Development of orientation preference maps in ferret visual cortex

Dissertation

zur Erlangung des Grades eines Doktors

der Naturwissenschaften

der Fakultät für Biologie der

Ludwig-Maximilians-Universität München

vorgelegt von

Diplom-Biochemiker

Marcus Leinweber

14. Oktober 2010

Ehrenwörtliche Versicherung:

Ich versichere hiermit ehrenwörtlich, dass ich die Dissertation mit dem Titel „Development of orientation preference maps in ferret visual cortex" selbständig und ohne unerlaubte Beihilfe angefertigt habe. Ich habe mich dabei keiner anderen als der von mir ausdrücklich bezeichneten Hilfen und Quellen bedient.

Erklärung:

Hiermit erkläre ich, dass ich mich nicht anderweitig einer Doktorprüfung ohne Erfolg unterzogen habe. Die Dissertation wurde in ihrer jetzigen oder ähnlichen Form bei keiner anderen Hochschule eingereicht und hat noch keinen sonstigen Prüfungszwecken gedient.

München, 14. Oktober 2010

Marcus Leinweber

Contents

Results   53

Discussion   87

Bibliography   101

Acknowledgements   121

Curriculum vitae   123

List of Figures

Summary

In the mammalian primary visual cortex, most neurons respond selectively to the orientation of a stimulus in visual space. In higher mammals, preferred stimulus orientation is mapped systematically and smoothly across the visual cortex, except at "pinwheel" centres, where all orientation preferences coalesce. It is not clear whether this peculiar functional architecture bears any significance for visual information processing, or whether it is merely a by-product of the developmental mechanism that leads to the generation of orientation selectivity. A crucial step in resolving this question is a detailed characterization of the development of the orientation preference map.

Ferrets are ideally suited to address this question, since they are born relatively

immature, thus allowing recording and imaging experiments in the visual cortex during early developmental stages. Previous intrinsic signal imaging studies in this species have revealed that a faint orientation preference map first appears around postnatal day 31. The map subsequently increases in strength, while its overall layout remains stable over the following weeks. Electrical recordings, however, have found orientation selective neurons about ten days before the appearance of the earliest orientation preference maps, but whether these neurons are organized into an orientation preference map remains unknown. Thus, there is a ten day gap in our knowledge of the critical steps of orientation map development in ferret visual cortex. Closing this gap is the aim of my thesis.

As the method of choice, I used, *in vivo* two-photon calcium imaging, as it allows to map orientation preference at cellular resolution in extended regions of the primary visual cortex. Neurons in ferrets as young as postnatal day 19 were not responding to visual stimulation, but many cells showed spontaneous calcium signals. Soon thereafter, around postnatal day 21, I was able to record the first visually evoked calcium signals. Neurons at this early age were sharply tuned for orientation, and, surprisingly, almost all cells responded strongly and nearly exclusively to horizontal stimuli. This unexpected regime of "all-horizontal" tuning lasted for about one week, up to postnatal day 27. Subsequently, around the time of eye-opening, cells lost their all-horizontal tuning and responded largely unselectively to all orientations. Despite such broad tuning during this period, cells were already organized into smooth maps of orientation preference with occasional pinwheel discontinuities. Later still, orientation selectivity improved further, but orientation map structure remained overall similar. Thus, during the initial development of visual response properties, neurons in ferret visual cortex undergo dramatic and exquisitely orchestrated changes in orientation tuning as one regime of functional organization gives way to another. In particular, the transition from all-horizontal tuning to the familiar pinwheel arrangement implies considerable, as yet unreported developmental changes in the neuronal circuits underlying the generation of orientation preference. These orchestrated developmental changes emphasize the significance of the map structure as at least one solution for cortical processing of orientations in the primary visual cortex.

Abbreviations

ACSF	artificial cerebral spinal fluid
AM	acetoxymethyl
ANOVA	analysis of variation
APB	DL-2-amino-4-phosphonobutyric acid
BP	band-pass
CSF	cerebral spinal fluid
CV	coefficient of variation
DiI	1,1'-dioctadecyl-3,3,3',3'- tetramethylindocarbocyanine perchlorate
DMSO	dimethyl sulfoxide

EKG	electrocardiogram
F	fluorescence
GABA	gamma-aminobutyric acid
Hz	Hertz
IC	inferior colliculus
LGN	lateral geniculate nucleus
MGN	medial geniculate nucleus
μm	micrometre
mm	millimetre
ms	milliseconds
MTF	modulation transfer function
NA	numerical aperture
NMDA	N-methyl-D-aspartate
NR2A	NMDA receptor subunit 2A
ODC	ocular dominance column
OGB-1 AM	Oregon Green® 488 BAPTA-1 AM
OSI	orientation selectivity index
P	postnatal day
PMT	photomultiplier tube
PW	postnatal week
ROI	region of interest
SC	superior colliculus
s	seconds
s. e. m.	standard error of the mean
TPLSM	two-photon laser scanning microscope
TTX	tetrodotoxin
V1	primary visual cortex

Introduction

1.1 Sensory processing in the visual system

The ability to process sensory information is essential for the survival of an organism in its rapidly changing world. Our brain consists of 100 billion neurons (Williams and Herrup 1988) of which many are devoted to gathering and processing sensory information in order to plan, initiate and finally execute behaviours. In many species, in particular many primates including ourselves, a substantial fraction of the brain is dealing with the processing

of visual information. In macaque monkeys, for example, a large part of the cerebral cortex, about 30–40 individual areas, comprising approximately 55% of the cortical surface area, process almost exclusively visual information (Felleman and Van Essen 1991). In humans, the visual system is a highly developed sensory system, enabling us to acquire and process very complex patterns of light in a precise manner, ultimately enabling us to carry out tasks – in a fraction of a second – like face recognition, which the best of today's computers still fail with. In a very general sense, visual information processing is based on decomposing the complex information present in the visual world by an array of initially simple spatial filters, whose properties are becoming more and more complex when moving from one cortical area to another one.

Visual processing starts with the formation of an image onto the retina by the eye's refractive structures, mainly the cornea and the lens. Rhodopsin (Shichida and Matsuyama 2009), a protein located in the photoreceptors, absorbs incident photons, which through a second messenger cascade ultimately leads to the hyperpolarisation of the photoreceptor. Within the retina, neuronal signals are further conducted through a network of bipolar, amacrine, and horizontal cells to the ganglion cells (Wässle 2004). The axons of retinal ganglion cells form the optic nerve exiting the eye, and they project via the optic chiasm to the lateral geniculate nucleus (LGN) of the thalamus. Through partial bifurcation of the optic nerve at the chiasm, the ganglion cells from the nasal retina send their projections to the contralateral LGN, whereas the temporal ganglion cells project to the ipsilateral LGN. From there, projections terminate in the primary visual cortex (also called striate cortex, V1 or area 17), located in the occipital part of the neocortex.

A primary visual cortex can be found in all mammals (Krubitzer and Kaas 2005), from highly visual primates to almost blind mole rats (Cooper *et al.* 1993). Like most other areas of the neocortex, the primary visual cortex consists of six layers. LGN neurons target cortical cells in layer 4, the main thalamic recipient layer, but some also send axons into cortical layer 6. A key feature of these projections is their topographic organization, such that visual space is orderly mapped onto the primary visual cortex, a principle that is maintained in most, but not all, higher visual areas.

Most of our knowledge about the structure of the visual system and visual information processing originates from research in the cat (*Felis catus*) that served as a model

organism in the field for decades. More recently, the ferret (*Mustela putorius furo*) has been introduced as an additional animal model with an overall similar anatomical and functional architecture of the visual system.

In the following, I will explain those steps of visual information processing, studied over many years in cats and ferrets, which are important in the context of the experiments described in my thesis.

A photoreceptor in the retina is activated by light coming from a particular region of the visual world, termed the receptive field. By definition, only visual stimuli inside this region are able to modulate the activity of that individual cell. Size, location and shape of a receptive field are basic neuronal properties, which can be determined experimentally. The definition of a receptive field can also be extended to cells higher up in the visual system. But while photoreceptors are pure light detectors, responding to local luminance, most other cells in the retina respond to more complex stimuli. For example, ganglion cells of the ON-type fire strongly in response to spots of light of an optimal size surrounded by a dark background (**FIGURE 1-1**). In contrast, OFF ganglion cells have the same concentric receptive field architecture, but with opposite sign (Kuffler 1953).

Retinal ganglion cells in the cat and ferret can be further subdivided into X, Y and W cell classes, based on additional response criteria. X and Y ganglion cells form two cell classes, each with physiological homogeneous properties and brisk responses (Cleland *et al.* 1971b), whereas W cells form a heterogeneous group with rather sluggish responses to visual stimulation. X cells typically have small receptive fields and exhibit sustained activity with linear summation of visual inputs; they show relatively long latencies between stimulus and response. Y cells have larger receptive fields and show phasic responses with shorter latencies. Moreover, they sum visual inputs over space in a nonlinear fashion (Enroth-Cugell and Robson 1966). It is also known that Y cells prefer higher temporal and lower spatial frequencies and have a higher contrast sensitivity than X cells (reviewed by Sherman 1985).

Anatomically, three main classes of retinal neurons could be identified, the alpha, beta and gamma ganglion cells. Each morphological class can be clearly related to its physiological counterpart. Cells of the alpha type are the equivalent to Y neurons, beta cells

correspond to X cells and gamma cells to W cells (for more details see Wässle and Boycott 1991).

LGN cells are segregated into three principal functional layers (A, A1 and C) in which the monocular nature of visual inputs is still preserved (**Figure 1-1**). Layer A1 receives inputs from the contralateral retina, whereas neurons in layer A receive projections from the ipsilateral retina (McConnell and LeVay 1986). In contrast, layer C receives inputs from
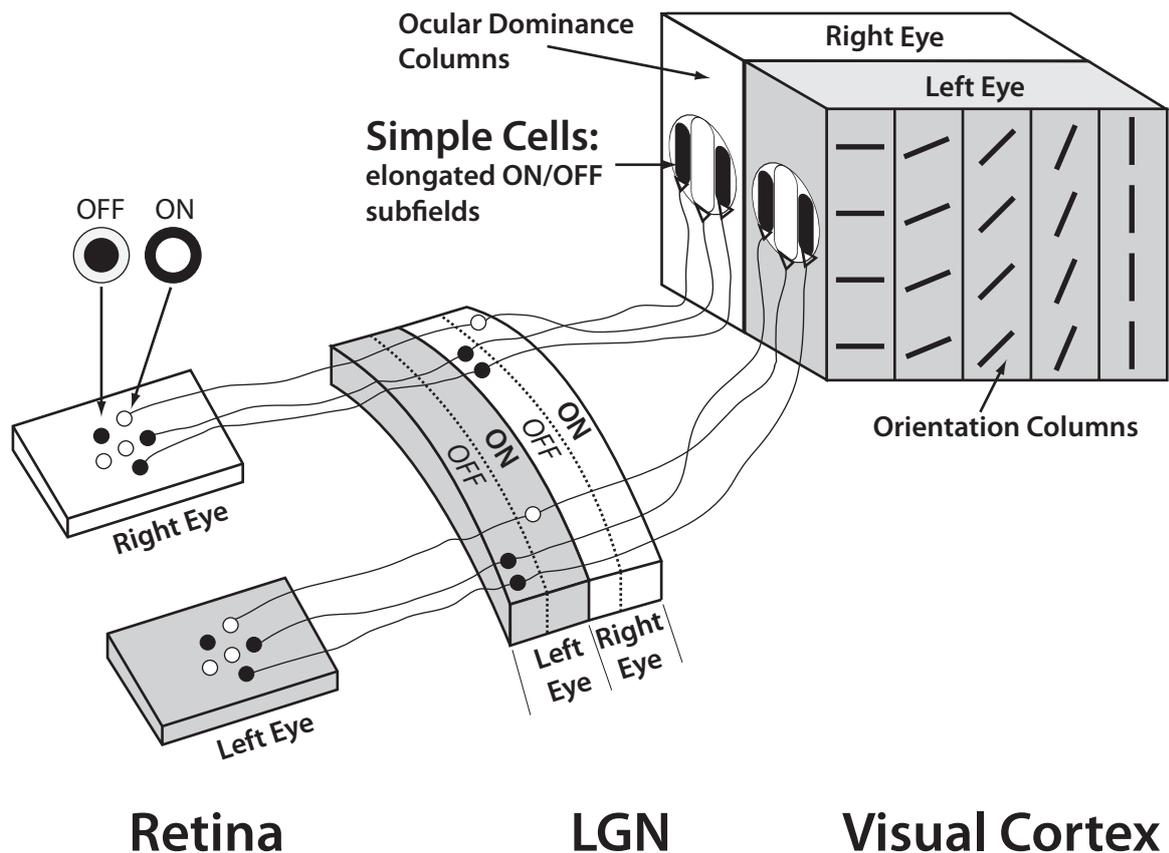
Figure 1-1: **Anatomical and functional organization of early visual pathways in the ferret.**

In the retina, ganglion cells, either ON- or OFF-centre type, have concentric receptive fields and project to the lateral geniculate nucleus (LGN). Receptive fields in the LGN are very similar to those in the retina. LGN neurons form synaptic contacts with cells in layer 4 of the primary visual cortex. The receptive fields of these simple cells are elongated and exhibit separate, antagonistic ON and OFF subzones, endowing them with the property of orientation tuning. Neurons with similar orientation tuning are grouped together, forming iso-orientation domains which are arranged in a systematic fashion across the cortical surface. Reproduced from Weliky 2000.

both retinas. Like retinal ganglion cells, LGN neurons can be subdivided into X, Y and W cells, which have antagonistic centre-surround receptive fields like their retinal counterparts. In the cat, ON- and OFF-centre cells are intermingled, whereas in the ferret each layer is further separated into ON and OFF sublaminae (Stryker and Zahs 1983; Bowling and Caverhill 1989; Thurlow *et al.* 1993).

Thus, connections between retina and LGN preserve the centre-surround receptive field organization pandered by the fact that geniculate neurons receive input from only one or few retinal ganglion cells (Bishop *et al.* 1958; Freygang 1958; Hubel and Wiesel 1961; Bishop *et al.* 1962; Kaplan *et al.* 1987). Dual recordings from neurons in the retina and LGN also demonstrated a convergence of few presynaptic retinal cells onto a single geniculate neuron (Cleland *et al.* 1971a,b; Levick *et al.* 1972; Usrey *et al.* 1999). Importantly, these studies confirmed that retinal and LGN cells with spatially overlapping receptive fields have the same sign, either ON or OFF. Apart from the overall similarity of receptive fields in the retina and LGN, there are a few notable differences; the most important one being the strengths of their surrounds: LGN surround responses are stronger than those from retinal ganglion cells.

In comparison to retina and LGN, the receptive field structure is dramatically different in the primary visual cortex, with new types of receptive fields present already in the input layer 4 (**Figure 1-1**). These differences are probably best characterized and described in cat visual cortex (Hubel and Wiesel 1962), where neurons in layer 4 receiving direct geniculate input feature separate, elongated ON and OFF zones. These ON and OFF subregions are likely formed by multiple, spatially aligned inputs from the LGN (Hubel and Wiesel 1962; Chapman *et al.* 1991; Alonso *et al.* 1996; Ferster *et al.* 1996).

1.2 Orientation selectivity in the primary visual cortex

In the course of characterising receptive field properties in cat visual cortex, Hubel and Wiesel discovered that many cortical neurons responded best to moving bars of light (Hubel and Wiesel 1959, 1963). Importantly, the angle of the bar was critical, such that only a certain orientation elicited a strong response, while an orthogonally angled bar evoked a weak response. Hubel and Wiesel coined the term orientation selectivity for this

receptive field property. Most neurons in the visual cortex, except those in layer 4C in monkeys (Bauer *et al.* 1980; Bullier and Henry 1980; Blasdel and Fitzpatrick 1984; Hawken and Parker 1984; Leventhal *et al.* 1995), exhibit orientation selectivity: In cat visual cortex around 90-95% of the neurons show tuned responses to stimulus orientation (Bishop and Henry 1972; Chapman and Stryker 1993). The adult ferret visual cortex contains slightly fewer orientation selective neurons, around 75% (Chapman and Stryker 1993). The degree of orientation selectivity is characterized by a neuron's orientation tuning curve, which plots response strengths as a function of stimulus orientation. Tuning width in the visual cortex, typically measured as half width at half maximum of the tuning curve, is surprisingly conserved in animals with very different visual acuities. It ranges from 19° - 25° in cat to around 30° in rodents (van Hooser 2007).

Several subclasses of orientation selective neurons have been described. Neurons termed simple cells by Hubel and Wiesel respond best to properly oriented bars at particular positions within their receptive field (Hubel and Wiesel 1962). At each position, a light stimulus of a specific sign evokes activity in a simple cell, either a bright bar on a dark background or dark bar on a bright background. Complex cells, the most common group in the visual cortex, are orientation selective as well. However, they are less sensitive to the exact position of the light bar within the receptive field and are rather driven by a moving bar of the preferred orientation.

In addition, the responses of simple and complex cells to oriented bars also vary depending on the presence of stimuli outside of their central receptive fields. Some neurons, termed end-stopped cells, decrease their responses as the length of the bar or grating extends beyond the central receptive field (Henry *et al.* 1974; Gilbert 1977; Murphy and Sillito 1987; Hammond 1994). Other cells, so-called length-summing cells, increase their activity when the length of the bar or grating increases (Gilbert 1977; Hammond 1994).

In summary, receptive fields of neurons in the visual cortex are very different from those in the LGN, which provide the input to the cortex. So, how does the cortex achieve the transformation of receptive field properties from non-orientation tuned cells in the LGN to orientation selective neurons in the primary visual cortex?

When Hubel and Wiesel (1962) published their findings on orientation selectivity, they proposed a simple and elegant model for its origin. Simple cells achieve orientation

selectivity by a specific arrangement of their convergent thalamic inputs (**Figure 1-1**). ON regions of a simple cell are constructed from inputs of ON-centre geniculate neurons overlapping in a row-like fashion along the axis of the receptive field. The assembly of parallel, adjacent OFF regions occurs in a corresponding manner. When a bar of light is oriented correctly along the axis of the receptive field, all presynaptic geniculate neurons get activated, causing the cortical neuron to fire to this optimally oriented stimulus. In contrast, the orthogonal, non-optimal stimulus activates only a few geniculate input neurons at a time, whose joint synaptic inputs are insufficient to drive the cortical simple cell's membrane potential above the spiking threshold.

This model was later referred to as the *feedforward model* since the information flows forward in one direction from the cells in the LGN to cortical simple cells and later complex cells (Hirsch *et al.* 1995; Reid and Alonso 1996). Support for this model is provided by several studies. Cortical layers 4 and 6 are dominated by simple cells (Martinez *et al.* 2005), receiving monosynaptic geniculate inputs (Ferster and Lindstrom 1983; Ferster *et al.* 1996). The receptive fields of geniculate afferents recorded in a pharmacologically silenced cortex are aligned along an axis that matches the preferred orientation of nearby cortical cells recorded before they were silenced (Chapman *et al.* 1991). Further strong support for a spatially elongated arrangement with subfields of opposite sign comes from dual recordings of LGN and cortex (Reid and Alonso 1995). Using cross-correlation techniques, these authors found that the centres of geniculate relay cells only overlap with a simple cell's subregion of the sample polarity (ON or OFF) as predicted by the feedforward model (Ferster *et al.* 1996).

However, pure feedforward models raised criticism, since they were not able to explain entirely the behaviour of simple cells: (1) The spatial arrangement of the geniculate inputs does not predict the narrow orientation tuning observed in many cortical cells. (2) Orientation selectivity is contrast invariant (Freeman *et al.* 1983), meaning that the width of the orientation tuning curve stays constant with increasing stimulus contrast, and a simple cell never responds to non-preferred orientations at any contrast. (3) Preferentially oriented stimuli overlaid with an orthogonal pattern reduce the responses of simple cells, a phenomenon referred to as cross-orientation suppression (Bishop *et al.* 1973).

Therefore, *feedback models* were suggested, that added intracortical inhibition and excitation to the feedforward circuitry. The pure excitatory nature of thalamocortical synapses is not disputed, so that any inhibitory contribution to the sharpness and contrast invariance of orientation selectivity must be of intracortical origin. The crucial importance of intracortical inhibition for the generation of orientation selectivity is based on theoretical work of many researchers (e. g. Troyer *et al.* 1998; McLaughlin *et al.* 2000; Wielaard *et al.* 2001). However, experiments gave ambiguous results. On the one hand, pharmacological inactivation of inhibition in the cortex was shown to lead to broader orientation tuning (Sillito 1975; Pfleger and Bonds 1995; Sato *et al.* 1996). Moreover, intracellular recordings in cat primary visual cortex showed that various forms of intracortical inhibition can alter orientation tuning (Borg-Graham *et al.* 1998; Monier *et al.* 2003). However, related experiments using cooling or electrical stimulation to silence cortical circuits came to a different conclusion: The remaining thalamocortical synaptic inputs showed sharp orientation tuning, not any different from that of cortical cells (Ferster *et al.* 1996; Chung and Ferster 1998).

A crucial role of intracortical excitation for orientation tuning was suggested by other theoretical models (Ben-Yishai *et al.* 1995; Adorjan *et al.* 1999; Tsodyks *et al.* 1999). These authors suggested that weak orientation tuning originating from feedforward connections is sharpened by strong recurrent excitatory feedback.

Contradictive lines of evidence for both, pure feedforward and feedback, models were a subject to a debate over many decades (Shapley *et al.* 2003; Priebe and Ferster 2005). Further studies are necessary to determine the precise connectivity. In particular, new imaging techniques in combination with genetic tools may facilitate identifying different cell types and their connectivity amongst each other.

1.3 Spatial organization of orientation preference across the cortical surface

Hubel and Wiesel already recognized in their first experiments that orientation selective neurons were not randomly distributed in cat visual cortex, but instead showed a highly

ordered organization. Neurons sharing a similar orientation preference cluster together, forming iso-orientation domains, which are repeated at regular intervals (800–900 μm), and extend vertically through all layers of the cortex, thereby forming what Hubel and Wiesel (1962, 1974) coined as orientation columns. The introduction of optical imaging techniques (Blasdel and Salama 1986; Grinvald *et al.* 1986) made it possible to visualize orientation columns over large cortical areas. Intrinsic signal imaging and later two-photon calcium imaging allowed studying the spatial arrangement of these orientation columns in great detail (Bonhoeffer and Grinvald 1991; Ohki *et al.* 2006). Apart from the mostly smooth and gradual progression of preferred orientation in these "orientation preference maps", discontinuities such as pinwheels and fractures were revealed. Iso-orientation domains containing the entire range of orientations converge at singularity points, termed pinwheel centres (Bonhoeffer and Grinvald 1991; Ohki *et al.* 2006). Here, orientation preference changes abruptly between adjacent neurons (**FIGURE 1-2A, B**). Furthermore, rapid changes of orientation preference occur along lines, termed fractures. They were first described in monkey visual cortex (Blasdel and Salama 1986), but are less pronounced in cats (Bonhoeffer and Grinvald 1993).

Orientation preference is not the only feature mapped across the surface of the visual cortex. Ocular dominance and spatial frequency are also organized into maps and are often, together with orientation preference maps, arranged in a systematic fashion towards each other (Bartfeld and Grinvald 1992; Hübener *et al.* 1997).

Orientation preference maps, subject to intense research for decades, were found in many mammalian species including primates (Hubel *et al.* 1978; Blasdel and Salama 1986), carnivores (Hubel and Wiesel 1963; McConnell and LeVay 1986; Bonhoeffer and Grinvald 1991; Rao *et al.* 1997), sheep (Clarke *et al.* 1976) and tree shrews (Humphrey and Norton 1980; Weliky and Katz 1994; Bosking *et al.* 1997). No evidence for orientation preference maps was found in rabbit (Murphy and Berman 1979), and hamster (Tiao and Blakemore 1976) and other rodents like mice and rats (Metin *et al.* 1988; Girman *et al.* 1999; Ohki *et al.* 2005) despite the presence of orientation selective neurons (**FIGURE 1-2C**). The fact that some species have orientation preference maps and others do not, raises the central question about their functional relevance (Horton and Adams 2005). Especially since many species lacking orientation preference maps have the same basic functional properties like

orientation selectivity, the presence of simple and complex cells, end-stopping and length-summation (Girman *et al.* 1999; Heimel *et al.* 2005; van Hooser *et al.* 2006) as animals with spatial clustering of orientation preference. The assumption that visual acuity correlates with the evolution of orientation preference maps is questioned by recent studies. The gray squirrel, a rodent, has all major cell types including cortical orientation selective neurons, and exhibits better visual acuity than many species with orientations preference maps (van Hooser *et al.* 2005; van Hooser *et al.* 2006). Importantly, their habitat and behaviour suggest that they have a highly developed visual sense. These observations as well as the
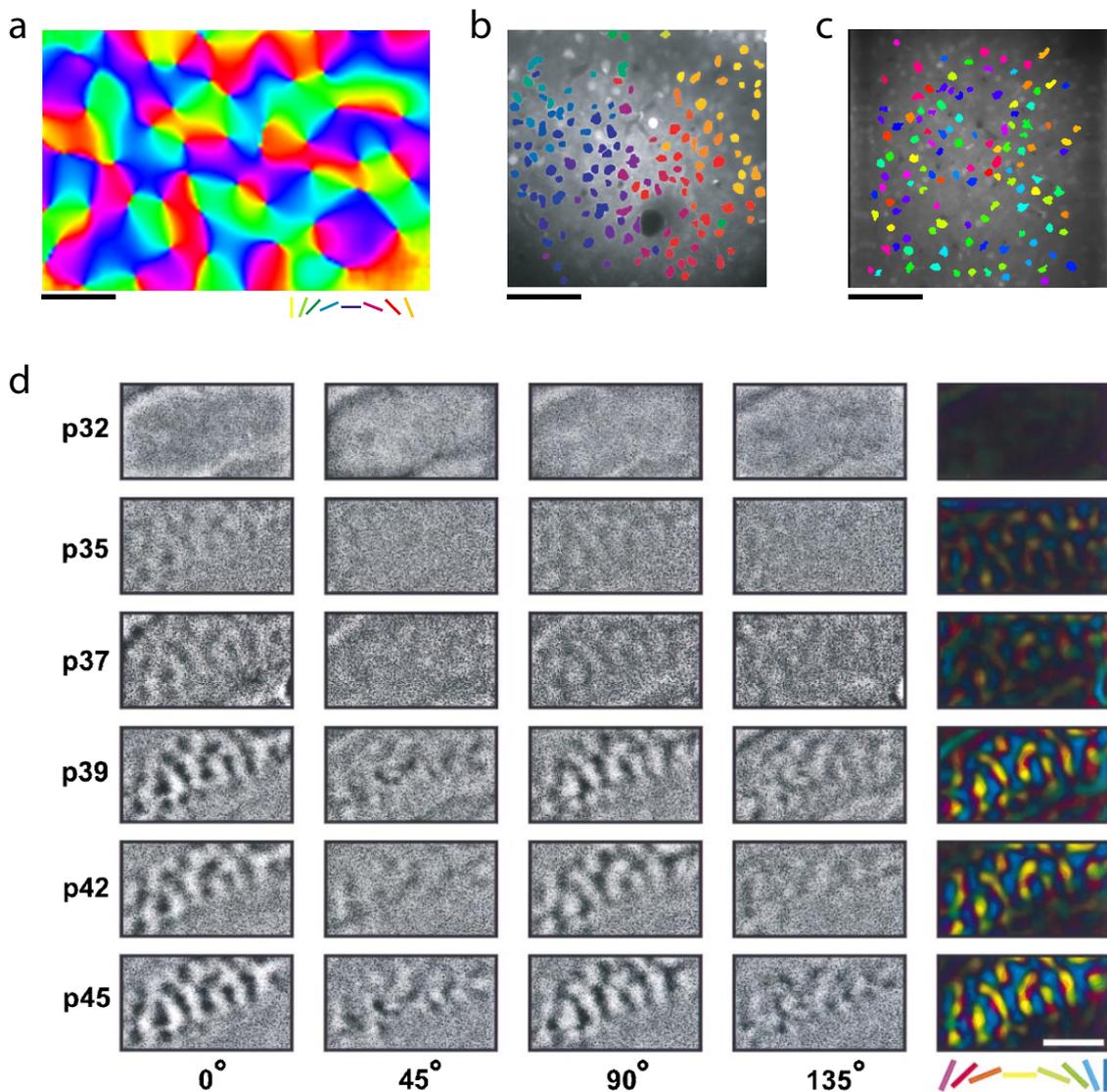
similarity in tuning sharpness between animals with and without orientation preference maps may have led many scientists to question that a modular organization of maps contributes significantly to cortical function (Horton and Adams 2005; van Hooser 2007). However, it is hard to imagine that evolutionary forces drive and maintain a highly ordered arrangement such as orientation preference maps over long time and many species. They might rather be a result of selective pressure during evolution to minimize the cortical wire length as first suggested by Hubel and Wiesel (1977). I will come back to this important question in the discussion.

Cortical connectivity on a fine scale is still poorly understood (Douglas and Martin 2004), mainly due to technical limitations of anatomical tracing and imaging techniques.

Figure 1-2: **Functional architecture of orientation preference maps and their development.**

a, Colour-coded orientation preference map in the adult cat derived with intrinsic signal imaging (Hübener and Bonhoeffer 2002). Colour indicates the preferred orientation as shown by the legend at the bottom. Neighbouring neurons prefer similar orientations and thereby form patches of the same colour called iso-orientation domains. Iso-orientation domains are arranged in a pinwheel-like fashion around point-like singularities, the pinwheel centre. Scale bar, 1 mm.

b, Orientation preference map in the cat at single cell resolution obtained with two-photon calcium imaging (Ohki *et al.* 2006). Neurons are coloured according to their preferred orientation as indicated in **a**. Scale bar, 100 µm.

c, Two-photon imaging of orientation selective neurons in mouse primary visual cortex (own data). Many mammals, including rodents, lack a functional organization for orientation preference. Scale bar, 100 µm. Colour-coding as in **a**.

d, Development of orientation preference maps in ferret visual cortex determined with chronic intrinsic signal imaging. Each row shows orientation maps recorded in one ferret at the age indicated at the left. The first four columns show single-condition orientation preference maps in response (dark regions) to a particular orientation of a moving grating stimulus. The fifth column displays polar maps determined from those single-condition maps whereby preferred orientation is colour-coded. The intensity in these maps indicates the magnitude of selectivity and/or responsiveness. In this example, an orientation preference map emerges first around postnatal day 35. Individual iso-orientation domains appear more visible over time, but otherwise remain stable and do not change their position or extent over the course of development. Scale bar, 2 mm. From Chapman and Bonhoeffer (1998).

New techniques with single cell resolution like two-photon calcium imaging (Stosiek *et al.* 2003; Helmchen and Denk 2005) and genetic tracing tools (Wickersham *et al.* 2007), will certainly improve our understanding of fine scale connectivity at the anatomical and functional level in the future (Ohki and Reid 2007; van Hooser 2007). Furthermore, a better understanding of the development of orientation preference maps in juvenile animals would allow disentangling the significance of such functional architecture also with respect to the general principles underlying cortical computation.

1.4   Development of orientation preference maps

While the significance of orientation preference maps remains a subject of controversy (Swindale 2000; Chklovskii and Koulakov 2004; Horton and Adams 2005), maps can serve as a conducive model to investigate the development and implementation of neural circuits to achieve selective response properties in the visual cortex.

As a framework of thinking, molecule-based and activity-based mechanisms are thought to be involved in the establishment and later refinement of neuronal maps. On one hand, genetic and molecular factors such as axon guidance cues and cell adhesion molecules might guide general map topology (Poskanzer *et al.* 2003; McLaughlin and O'Leary 2005; Chen and Flanagan 2006; Flanagan 2006; Huberman *et al.* 2008). On the other hand, patterned electrical activity adjusts further connectivity and guides the fine-scale formation of the map. The intimate interplay of both mechanisms is best understood for the development of the topography of visual space in the tectum (reviewed by Lemke and Reber 2005; Huberman *et al.* 2008). Gradients of molecular cues instruct retinal axons to the correct regions within the map, whereas waves of spontaneous activity refine topology of the map at later stages in development. Similar mechanisms also apply for the formation of the retinotopic map in the visual cortex (Cang *et al.* 2005; Cang *et al.* 2008). However, the development of maps representing other functional properties, like orientation preference, remains to be elucidated.

The first experiments investigating the development of orientation selective neurons were performed in traditional model organisms such as rhesus monkey and cat. Electrophysiological recordings in rhesus monkeys revealed some early orientation selective

neurons at birth (Wiesel and Hubel 1974). In kittens, the earliest cortical responses evoked by visual stimulation occur at the end of the first postnatal week, just before natural eye opening. At that time, orientation selective neurons were first found, but the actual percentage of tuned cells in kittens remains controversial. Electrophysiological studies reported very different fractions of orientation tuned neurons in the young cat visual cortex, ranging from 0% (Barlow and Pettigrew 1971; Pettigrew 1974), to 20% (Blakemore and Sluyters 1975) to 100% (Hubel and Wiesel 1963). Reasons for these discrepancies may lie in the difficulty in performing stable electrophysiological recordings in such young animals, where cells show sluggish responses which also habituate rapidly (Hubel and Wiesel 1963). Moreover, small changes in the physiological condition of the animal, in particular alterations in blood pressure and exhaled CO_2, can cause orientation selective neurons to become unselective or even non-responsive (Blakemore and Sluyters 1975). These problems can be minimized by using the ferret (*Mustela putorius furo*) as an animal model. The visual system is very similar to that of the cat (Law *et al.* 1988), but ferrets are born approximately three weeks earlier in development (Linden *et al.* 1981). The ferret therefore provides an appropriate model organism to study the mechanisms underlying the development of orientation selectivity at the earliest stages (Jackson and Hickey 1985; Chapman and Stryker 1993; Krug *et al.* 2001).

The first orientation selective responses in ferret visual cortex occur at postnatal day (P) 23, about nine days before natural eye opening at around P31. However, electrophysiological studies found that only 25% of neurons in these young ferrets showed orientation selectivity. Tuning was not very sharp and reached adult-like levels about one week after eye opening (Chapman and Stryker 1993; Krug *et al.* 2001; Akerman *et al.* 2004). Faint orientation preference maps were first detectable with intrinsic signal imaging at the time of natural eye opening (**Figure 1-2d**; Chapman *et al.* 1996; White *et al.* 2001; Li *et al.* 2006). Although chronic imaging revealed that the spatial layout of the emergent orientation preference maps in the ferret was quite stable over the course of development (Chapman *et al.* 1996), maps varied strongly in their signal strength. Interestingly, early maps were often biased towards cardinal orientations (vertical and horizontal) from the time of emergence to full functional maturation, approximately three weeks after eye opening (Chapman *et al.* 1996; White *et al.* 2001; Coppola and White 2004). The developmental time course seen

with intrinsic signal imaging generally matches with data on the maturation of orientation selectivity probed with electrophysiology (Chapman and Stryker 1993; Chapman *et al.* 1996; in the cat: Gödecke *et al.* 1997).

1.4.1 Structural changes during the development of orientation preference maps

Over the time course of development, several events and processes accompany the formation and maturation of orientation preference maps. The density of synaptic connections in the visual cortex is relatively low before the onset of visual experience. This changes dramatically after visually evoked activity starts, coinciding with the formation of the majority of cortical synapses, which increases rapidly in number before reaching stable adolescent levels (cat: Cragg 1975; rhesus: Bourgeois and Rakic 1993; ferret: Erisir and Harris 2003).

This remarkable increase in synaptogenesis coincides with the outgrowth of axons in different layers of the visual cortex. Long-range connections in layer 2/3 that preferentially connect iso-orientation domains (Malach *et al.* 1993; Bosking *et al.* 1997) expand and mature over the same period of postnatal map development (Durack and Katz 1996; Ruthazer and Stryker 1996; White *et al.* 2001). Anatomical reconstruction of horizontal long-range connections at different stages of map development around the time of eye opening revealed that anatomical and functional maturation are well correlated. At the time of eye opening, horizontal connections extent only shortly across the cortical surface and form crude clusters. Over the following two weeks, these horizontal connections grow in length and extent their degree of branching and clustering in layer 2/3 of the developing ferret (Durack and Katz 1996; Ruthazer and Stryker 1996). Importantly, this process is under activity control, since the extent of coverage and clustering was strongly reduced when sensory input was altered by dark rearing or binocular lid suture (White *et al.* 2001).

1.4.2 Molecular changes in neural circuits during the time of map formation

While a direct role of molecular cues in the development of orientation maps has not been shown (Huberman 2008, White 2007), molecular changes affect the excitatory and inhibitory balance of neuronal circuits in the visual cortex during this phase. NMDA receptors, which are key to detect correlations between pre- and postsynaptic activity (Bourne and Nicoll 1993), undergo changes in expression (Smith and Thompson 1999), accompanied by an up-regulation of the NR2A subunit of the NMDA receptor, which affects the duration of NMDA receptor currents (Roberts and Ramoa 1999). Furthermore, the blockade of NMDA receptors during this period perturbs the maturation of orientation selectivity (Ramoa *et al.* 2001). Thus, NMDA receptors play an important role in the specific strengthening of connections between pre- and postsynaptic neurons. A possible link between the development of inhibitory circuits and orientation preference maps is possible, but only poorly understood. In parallel, the composition of $GABA_A$ receptor subunits change in inhibitory neurons, but with a much slower time course than the maturation of orientation maps (Gao *et al.* 1999, 2000).

1.4.3 Role of different types of neuronal activity during map emergence

The role of visual experience during map formation has been intensely investigated. The observation that orientation selective neurons are already present more than a week before eye opening in ferret visual cortex suggests that the initial emergence of orientation preference maps occurs without visual experience. There is evidence that neurons respond in a selective manner to stimulus orientations through closed eye lids (Krug *et al.* 2001) suggesting that vision may play a role in the formation of orientation preference maps. However, earlier studies in ferrets and cats demonstrated that cortical orientation preference maps develop in a stable and orderly arranged manner after dark-rearing prior to natural eye opening (Gödecke *et al.* 1997; Crair *et al.* 1998; White *et al.* 2001).

Although orientation preference maps in dark-reared animals were very similar in their spatial layout to normal maps, they did not reach mature levels of orientation tuning. Moreover, experiments in young cats that were reared with only a limited set of stimulus

orientations (stripe rearing) showed very similar results. While orientation preference maps had a clear bias towards the experienced orientation, their overall layout was rather normal and they did contain domains tuned to orientations the animal had never experienced (Sengpiel *et al.* 1999). While dark-rearing completely prevents light stimulation of the retina, binocular lid suture only partially abolishes vision by allowing low spatial frequencies to be passed through the closed eye lid. Interestingly, visual deprivation by binocular lid suture produced more devastating effects on the maturation of orientation tuning (Chapman and Stryker 1993; White *et al.* 2001). Together, these results show that orientation preference maps develop initially without visual experience. Vision is necessary for full maturation and maintenance of the map, and degraded vision impairs map formation.

While visual experience has very little effect on the initial emergence of orientation selectivity, intrinsic neuronal activity does play an important role. Waves of activity propagate periodically across the ferret retina (Meister *et al.* 1991), starting from birth until the time of eye opening (Huberman *et al.* 2008). Different types of retinal waves are present during subsequent stages of visual system development, but all types generate patterned synchronous activity, resulting in high correlations among neighbouring retinal ganglion cells and low correlations between distant cells (reviewed in detail by e. g. Wong 1999; Huberman *et al.* 2008). Spontaneous, correlated activity is also present in the LGN during development. Correlations are higher between centre-type neurons of the same sign (ON or OFF), than between neurons of opposite sign (ON versus OFF). Moreover, spontaneous activity generates higher correlations between layers of the same eye (Weliky and Katz 1999). Interestingly, perturbation of spontaneous activity by electrical stimulation of the optic nerve during early development in the ferret (P15 - 17) results in a reduction of orientation selectivity in the mature visual cortex (Weliky and Katz 1997).

Similar patterns of activity were also found in the cortex of non-anaesthetized ferrets by multi-electrode recordings (Chiu and Weliky 2001). Synchronous bursts of spontaneous activity emerging around one week before natural eye opening occurred in patchy patterns over distances of about 1 mm. This long-range correlated activity is generated intracortically and is independent of input from the LGN (Chiu and Weliky 2001). In this context,

a

b

c

(1)　　　　　　　　　(2)　　　　　　　　　(3)
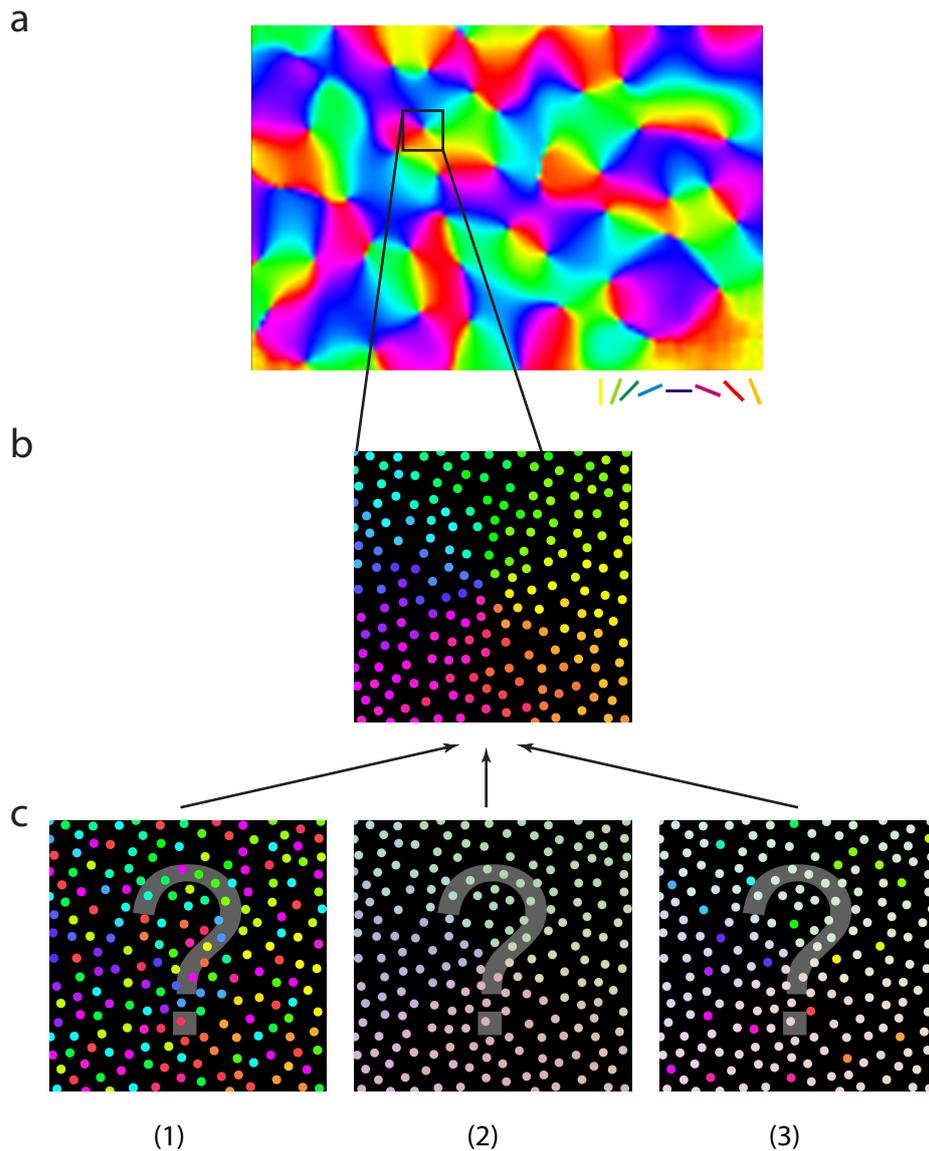
FIGURE 1-3: **Possible scenarios for the development of orientation preference maps at single cell level.**

a, Colour-coded orientation preference map obtained with intrinsic signal imaging.

b, Schematic of functional organization at the cellular level.

c, Three potential scenarios depicting early functional organization which might give rise to **b**. (1) Neurons with clear orientation preference, but arranged randomly in a "salt-and-pepper" layout. Many cells have to change their orientation preference during development. (2) Cells with broad orientation tuning (indicated by the low saturation in colour-coding) are already initially spatially clustered. All neurons may change the degree of selectivity over time. (3) "Seeding neurons" with clear orientation preference and narrow tuning may serve as templates for a mature orientation preference map and instruct neighbouring unturned cells. This step is potentially an intermediate step of either (1) or (2).

pharmacological silencing of spontaneous activity in visual cortex disrupts the maturation of orientation selectivity (Chapman and Stryker 1993).

In summary, the development of orientation preference maps is currently thought to proceed in two general phases: First, the initial map is formed by innate, experience independent mechanisms. Second, the refinement of the map is driven later through patterned visual activity (White and Fitzpatrick 2007; Huberman *et al.* 2008). However, for a precise understanding of the complex mechanisms leading to the formation of orientation preference maps, it is crucial to elucidate how the map develops in detail.

1.5   The goal of this thesis

While the layout of orientation preference maps has been studied intensively (Wiesel and Hubel 1974; Bonhoeffer and Grinvald 1991, 1993; Ohki *et al.* 2006), much less is known about map development. In particular, it is not clear whether the development of orientation tuning of individual neurons is coupled to the formation of the orientation preference map itself. More specifically, we do not know whether the earliest orientation selective neurons (Krug *et al.* 2001) are already organized into an orientation preference map. Does visual experience only serve to consolidate the layout of the map? Do individual neurons undergo changes in orientation preference and tuning in the process of map formation (**FIGURE 1-3**)? Are there 'seeding neurons', whose preferences and tuning establishes a basic scaffold of the orientation preference map prior to the onset of visual experience, subsequently instructing neighbouring neurons later during map maturation?

The most commonly used methods for mapping the functional architecture of developing orientation preference maps (Chapman *et al.* 1991; Chapman and Stryker 1993; Krug *et al.* 2001) have a number of limitations. Intrinsic signal imaging lacks single cell resolution, and the source of the intrinsic signals is still not very clear (Schummers *et al.* 2008; Sirotin and Das 2009). On the other hand, electrophysiological methods are notorious for introducing sample biases, they preferentially record from large and highly active neurons while at the same time missing weakly active or unresponsive units. Also, systematic mapping of large cortical regions is extremely time-consuming. The recently developed method of two-photon imaging of somatic calcium signals (Stosiek *et al.* 2003) overcomes

most of these problems and made it possible for the first time to investigate map structure at single cell resolution, for example demonstrating the highly ordered arrangement of direction and orientation selective neurons in cat visual cortex (Ohki *et al.* 2006).

In summary, the goal of this thesis is to investigate the functional architecture of early developing orientation preference maps at single cell resolution using two-photon calcium imaging in ferret visual cortex. While prior electrophysiological work (Chapman and Stryker 1993; Krug *et al.* 2001) has found orientation selective neurons around postnatal day 21, the earliest orientation preference maps, obtained with intrinsic signal imaging, emerge ten days later (Chapman *et al.* 1996). How these early orientation selective neurons become organized over time to finally establish an orientation preference map (**Figure 1-3**), remains to be elucidated. Thus, there is a ten day gap in our knowledge of the critical steps of orientation map development in ferret visual cortex. Closing this gap is the central goal of my thesis.

Materials and Methods

2.1 Materials

2.1.1 Drugs and Chemicals

1,1'-dioctadecyl-3,3,3',3'- tetramethylindocarbocyanine perchlorate,
    Invitrogen, Carlsbad, USA

Acepromazine, Vetranquil 1% Ceva, Düsseldorf, Germany

Agarose, biomol, Hamburg, Germany

Atropine 1.0 mg, Eifelango, Bad Neuenahr-Ahrweiler, Germany

Atropine EDO 0.5%, Dr. Mann Pharma, Berlin, Germany

Black pigment, Elfenbeinschwarz, Kremer, Aichstetten, Germany

Calcium chloride dihydrate, Merck, Darmstadt, Germany

Dental cement, Paladur, Heraeus Kulzer, Hanau, Germany

Dexamethasone, Fortecortin 4 mg, Merck, Darmstadt, Germany

Eye lubricant, Isopto-Max, Alcon, Freiburg, Germany

Glucose infusion solution, Sterofundin VG-5, Braun, Melsungen, Germany

Glucose monohydrate, Roth, Karlsruhe, Germany

Halothane, Nicholas Pharma, Ennore, India

HEPES, Roth, Karlsruhe, Germany

Iodine solution, Braunol 7.5, Braun, Melsungen, Germany

Ketamine 10%, WDT, Giessen, Germany

Magnesium sulfate heptahydrate, Merck, Darmstadt, Germany

Neosynephrine-POS 5%, Ursapharm, Saarbrücken, Germany

Oculotect, Novartis, Nürnberg, Germany

Oregon Green® 488 BAPTA-1 AM, 50 µg, Invitrogen, Carlsbad, USA

Pluronic 20% solution in DMSO, Invitrogen, Carlsbad, USA

Potassium chloride, Roth, Karlsruhe, Germany

Ringer's solution, Isotone 0.9%, Braun, Melsungen, Germany

Sodium chloride, Merck, Darmstadt, Germany

Sodium hydroxide, 1 N, VWR, Briare, France

Sulforhodamine 101, Invitrogen, Carlsbad, USA

T61, intervet, Unterschleißheim, Germany

Vaselium album, Rhenania, Bonn, Germany

Xylocaine, AstraZebeca, Wedel, Germany

2.1.2 Surgical instruments and material

Bone wax, Ethicon, Norderstedt, Germany

Borosilicate glass capillaries, GC150F-10, Harvard Apparatus, Holliston, USA

Centrifugal filter, 0.22 μm, Millipore, Ireland

Contact lenses, Ocular Contact Lenses, Benicia, CA, USA

Cover glass, Ø 5 mm, Electron Microscopy Sciences, Hatfield, USA

Forceps, #5, angled, No. 555229F, WPI, Sarasota, USA

Forceps, #5, straight, No. 11251-30, Fine Science Tools, Germany

Forceps, #7, angled, No. 11271-30, Fine Science Tools, Germany

Hair trimmer, Aesculap, Melsungen, Germany

Hand silk, #3-0, Ethicon, Norderstedt, Germany

Hand silk, #5-0, Ethicon, Norderstedt, Germany

IV cannula, Introcan-W, 22 gauge, Braun, Melsungen, Germany

Needle Holder, No. 12002-12, Fine Science Tools, Germany

Needle, 20 gauge, Terumo, Leuven, Belgium

Needle, 23 gauge, Terumo, Leuven, Belgium

Needle, 27 gauge, Terumo, Leuven, Belgium

Needle, 19 gauge, Sterican, Braun, Melsungen, Germany

Operating microscope, KAPS, Asslar, Germany

Particle filter, Mini-Spike Plus, Braun, Melsungen, Germany

Perfusor tubing, Braun, Melsungen, Germany

Pipette tips for Microloader, Eppendorf, Hamburg, Germany

Pipettes, various models, Gilson, Middleton, USA

Scalpel blades #10, No. 10010-00, Fine Science Tools, Germany

Scalpel handle #7, No. 10007-16, Fine Science Tools, Germany

Scissors, straight 8.5 cm, No. 14090-09, Fine Science Tools, Germany

Spring scissors, 2.5 mm blades angled, No. 15002-08, Fine Science Tools, Germany

Spring scissors, 3 mm blades straight, No. 15000-00, Fine Science Tools, Germany

Sterile swabs, Sugi, Kettenbach, Eschenburg, Germany

Syringe, Injekt 10 ml, Braun, Melsungen, Germany

Syringe, Omnican 50, Braun, Melsungen, Germany

Syringe, Omnifix 1 ml, Braun, Melsungen, Germany

Syringe, OPS 50ml, Braun, Melsungen, Germany

Tissue adhesive, Histoacryl, Aesculap, Tuttlingen, Germany

2.1.3   Instrumentation

Axoporator 800A, Molecular Devices, Sunnyvale, USA

Brownlee 440 amplifier, Brownlee Precision, San Jose, USA

Dentral drill, MF-perfecta with handpiece WS92 E/3, W&H, Bürmoos, Austria

Drill bits, HM 1005, Meisinger, Neuss, Germany

End-tidal CO_2 analyser, microCapStar, CWE, Pennsylvania, USA

Epifluorescence microscope, Lumar V12, Zeiss, Jena, Germany

Gas regulator N_2O 150-2150cm^3, ABB, Zurich, Switzerland

Gas regulator N_2O 40-580cm^3, ABB, Zurich, Switzerland

Gas regulator O_2 150-2100cm^3, ABB, Zurich, Switzerland

Gas regulator O_2 40-580cm^3, ABB, Zurich, Switzerland

Halothane vaporizer, Dräger, Lübeck, Germany

Homoeothermic blanket with rectal probe, Harvard Apparatus, Holliston, USA

Micromanipulator, MO-10, Narishige, Tokyo, Japan

Micromanipulator, Sutter MP285, Sutter Instrument, Novato, Germany

Ophthalmoscope, Beta 200, Heine, Herrsching, Germany

Patient monitor, UltraCare SLP, Spacelabs Healthcare, Issaquah, USA

Perfusor secura, Braun, Melsungen, Germany

Small animal respirator, KTR 5, FMI, Engelsbach, Germany

Stimulation monitor, L227WTP, LG, Jaebeol, South Korea

Toohey Spritzer Pressure System IIe, Toohey, Fairfield, USA

Tripod Cullmann 40300, Cullmann, Langenzenn, Germany

Two-step vertical puller, P-10, Narishige, Japan

2.1.4   Two-photon microscope

Autocorrelator, Carpe, APE, Berlin, Germany

CCD camera, Adimec 1000m/D, Eindhoven, Netherlands

Controller for Pockels cell, model 302RM, conoptics, Danbury, USA

Data acquisition card, NI 6115, National Instruments, Austin, USA

Data acquisition card, NI 6008, National Instruments, Austin, USA

Dichroic mirror, 670 nm, Chroma, Bellows Falls, USA

Emission filter, 535 nm, 50 nm bandwidth, 18° optimized, Chroma, Bellows Falls, USA

Emission filter, 610 nm, 75 nm bandwidth, 18° optimized, Chroma, Bellows Falls, USA

Eye shutters, workshop, MPI

Linear stage and motor, LTA-HS and M-UMR8.51, Newport, Santa Clara, USA

Linear stage, M-VP-25-XA, Newport, Santa Clara, USA

Low-noise current amplifier, SR570, Stanford Research Systems

MaiTai HP DeepSee, SpectraPhysics/ Newport, Santa Clara, USA

Mirrors, E03, Thorlabs, Dachau, Germany

Motion controller, ESP300, Newport, Santa Clara, USA

Mounting material, Thorlabs, Dachau, Germany

Objective, water immersion, 40×, 0.8 NA, Olympus, Tokyo, Japan

Photomultiplier tube, R6357, Hamamatsu, Toyooka, Japan

Pockels cell, model 350–80, conoptics, Danbury, USA

Power supply, NMC–100, Conrad, Germany

Scan lens, 50 mm, Leica, Wetzlar, Germany

Tube lens, 300 mm, Thorlabs, Dachau, Germany

Yanus Scanhead, TILLPhotonics, Martinsried, Germany

2.1.5 Electrophysiological equipment

16 channel silicon probes, A-style, NeuroNexus, Ann Arbor, USA

Audio monitor, AM10, GRASS Technologies, West Warwick, USA

Headstage RA16AC, Tucker-Davis, Alachua, USA

Luigs-Neumann, LM1 with 3 mini 25 motors, Ratingen, Germany

Multi-function processor RX5, Tucker-Davis, Alachua, USA

Oscilloscope, Tektronix, USA

Preamplifier RA16PA, Tucker-Davis, Alachua, USA

Real-time processor RP2.1, Tucker-Davis, Alachua, USA

Tungsten electrodes, 1 MΩ, AM Systems, Carlsbourg, USA

2.1.6 Photorefraction

CCD monochrome camera, DMK 21AU04, Imaging Source, Bremen, Germany

Focal length extender ring 2×, Computar EX2C, Imaging Source, Bremen, Germany

IR filter, type 092, 46×0.75, Imaging Source, Bremen, Germany

IR LEDs 5 mm, Conrad, Hirschau, Germany

Lens, f = 50 mm, C5028-M(KP), Imaging Source, Bremen, Germany

Plastic holder for IR LEDs, workshop MPI of Neurobiology, Munich

2.1.7 Software

Brainware, version 8.12, Tucker-Davis, Alachua, USA

Colibri, TPLSM controlling software written in LabView (LMU Biocenter and MPI of Neurobiology, Munich)

Fluoview, Olympus, Tokyo, Japan

ImageJ, National Health Institute, USA, http://rsbweb.nih.gov/ij

   Including the plug-in „Register ROI", http://bij.isi.uu.nl

LabView, National Instruments, Austin, USA

Matlab, Mathworks, Natick, USA

Photorefraction, custom written software (Frank Schäffel, University Tübingen)

Psychophysics Toolbox, http://psychtoolbox.org

2.2 Methods

2.2.1 Solutions

2.2.1.1 *Artificial cerebral spinal fluid (ASCF)*

Substance	Molarity [mM]	Concentration [g l^{-1}]
NaCl	125	7.305
KCl	5	0.372
Glucose * H_2O	10	1.981
Hepes	10	2.383
$CaCl_2$ * 2 H_2O	2	0.294
$MgSO_4$ * 7 H_2O	2	0.492

The buffer was adjusted to pH 7.4 with 1 N NaOH and filtered sterile.

2.2.1.2 *Dye buffer*

Substance	Molarity [mM]	Concentration [g l^{-1}]
NaCl	150	8.766
KCl	2.5	0.186
Hepes	10	2.383

The buffer was adjusted to pH 7.4 with 1 N NaOH and filtered sterile.

2.2.1.3 *Infusion*

40 ml   glucose infusion solution (Sterofundin VG-5)

10 ml   Ringer's solution (Isotone 0.9%)

0.5 ml dexamethasone (4 mg ml^{-1})

1 ml   atropine (1 mg ml^{-1})

2.2.1.4 Dye preparation

The calcium indicator Oregon Green BAPTA-1 AM (OGB-1 AM, 50 μg) was mixed with 4.7 μl pluronic acid in dimethyl sulfoxide (DMSO) and vortexed for one minute. Then, 47 μl dye buffer (see above) were added to yield a final concentration of 0.76 mM OGB-1 AM. The solution was finally filtered sterile and kept on ice before usage.

2.2.2 Animal preparation and surgery

All animal experiments were performed in compliance with institutional guidelines and were approved by the local authorities (Regierung von Oberbayern).

Experiments were carried out on sable ferrets. Pregnant sable jills were obtained from Marshall Farms (North Rose, USA) 28 days after conception. The ferrets were reared under a twelve hour light-dark cycle. The day of birth was defined as postnatal day 0 (P0). Experiments were carried out on ferrets ranging in age between P19 and P179.

For surgery, ferrets were administered with atropine (0.05 mg kg^{-1}, intraperitoneally) and initial anaesthesia was induced with ketamine (25 mg kg^{-1}, intramuscularly) and either xylazine (1 mg kg^{-1}, intramuscularly) or acepromazine (0.2 mg kg^{-1}, intramuscularly) (Wixson 1999 p. 274ff; Williams 2000 p. 138). The animal was placed on a homoeothermic blanket to maintain its body temperature at 37.5°C. The tempera-
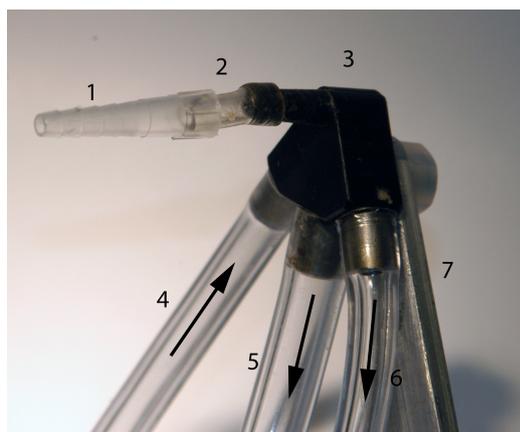
FIGURE 2-1: **Trachea cannula for artificial ventilation attached to manifold.**

1, trachea cannula (cut and fluted 20 μl pipette tip)

2, silicon tube

3, manifold

4, tube for inspiration

5, tube for expiration

6, tube for measuring exhaled CO_2 and pressure

7, post
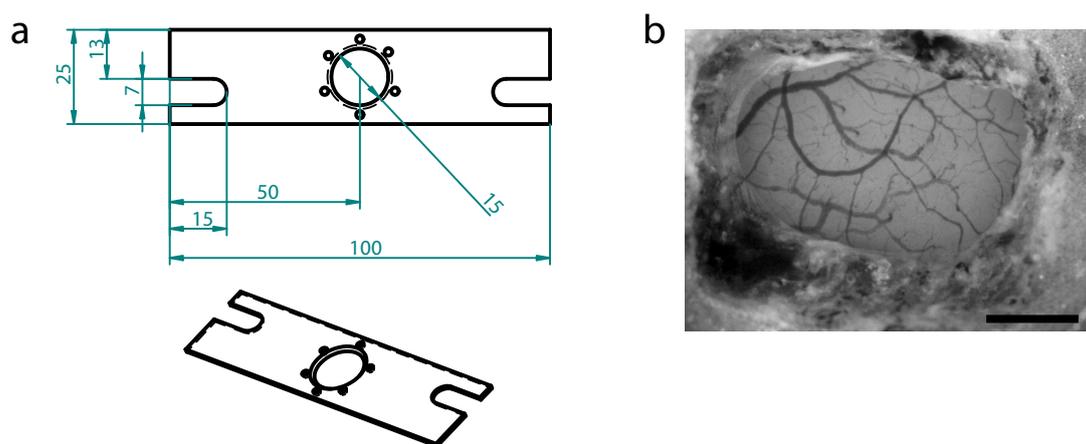
FIGURE 2-2: **Head mount design and craniotomy.**

> **a,** Custom-built head mount made of stainless steel (V4A). The bar is 1 mm thick. Numbers are dimensions in mm.

> **b,** Image of the exposed visual cortex with blood vessel pattern. The dura mater was reflected and is still visible at the edges of the craniotomy. Scale bar, 1 mm.

ture was closely monitored, since ferrets tend to become hypothermic during anaesthesia (Williams 2000 p. 137).

For mechanical ventilation via a tracheostomy, the hair over the cervical trachea was shaved, the skin was disinfected with iodine, a longitudinal skin incision was made and the muscles were retracted to expose the cervical trachea before a transverse intercartilaginous incision was performed. The tracheal cannula (**FIGURE 2-1**), a pipette tip fluted and cut to match the appropriate diameter of the trachea, was inserted and stabilized with tissue adhesive. The skin was sutured and the tracheal cannula was connected via a short silicon tube to the manifold (**FIGURE 2-1**). This custom-built manifold was particularly optimized to minimize mechanical dead space ventilation for small animals and to maximize unobstructed vision during visual stimulation.

Ventilation was controlled by an animal respirator (respiratory rate: 25–33 breaths min^{-1}; inspiratory time: 26–33% of a single stroke cycle), such that the expired CO_2 level was maintained at 3.8 to 4.2%. End-tidal CO_2 was monitored using a microCapStar analyser. Anaesthesia was maintained by halothane (1.0% during surgery, 0.2–1.0% during data acquisition) in a 3:1 mixture of N_2O and O_2. The electrocardiogram (EKG) (Zandvliet 2005) was recorded with two needle electrodes, inserted subcutaneously into the right shoulder and the left hind limb, and amplified with a custom-built preamplifier (MPI

workshop). The EKG was further processed and filtered with a Brownlee amplifier. The EKG signal, together with all other physiological parameters (end-tidal CO_2, O_2, N_2O, halothane, body temperature), were digitized with a data acquisition card (NI 6008), analysed online and saved to the computer's hard disk with a custom written programme (LabView). Atropine (0.02 mg ml^{-1}) and dexamethasone (0.04 mg ml^{-1}) were infused continuously in 5% dextrose in Ringer's solution (0.5–1.5 ml h^{-1}, subcutaneously).

A longitudinal incision on the dorsal midline of the skull along the rostro-caudal axis was carried out, the pericranium scraped off, the muscles retracted and the cranial bone abraded. For stabilization, the wound edges were sealed with tissue adhesive before the custom-built head mount (**Figure 2-2a**) was positioned with cyanoacrylate glue and finally fixated with dental cement. In some cases, a head mount with a larger borehole (10 mm) was used to access the visual cortex and the lateral geniculate nucleus (LGN) simultaneously. A craniotomy (2 × 2 mm) was performed over the visual cortex (**Figure 2-2b**), centred 7–9 mm lateral from the midline and 0–2 mm rostral of lambda (Krug *et al.* 2001), using a dental drill. For LGN recording experiments, an additional craniotomy was made 4–5 mm lateral from the midline and 8–9 mm rostral of lambda (Krug *et al.* 2001). Following the trepanation, the dura mater was gently opened with a hooked 27 gauge needle and fine forceps. In case of brain oedema, cerebral spinal fluid (CSF) was withdrawn from the *cisterna magna* through a spinal needle (Bonhoeffer *et al.* 1995).

Following dye loading, the cortex was stabilized with agar (2%, in ACSF) and a cover glass. To this end, hot, melted agarose was taken up with a 1 ml syringe, cooled down to body temperature, and a small drop was placed over the exposed cortex. Immediately thereafter, a clean cover glass was placed on top of the agarose, and pressure was applied with forceps until the agarose solidified to minimize the space between the cover glass and the cortical surface. To prevent light from the visual stimulus monitor entering the objective, a black cone was mounted above the head mount's borehole with dental cement containing black ink pigment. The cone also served as a reservoir for ACSF into which the water corrected objective dipped.

If necessary, the eye lids were surgically opened, nictitating membranes were retracted with neosynephrine eye drops, and pupils were dilated with atropine eye drops. The eyes were protected and kept moist by contact lenses (0 D).

2.2.3 Bolus loading

The calcium sensitive dye Oregon Green BAPTA-1 AM (OGB1 AM) was used for bolus loading of cortical neurons (Stosiek *et al.* 2003; Ohki *et al.* 2005). The dye solution was prepared freshly (**SECTION 2.2.1.4, PAGE 38**) to yield a final concentration of 0.76 mM and was injected under constant pressure with a glass micropipette (4–6 MΩ tip resistance, 0.4–0.55 bar, 60–90 s) inserted 350–450 μm into the cortex at an angle of 45 degrees to aim a depth of 250–350 μm below the cortical surface. Pipette resistance was monitored during the injection to detect clogging of the tip. In some experiments, the dye-loading procedure was carried out under visual control using an epi-fluorescence binocular (**FIGURE 2-3**). The resulting spherical bolus of stained tissue had a diameter of about 300 μm. In most ferrets, multiple dye injections were carried out.
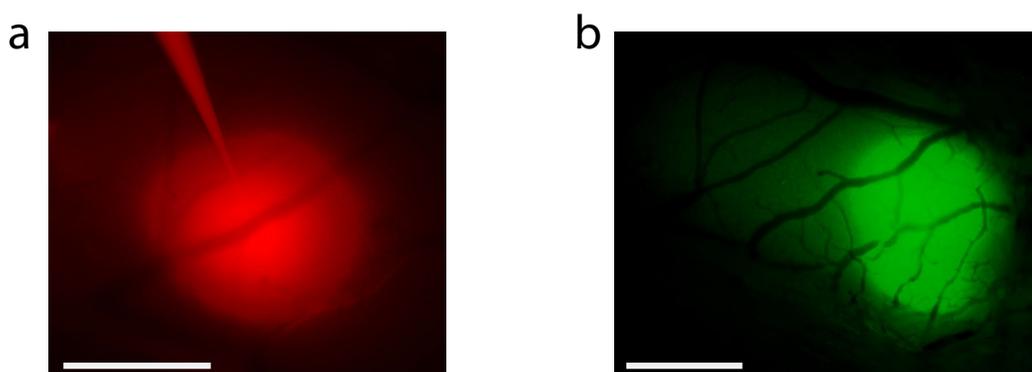
FIGURE 2-3: **Pressure injection of the calcium indicator Oregon Green BAPTA-1 AM under visual control.**
Visual inspection of the dye loading was achieved using a epi-fluorescence microscope during and after injection.

a, Since OGB BAPTA-1 AM is only marginally fluorescent before the uptake into neurons, the fluorescence dye Alexa 594 was co-injected to visualize diffusion of the solution in the cortex. The injection pipette is visible at the top. The image was acquired during pressure injection (excitation: BP 545/25; emission: BP 605/70). Scale bar, 100 μm.

b, Fluorescence wide field image of the cortex after a successful injection of OGB BAPTA-1 AM (excitation: BP 470/40; emission: BP 525/25). Scale bar, 1 mm.

2.2.4 Two-photon calcium imaging

A custom-built two-photon laser scanning microscope (TPLSM) was used to monitor the activity of cortical neurons by imaging fluorescence changes (Majewska *et al.* 2000; Tsai *et al.* 2002; Helmchen and Denk 2005). For the initial experiments, a custom-built microscope was used, equipped with a mode-locked Ti:Sapphire laser (Mai Tai) tuned to 830 nm (**Figure 1-1**). The intensity of the laser beam was attenuated by a Pockels cell and the size was adjusted by telescopes to match the size of the back aperture of a 40× water immersion objective. The scanning was accomplished by a Yanus I galvometric system operated in analog mode. Scanning control and image acquisition was conducted by Fluoview software. The emitted light from the sample was separated by a dichroic beamsplitter mirror (λ_{cut} = 585 nm with long-pass characteristics) and optically filtered (transmission filter 680 nm with short-pass characteristics) before it was collected by a photomultiplier tube. The resulting current was boosted by a current amplifier. The processed signals were read by a data acquisition card into the computer in order to reconstruct the images (350 × 350 μm, 256 or 512 pixel side length, frame rate 1 or 2 Hz) and store the data. At each injection site, data were obtained from several depths in layer 2/3 of the visual cortex, with a spacing of at least 22 μm.

For later experiments, I assembled a custom microscope with a few improvements. The illumination source was a mode-locked Ti:Sapphire laser with automated dispersion compensation (Mai Tai HP DeepSee). The added pre-compensation allows correcting dispersion of the optical setup in order to maximize fluorescence signals and decrease damage of the sample. Furthermore, two inch optics were used, shaping and guiding the beam, to minimize optical aberrations and to reduce neuropil contamination by beam expansion (Kerr and Denk 2008). The emitted light from the sample was separated by a dichroic filter and further split into two channels using a similar design to the movable objective microscope (MOM) (Sutter Instruments; W. Denk, personal communication). The following wavelength and emission filters were employed: 830 nm excitation light, 680 nm short-pass (Semrock) IR blocking filter, 535/50 18° reflection filter (OGB-1 AM) for green emission and 610/75 (SR101) for red emission (Chroma). Custom developed software (Colibri written in LabView) was used for microscope control and image acquisition.

2.2.5 Electrophysiology

Extracellular spikes in the visual cortex were recorded, usually following calcium imaging, using silicon electrode arrays placed at depths between 100 and 500 μm. Data collection and stimulus onset was controlled by the Pentusa multichannel processor and BrainWare software. Signals were sampled at 25 kHz and band-pass filtered, before action potentials were isolated automatically based on waveform and saved in BrainWare for offline analysis.

For LGN recordings, tungsten electrodes (1–2 MΩ) were inserted perpendicular to the cortical surface and about 5.5–7.5 mm deep into the brain (Krug *et al.* 2001). Since it is difficult to locate the LGN in juvenile ferrets based on stereotaxic coordinates alone, we relied on characteristic neuronal signals (audible on the audio monitor) to determine its position while first passing the hippocampus, a zone with high spontaneous firing rate, and then reaching a region with less spontaneous, but visually evoked activity. The tungsten electrodes were mounted in a similar way as the silicon electrode arrays and signals were processed with the same recording system (Tucker Davis). Prior to insertion, the electrodes were painted with red fluorescent 1,1'-dioctadecyl-3,3,3',3'- tetramethylindocarbocyanine perchlorate (DiI, 10% in ethanol) for later anatomical confirmation of the position of the electrode. DiI as lipophilic neuronal tracer is taken up by neurons next to the recording site (DiCarlo *et al.* 1996; Blanche *et al.* 2005).

2.2.6 Visual stimulation

All visual stimuli were programmed with Psychophysics Toolbox extensions (Brainard 1997; Pelli 1997) in Matlab and displayed on a 20 inch LCD monitor (60 Hz) mounted on a tripod at a distance of 25–30 cm. The angle of the monitor was adjusted according to the animal's head position.

For calcium imaging, square-wave grating stimuli (100% contrast, black white) were presented. Gratings were displayed in four or eight orientations, each moving in two directions (spacing spaced 45° or 22.5°). Each stimulus block consisted of a stationary grating (6600 ms) followed by a unidirectionally drifting grating of the same orientation (4300 ms, temporal frequency 1 Hz). The stationary grating was used as blank with identical mean luminance to record the baseline fluorescence. Spatial frequency of the gratings varied

between 0.025 and 0.25 cycles deg^{-1} depending on the age of the animal. The appropriate spatial frequency, evoking the strongest responses, was tested during an initial phase of the experiment. The complete stimulus sequence was repeated seven times. Stimulus order was serially clockwise in some earlier experiments, but randomly permuted in most experiments. Stimuli were presented in the central visual field and were delivered monocularly or binocularly.

For electrical recordings in the visual cortex and the LGN, the same stimuli were used, except that gratings were presented for shorter durations.

Overall retinotopy was mapped using square-wave drifting gratings with same spatial and temporal frequencies as described above. Stimulation was restricted to abutting patches (13° × 15°, 6 × 4 grid design or 20° × 20°, 4 × 3 grid design) which were displayed in a random manner at the different positions of the visual field (80° azimuth and 60° elevation). The gratings changed their orientation every 0.6 s randomly and each 4.8 s stimulus presentation at one position was followed by a blank screen for 5 s matching the same mean luminance. The whole stimulus sequence was repeated as least five times.

2.2.7 Photorefraction

Measurements of the refractive power were carried out by an eccentric infrared photorefractor (Schaeffel *et al.* 1987; Choi *et al.* 2000). Briefly, the eccentric photorefractor operates as follows: Light, emitted from a light source (infrared LEDs) located on a ring of the camera lens, generates a reflection (bright spot) on the retina and is captured by the sensor of the camera (**Figure 2-4**). In case of normal refraction, the image of the pupil is evenly illuminated without any gradient in the intensity distribution. If the eye is focussed close (myopia), the reflected light diverges behind the plane of focus and is partly blocked by the aperture in front of the camera resulting in an intensity gradient (**Figure 2-4b**). Conversely, the intensity distribution is inverted if the eye is hyperopic. Through the use of several infrared LEDs, the intensity gradient can be fitted by linear regression. The slope of the linear regression in turn is linearly related to the refractive power which can be quantified after calibration with trial lenses. The software automatically recognized the pupil and determined its diameter and the average refractive power of the eye.
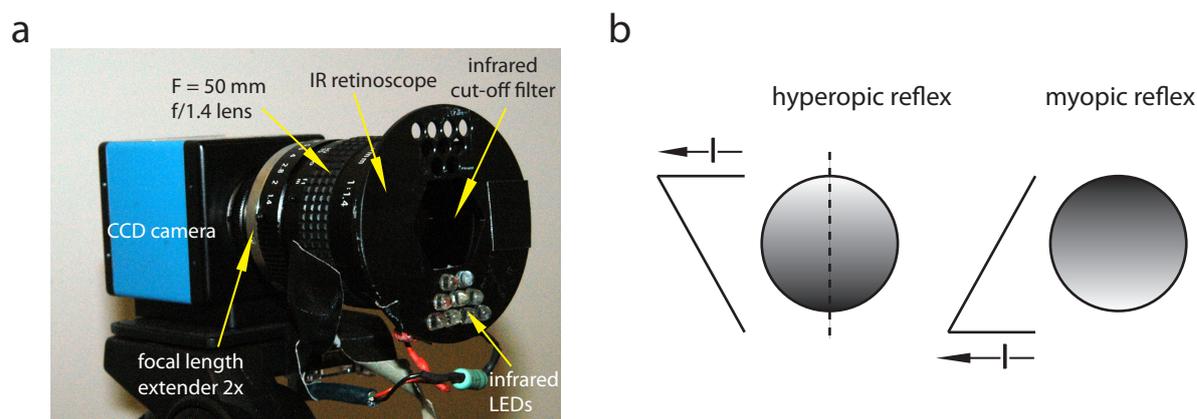
FIGURE 2-4: Measurement of the refractive power.

a, Arrangement of an eccentric photorefractor based on a design by Schaeffel *et al.* (1987).

b, Intensity distribution or reflex that appears in the pupil. The reflex fills the pupil and the slope of the intensity profile is used to deduce the refractive state. The line to the left of each pupil shows the intensity profile across the vertical meridian of the pupil (shown by the dashed line). As the refractive state augments in either direction, the slope of the intensity profile increases.

2.2.8 Data analysis

Imaging data were analysed with custom software programmed in Matlab and ImageJ based on software used by Ohki *et al.* (2005, 2006).

2.2.8.1 Pre-processing of imaging data

First, time-lapse movies of cortical neurons labelled with OGB-1 AM were inspected visually. Data were discarded if drift in the z-axis was observed. To correct for lateral drift and motion, typically on the order of a few pixels, time-lapse images were realigned by maximizing the cross-correlation between frames using an ImageJ plug-in ("Register ROI"). Following alignment, a set of morphological filters (Ohki *et al.* 2005; Ohki *et al.* 2006), delineating the contours of the cell somata based on intensity, size and shape, was applied to the average image of each set of time-lapse images to identify regions of interest (ROIs).

2.2.8.2 Determination of tuning properties

For each neuron identified, the fluorescence time course signal of the cell was obtained by averaging the signals of all pixels contained in the ROI. Fluorescence time courses $\Delta F/F_0$ were normalized relative to the baseline fluorescence level F_0, recorded during the stationary phase of the stimulus, either for each pixel or for each identified cell. Slow drift of the baseline signal over minutes was removed by a low-cut filter (cut-off, 2–4 min). Cells were defined to be "visually responsive" if $P < 0.01$ for one-way analysis of variance (one-way ANOVA) across responses to the blank and to all N stimuli presented, which evenly spanned the orientation space. Visually responsive cells were defined to be "orientation selective" if $P < 0.01$ for one-way ANOVA across responses to all N stimuli. A normalized response of magnitude $r \in [0,1]$ to a stimulus with orientation θ was encoded as a polar response vector, $R_\theta = (r, \theta)$. $\theta = 0^\circ$ corresponded to a horizontally oriented stimulus, with θ increasing as stimulus orientation rotated counter-clockwise. Stimulus orientations were identified modulo 180°. Orientation preference, $\overline{\theta}$, was calculated as the angle of the vector average, $\overline{R}$, of the response vectors, R_θ, corresponding to all N stimuli presented (Bonhoeffer *et al.* 1995):

$$\overline{R} = (\overline{r}/\overline{\theta}) = \frac{1}{N}\sum_1^N R_\theta$$

As a measure for selectivity, an orientation selectivity index (OSI) value was calculated as the magnitude of the average response vector, $\overline{R}$, normalized by the sum of all response magnitudes, r, corresponding to all N stimuli (Thibos and Levick 1985; Wörgötter and Eysel 1987; Chapman and Stryker 1993):

$$OSI = \frac{|\overline{R}|}{\sum_1^N r}$$

A value between 0 and 1 is assigned – high values indicate strong orientation tuning, whereas a value of 0 denotes the lack of any orientation tuning. Orientation selective cells were examined to obtain a distribution of orientation preferences and a distribution of OSI values for each orientation map. Throughout, the term "map" refers to the set of cells z-projected from usually three cortical depths up to typically 400 µm below a single region on

the cortical surface. Probability distributions were obtained by normalizing by the number of orientation selective cells. Average probability distributions for orientation preference were compared using circular variance (CV; see below). Once probability distributions had been categorized by functional organization and age, probability distributions were also compared across categories by mixed-model ANOVA using SPSS 16.0.

When OSI or the proportion of non-selective, but responsive, cells was plotted as a function of postnatal day or body weight, trend lines serving as a visual guide were generated by local regression using weighted linear least-squares and a 1st degree polynomial model. To increase the robustness of the regression, no weight was assigned to data outside six mean absolute deviations.

The CV of orientation preferences $\theta_1, \ldots, \theta_n$ was calculated as the magnitude of the average response vector when all orientation preferences were assigned equal response magnitude, arbitrarily 1 (Mardia 1972; Batschelet 1981). The result was then subtracted from 1 so that the minimum CV, 0, would indicate that all orientation preferences $\theta_1, \ldots, \theta_n$ are the same, while the maximum CV, 1, would indicate a uniform distribution of orientation preferences:

$$CV = 1 - \frac{\left| \sum_{1}^{n} (1, \theta_i) \right|}{\sum_{1}^{n} 1} = 1 - \frac{1}{n} \left| \sum_{i=1}^{n} (1, \theta_i) \right|$$

Accordingly, we calculated CV to quantify the width of any distribution of orientation preferences. For average probability distributions (**Figures 3-3e, 3-6g, 3-10e**) as well as for one-day bins (**Figure 3-12c**), each region on the cortical surface was weighted equally in the calculation of CV. To ensure adequate sampling, we discarded one-day bins if they included orientation maps from less than three regions. CV time series were analysed by one-way ANOVA across orientation map categories with *post hoc* Tukey's tests using a *P = 0.01* significance level.

2.2.8.3   Calculation of maps

The calculated functional properties were displayed in various maps. Regions of interests were colour-coded for their preferred orientation in maps for visually responsive cells (e. g. **Figure 3-2f**), where e. g. 0° (horizontal preference) corresponds to blue and 90° (vertical)

is encoded by yellow (**Figure 3-2c** colour-legend, **Figure 2-5**). In these cell-based maps, only visually responsive cells were considered and overlaid on the anatomical image.

For pixel-based analysis, images were averaged over stimulus repetitions, and spatially smoothed (Gaussian, σ = 1 μm). Single condition maps (**Figure 3-2b**) were obtained by subtracting images during the stationary (blank) period from images during which one of the orientations was drifting. Functional pixel maps were calculated as so-called "hue-lightness-saturation maps" (HLS maps) (e. g. **Figure 3-2c**). This type of map displays simultaneously three values: (1) preferred orientation, (2) overall response strength, and (3) orientation tuning (Ts'o *et al.* 1990; Bonhoeffer and Grinvald 1993, 1996). The colour (hue) encodes the orientation preference and the overall response magnitude at each pixel (i. e., the response of one particular site summed over all orientations) is represented by colour intensity (lightness). And last, the quality of the orientation tuning (calculated as OSI) is encoded by the colour saturation (the worse the tuning the less saturated, i. e., the "whiter" the colour). The HLS pixel maps were clipped at OSI = 0.5 for better presentation. The relationship of hue, lightness and saturation as representation of the three functional properties is illustrated in **Figure 2-5**.

For depth-projected cell-based maps, the same HLS colour coding was employed.

2.2.8.4 *Analysis of fine scale functional organization*

Fine scale functional organization was assessed in each orientation map by comparing the functional similarity of anatomically proximal cells to the functional similarity of anatomically distant cells. For each pair of orientation selective cells with ROIs with centres of gravity at $p_1 = (x_1, y_1)$ and $p_2 = (x_2, y_2)$, the anatomic distance separating the cells $d = (p_1, p_2)$ was calculated as the Euclidean distance:

$$d = (p_1, p_2) = |p_1 - p_2| = \sqrt{(x_1 - x_2)^2 + (y_1 - y_2)^2}$$

"Nearby" cells were defined to be within 20 μm of one another. "Distant" cells were defined to be separated by 100–120 μm. The functional difference, $f = (\theta_1, \theta_2)$, between orientation preferences θ_1 and θ_2 was calculated as the smaller of the two angles determined by lines extended from the vectors $(1, \theta_1)$ and $(1, \theta_2)$:
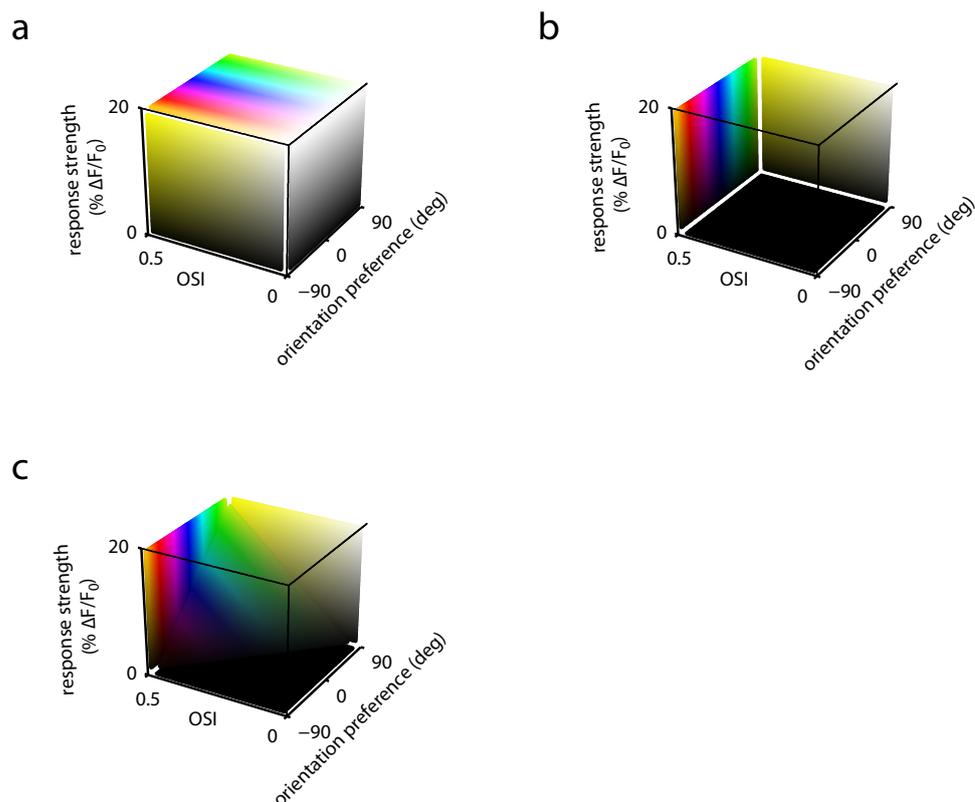
FIGURE 2-5: **Representation of hue-luminance-saturation (HLS) coding-space in three dimensions as a rectangular prism.**

> **a,** View of near-side surfaces of the coding space. On the top face, response strength is constant at its maximum, while orientation preference and orientation selectivity index (OSI) vary. On the left face, orientation preference is constant at 90°, while response strength and OSI vary. On the right face, OSI is constant at its minimum, while response strength varies.
>
> **b,** View of far-side surfaces of the coding space. Near-side surfaces and interior points have been removed. On the left face, OSI is constant at its maximum, while orientation preference and response strength vary. On the right face, orientation preference is constant at 90°, while response strength and OSI vary.
>
> **c,** HLS coding on a plane through the interior of the HLS coding-space. In this plane, orientation preference, response strength, and OSI vary simultaneously. Planes from **b** are reproduced here for reference.

$$f(\theta_1, \theta_2) = \min(|\theta_1 - \theta_2|, 180 - |\theta_1 - \theta_2|)$$

Thus, for *n* orientation selective cells in a given orientation map, *n(n−1)* pairs *(d, f)* were obtained. The mean functional distance between nearby cells was calculated by selecting all such pairs for which $0 < d \leq 20$, in μm, and taking the mean of the respective *f* values. The mean functional distance between distant cells was calculated in the same manner, except for pairs for which $100 < d \leq 120$, in μm. This calculation was further carried out for all consecutive 20 μm bins out to a distance of 300 μm. Finally, mean functional distances between cells were compared (1) across orientation map categories by one-way ANOVA and (2) between anatomic distance bins by Mann-Whitney U test.

The true orientation preference of a neuron is estimated from its visually evoked responses, but visually evoked responses are contaminated by spontaneous activity and other sources of random noise, all of which spuriously cause the estimated orientation preference to deviate from the true orientation preference. For this reason, the estimation of orientation preference is more accurate for neurons with high OSI values.

Consequently, we analysed fine scale functional organization using subsets of orientation selective cells chosen using OSI-based criteria. First, cells were selected for analysis using a criterion of OSI ≥ 0.275, which was approximately the OSI value at which cells began to fail to respond to at least one out of eight stimulus orientations (**Figure 3-3B**). This criterion thus enforced a slightly stronger definition of orientation selectivity than our standard statistical criterion based on one-way ANOVA. Second, cells were selected from OSI value intervals of width 0.1 to ensure that the distribution of OSI values was approximately the same across orientation map categories, which without this type of selection criterion exhibited significantly different distributions of OSI values (e. g. **Figure 3-3F**). Our interpretations of the data were robust to these variations in our analysis of fine scale functional organization. In **Figure 3-12**, we present our results for the criterion 0.25 ≤ OSI ≤ 0.45.

2.2.8.5   *Analysis of electrophysiological recordings*

Single-units were isolated by delineating clusters of action potentials manually in Brainware. Action potential waveforms were selected by their metrics like total amplitude,

amplitude of the 1st and 2nd peak, and area under the spike in the feature space. Action potentials from a single-unit were examined for uniformity and to have very similar shapes. A refractory period of ≥ 2 ms seen in the autocorrelogram was used as an additional criterion for a putative single-unit. Spike times of multi- and single-units were exported from Brainware and then further analysed with software programmed in Matlab. The activity of each neuron was normalized to the average firing rate of the period before stimulation onset. Functional properties of single- and multi-units were calculated in the same way as for the calcium imaging data.

2.2.8.6 *Estimation of the modulation transfer function*

The contrast transfer for a presented stimulus of a certain spatial frequency (SF) is described by the modulation transfer function:

$$MTF_{SF} = \frac{modulation(in)}{modulation(out)}$$

where modulation (in) is the contrast of the grating displayed and modulation (out) is the contrast of the grating on the retina. Neglecting effects of diffraction, the geometrical MTF can be calculated as follows (Smith 2008; Bass *et al.* 2010):

$$MTF_{SF} = \frac{2J_1(\pi\beta SF)}{\pi\beta SF}$$

where SF is the spatial frequency in cycles deg^{-1} and J_1 is the first-order Bessel function of the first kind. With large focusing errors, the point spread function of the defocus can be assumed as a uniform blur circle (Bass *et al.* 2010). The angular diameter β of this retinal blur circle for a pupil diameter p in mm and defocus D in dioptres is:

$$\beta = \frac{0.18pD}{\pi}\deg$$

which was also experimentally demonstrated as a good predictor for pupils between 2 and 6 mm in diameter and a defocus of 1 and 12 D (Chan *et al.* 1985).

The different MTFs in **Figure 3-18c** were then computed in Matlab taking a pupil diameter p = 2.8 mm into account as measured for young ferrets.

Results

3.1 Calcium imaging at single cell resolution in ferret visual cortex

We initially carried out two-photon calcium imaging in adult ferrets in order to establish the method for very young animals, and since we wanted to study the fine-scale functional architecture of orientation preference in mature ferrets. Pressure injection of the calcium indicator Oregon Green BAPTA-1 acetoxymethyl ester (OGB-1 AM) into the primary visual
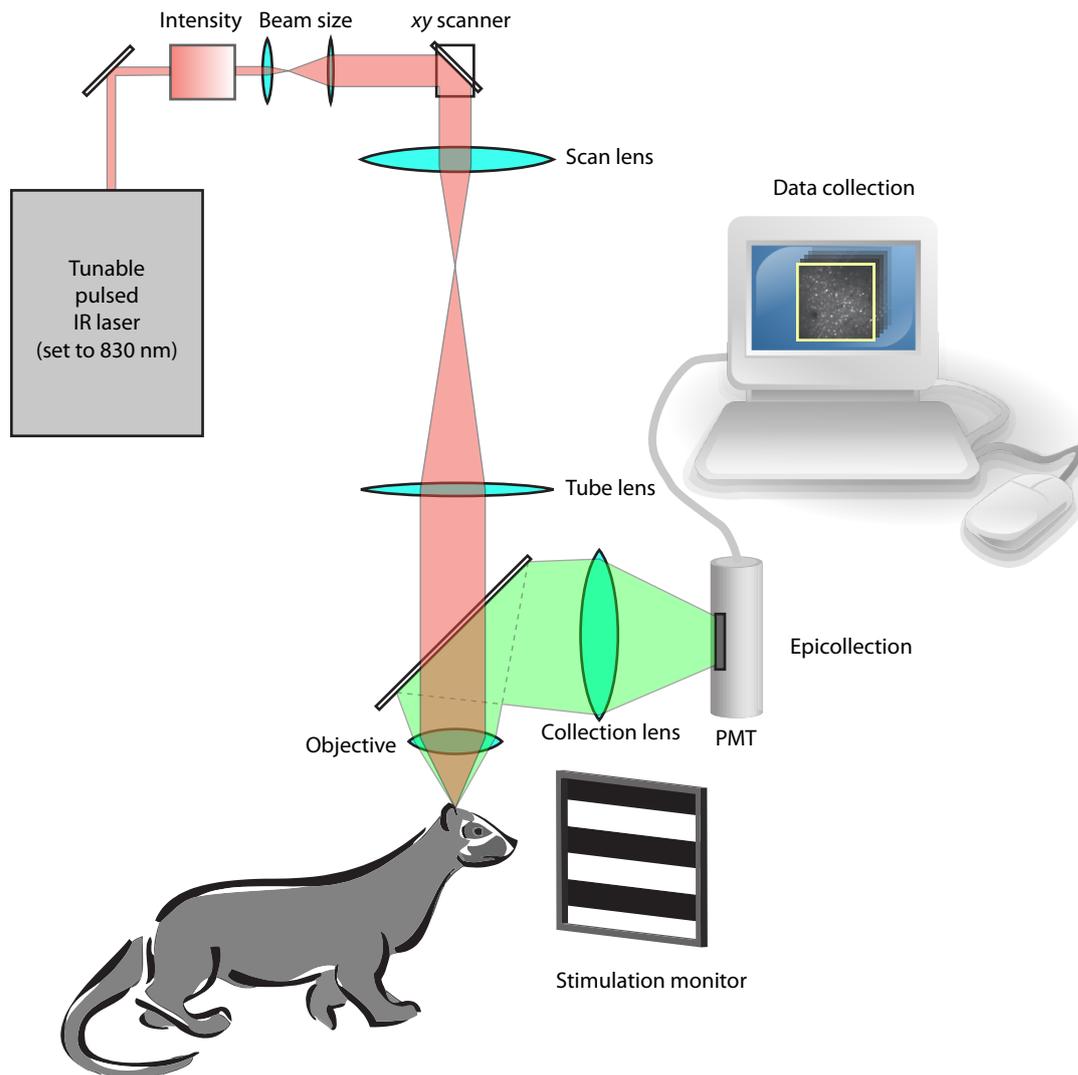
FIGURE 3-1: **Experimental setup for *in vivo* two-photon calcium imaging.**
The schematic displays the optical pathways for excitation (red) and emission (green) of a custom-built two-photon microscope. Moving grating stimuli were presented binocularly to the anaesthetized ferret and by this, evoked orientation specific responses in neurons in the primary visual cortex.

cortex yielded a bolus of labelled cells (**FIGURE 3-1**; Stosiek *et al.* 2003; Ohki *et al.* 2006). The injection was adjusted to give a bolus with a size of approximately 300–400 µm in diameter. The calcium indicator was taken up by the cells within an hour and typically stained thousands of neurons. Two-photon calcium imaging then allowed us to record simultaneously from 20–100 labelled cells within a given optical section running parallel to the cortical surface. Fluorescence changes (ΔF/F) of the calcium indicator in neuronal cell

bodies and the surrounding neuropil were evoked by visual stimuli consisting of moving, square wave gratings presented at different orientations (**Figure 3-1**).

We found that many neurons in ferrets older than six weeks responded to moving grating stimuli, and a large fraction of these showed preference for a particular orientation (**Figures 3-2** and **3-3**). The orientation preference and tuning of individual neurons is best illustrated by the time course of the calcium signals. Calcium responses were usually very reliably locked to the stimulus over several repetitions, and they were thus averaged to compute the mean signal (**Figure 3-2h**, **Figure 3-3b**). This allowed us to construct orientation maps which reveal the orientation preference and tuning width for each cell or pixel (Bonhoeffer *et al.* 1995) in the imaged region, typically 350 × 350 μm large (**Figure 3-2c-g**; **Figure 3-3a, c-d**). From these maps, we derive that orientation selective neurons in juvenile and adult ferrets are arranged in an orderly fashion in a pinwheel-like pattern (Bonhoeffer and Grinvald 1991), with orientation preference changing smoothly around the pinwheel centre without much scatter across the cortical surface. There was virtually no mixing of cells with different orientation preferences, even close to pinwheel centres (**Figure 3-2f**, **Figure 3-3a**). This became particularly evident when cells from optical sections obtained at five different depths in the same cortical region were superimposed (**Figure 3-3c**). The orientation preference maps, we observed in juvenile and adult ferrets, were mature and matched on a fine scale the maps that have been obtained in kittens (Ohki *et al.* 2006). They were also very similar to the maps from a recent study carried out in ferrets (Schummers *et al.* 2008).

In ten juvenile ferrets (aged P35 to P44), we extracted altogether 12,714 cells from 24 stained regions. At each region, cells were usually sampled from three to five depths in layer 2/3 of ferret primary visual cortex. Statistical analysis (ANOVA across blank and all direction periods, $P < 0.01$) revealed that on average 57.3% ± 4.0% (mean ± s. e. m.) of the labelled cells were visually responsive. Of those, 81.0% were selective for orientation (ANOVA across all direction periods, $P < 0.01$), a value, very close to that found in young cats (Ohki *et al.* 2006). As a quantitative measure for the degree of orientation selectivity, we calculated the orientation selectivity index (OSI) for each selectively responding cell (**Methods 2.2.8.2, page 46**). The minimum OSI value, 0, corresponds to the absence of orientation selectivity, while the maximum, 1, corresponds to exclusive preference for
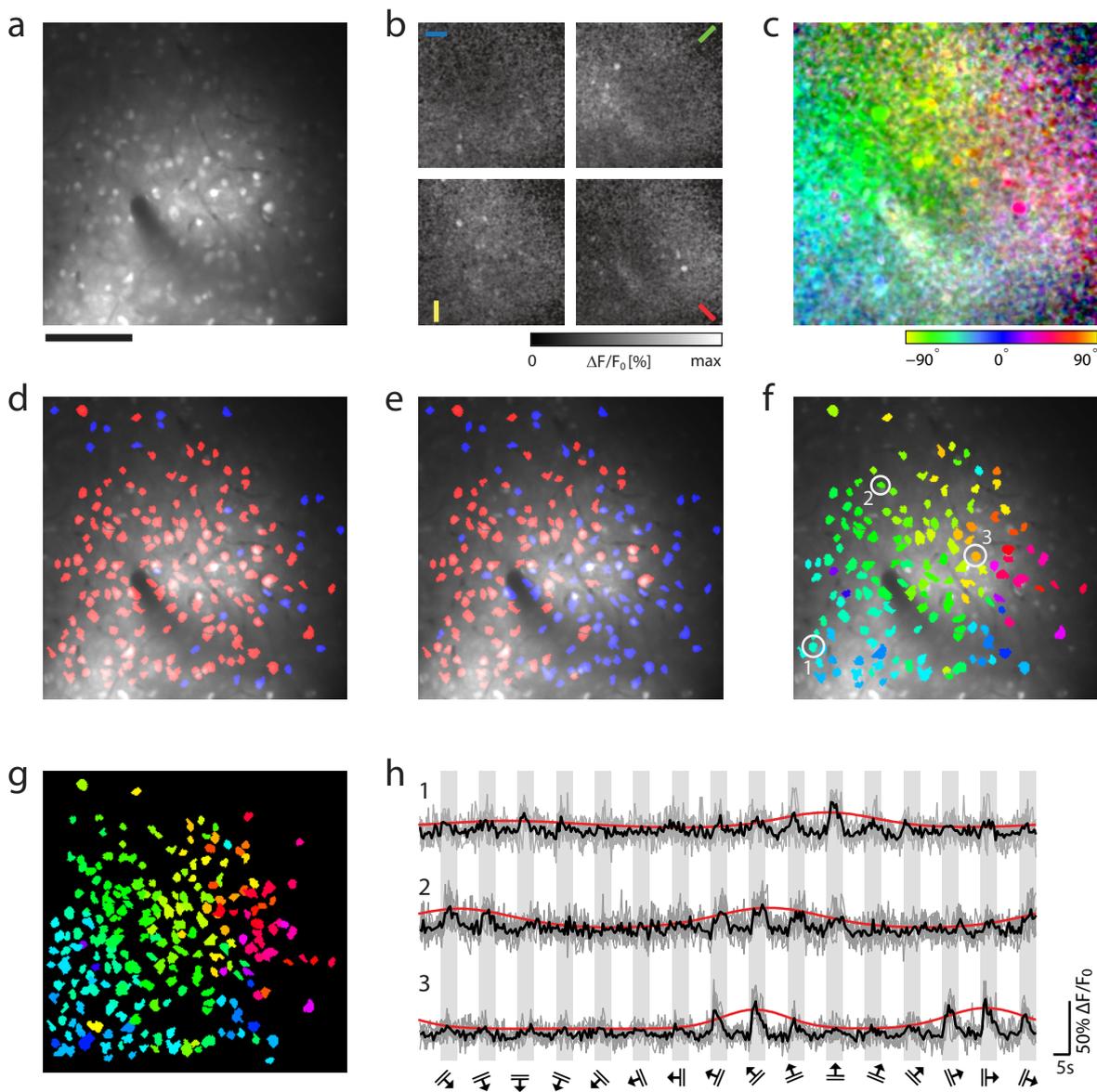
FIGURE 3-2: **Two-photon calcium imaging of orientation preference in mature ferret primary visual cortex.**

a, Cortical cells *in vivo* stained with the calcium indicator OGB-1 AM. The image is the motion corrected average of all 2,576 frames recorded during the visual stimulation protocol. Data were recorded in a P179 animal, 191 μm below the cortical surface. Scale bar, 100 μm.

b, Single-condition maps (quarter scale) calculated pixel-wise for the orientations indicated by the coloured bars in each map.

c, Colour-coded orientation preference map calculated pixel-wise as a hue-lightness-saturation (HLS) map. Hue codes for preferred orientation according to the

legend at the bottom, lightness for response strength, and saturation for tuning width (**Methods 2.2.8.3, page 47**). This example demonstrates the overall functional architecture of the orientation preference map, with iso-orientation domains arranged around a pinwheel centre. The relative high level of saturation illustrates the strong tuning of cells and neuropil, even at the pinwheel centre.

d, Cell-based categorization of visual responsiveness. Cells were extracted by a set of morphological filters, overlaid onto the average image (**a**) and coloured as visually responsive in red (ANOVA across blank and all 16 directions, *P < 0.01*) whereas blue indicate the absence of responsiveness.

e, Cell-based categorization of orientation selectivity. Selective cells (ANOVA across all 16 directions, *P < 0.01*) were overlaid in red. Cells labelled in blue indicate absence of selectivity, partly due to non-responsiveness as shown in **d**.

f, Cell-based orientation preference map for all visually responsive cells. The colour encodes the preferred orientation as indicated by the legend in **c**.

g, Depth-projected orientation preference map over two depths (191 μm and 260 μm), clearly demonstrating the columnar organization of orientation preference. Another example with tighter spacing is shown in **Figure 3-3c**.

h, Fluorescence time courses of representative cells indicated in **f**. The grey bars indicate the periods of visual stimulation consisting of oriented gratings drifting in 16 directions, interspersed with standing gratings of the following orientation in the sequence. Stimuli were presented in a pseudorandom manner and were shuffled into clockwise order for presentation. Light traces represent single trials, heavy traces show average responses over seven repetitions. Red traces are orientation tuning curves fitted with the sum of two circular Gaussian functions to the peak responses (Swindale *et al.* 2003).

a single orientation. The distribution of orientation tuning, calculated as OSI, is shown in **Figure 3-3f**. The mean OSI value of 0.51 reflects the high degree of orientation selectivity also seen in individual examples (**Figure 3-3b**), and is also in agreement with previous electrophysiological studies (Chapman and Stryker 1993; Chapman *et al.* 1996).

Intrinsic signal imaging, used in earlier studies, does not allow examining the development of orientation preference maps at single cell resolution (Chapman *et al.* 1996; Chapman and Bonhoeffer 1998). As shown above, two-photon calcium imaging overcomes this limitation in spatial resolution, allowing us to study the orientation preference, tuning and response strength of individual neurons at multiple depths below the cortical surface, as well as visualizing the spatial arrangement of iso-orientation domains and pinwheels.
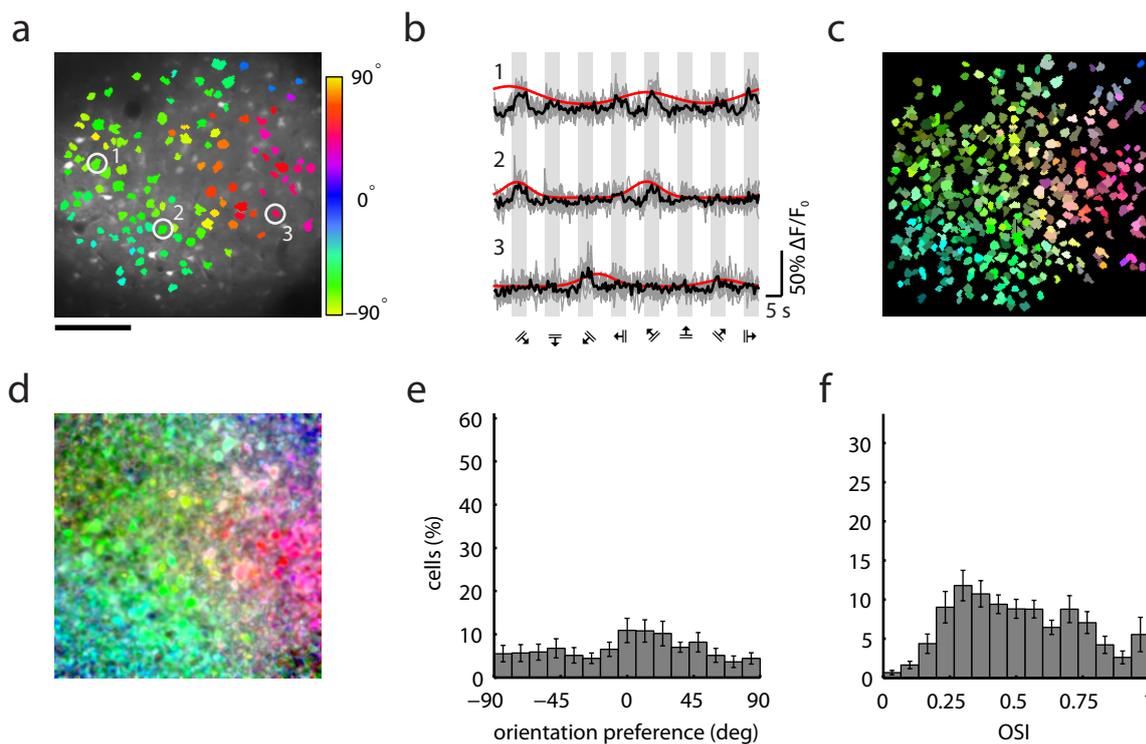
FIGURE 3-3: **Orientation preference and tuning in juvenile ferrets between P35 and P44.**

a, Visually responsive cells overlaid on the anatomical image and colour-coded for preferred orientation. Data were imaged in a P43 ferret at a depth of 191 μm below the cortical surface. Scale bar, 100 μm.

b, Fluorescence time courses of representative cells indicated in a. Tuning curves in red. Same conventions as in **FIGURE 3-2H**.

c, Depth-projected orientation preference map (5 depths, from 135–304 μm with a spacing of 33.75 μm).

d, HLS colour-coded orientation preference map calculated pixel-wise. Conventions as in **FIGURE 3-2C**.

e, Mean distribution of orientation preference (n = 24 regions, including 6,350 orientation selective cells from 10 ferrets). Error bars indicate the standard error of the mean (s. e. m.).

f, Mean distribution of orientation selectivity index (OSI). An OSI value of 0 indicates the absence of orientation tuning whereas the maximum value of 1 indicates perfect tuning. Error bars indicate s. e. m.

3.2 Confirmation of calcium imaging data with extracellular recordings

In vivo two-photon calcium imaging uses changes in intracellular calcium concentration to assess the functional properties of neurons in the visual cortex. Several studies have shown that intracellular calcium reliably indicates the firing of action potentials by neurons under a variety of experimental conditions (Smetters *et al.* 1999; Mao *et al.* 2001). In turn, subthreshold activity does generally not lead to calcium transients in neuronal cell bodies (Smetters *et al.* 1999; Mao *et al.* 2001; Stosiek *et al.* 2003). To address the relationship between electrical activity and calcium signals in juvenile ferrets, we carried out extracellular electrical recordings in some ferrets which we had imaged before. Recordings were made from up to four penetrations per animal, using a multi-channel silicon probe allowing to record from 16 sites simultaneously.

We recorded electrical multi-unit activity from three animals (P35, P39, P71) with mature orientation preference maps (**Figure 3-4a, e**). In the upper layers, over 80% of all units were orientation selective (ANOVA; *P < 0.01*; **Figure 3-4f**), a value comparable to our imaging experiments. The degree of selectivity was lower (median OSI = 0.29; *n* = 101 multi-units) than for imaged cells, most likely because multi-unit data reflects the activity of many neurons with different orientation preferences. Another potential sampling bias of electrical recordings becomes evident when analysing the distributions of orientation preference (**Figure 3-4e, f**). The bias results in a non-uniform distribution of orientation preference and apparently reflects the lack of equidistant probing of mature orientation preference maps characterized by iso-orientation domains and pinwheels. However, examples of single-units (**Figure 3-4a**), which were manually isolated, showed tuning curves very similar to those from individual imaged neurons.

In summary, our electrical recordings demonstrate that two-photon calcium imaging is a reliable method for studying the spatial layout of orientation preference maps.
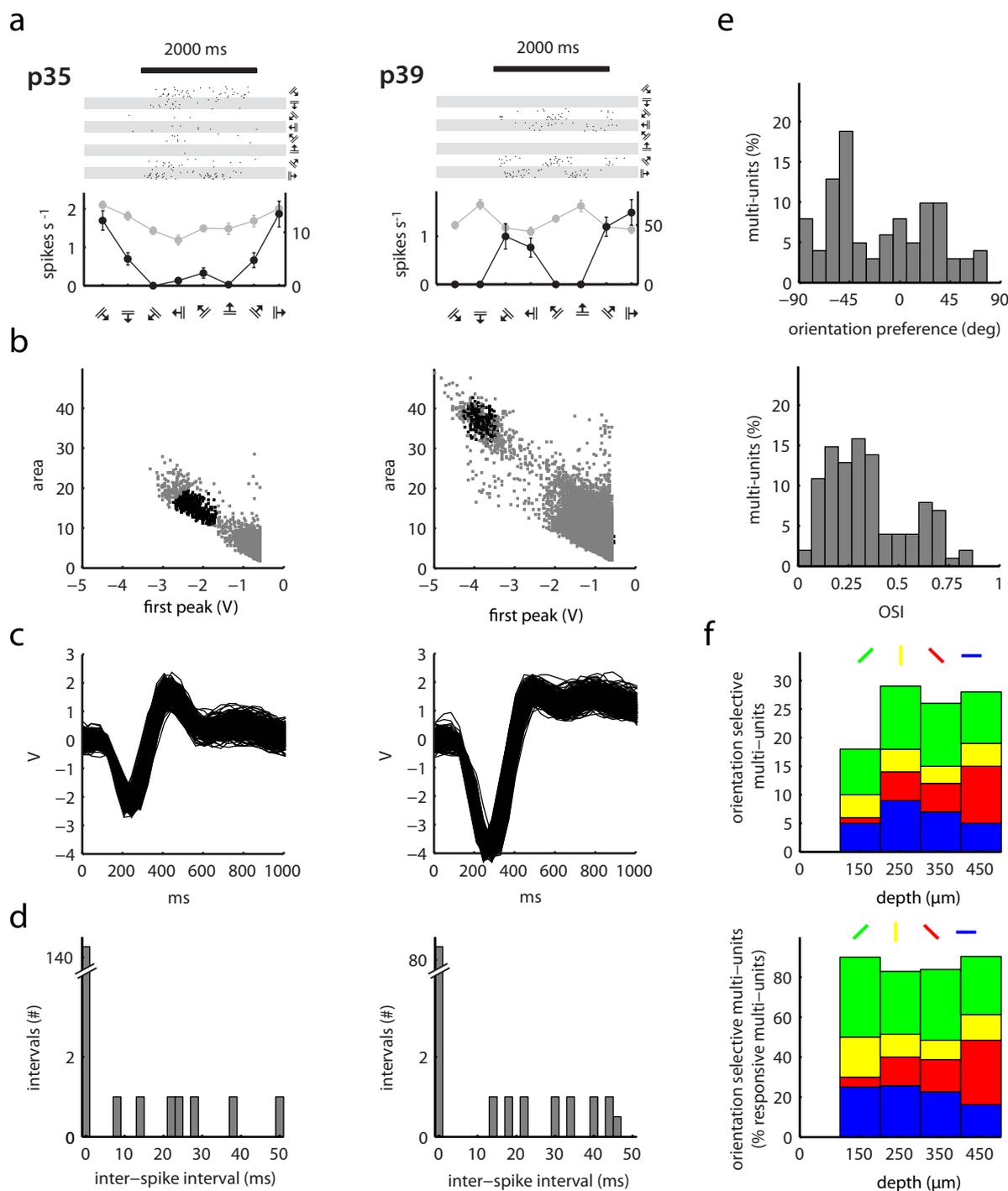
FIGURE 3-4: **Orientation tuning of electrically recorded multi- and single-units.**
a, Spike rasters (top) and tuning curves (bottom, black) of example single-units isolated from their respective multi-units from two animals (age indicated at the left). The bars above the spike raster plots indicate the period of visual stimulation. The 15 sweeps are grouped by stimulus orientation, starting with −45° and proceeding from bottom to top in 22.5° clockwise steps as indicated by the stimulus symbols and alternating white and grey bars. The tuning curves of

the respective multi-units (bottom) are shown in grey. Left- and right-hand ordinates indicate multi- and single-unit average firing rates above baseline, respectively. Error bars, s. e. m.

b, Representative feature spaces used in cluster cutting to identify spikes generated by a single neuron. Black dots indicate spikes assigned to the putative single unit, grey dots are unassigned spikes. Clusters may appear incomplete because clustering was performed in multiple arbitrary feature spaces.

c, Spike waveforms of the two isolated single-units in **b**. Amplifier gain was 29,000.

d, Auto-correlation histograms of spike trains of the respective single-units. Here, the histograms are used to test the "purity" of a cluster. Due to the refractory period in the firing of a given neuron, the auto-correlation histogram should show a paucity of at least 2 ms intervals. If there is no sharp dip at the first bin, the cluster probably does not reflect single-unit activity but contains spikes from several neurons.

e, Distribution of orientation preference (top) and OSI values (bottom) of electrically recorded multi-units (101 multi-units from 10 penetrations in three ferrets).

f, Preferred orientations were grouped into bins centred on the cardinal and oblique orientations and plotted as a function of depth below the cortical surface for ferrets with full orientation maps. Proportions of multi-units by depth (top) and cumulative proportion of visually responsive multi-units that were orientation selective as a function of depth (bottom).

3.3 Spontaneous activity in early ferret visual cortex

Having established two-photon calcium imaging in ferret visual cortex, we explored the period during which the first visually evoked signals could be detected in very young animals. Overall, this early period of development was characterized by a preponderance of spontaneous neuronal activity over visually evoked responses. Since spontaneous activity, in particular retinal and cortical waves, might be important for the initial development of orientation preference maps (Chiu and Weliky 2001, 2002; Cang *et al.* 2005; Huberman *et al.* 2008; Colonnese and Khazipov 2010), I will first describe the spatiotemporal structure of spontaneous calcium signals in very young and also in older ferrets.

We recorded spontaneous activity in 14 animals (P19–P35) in total. In all cases, we first recorded spontaneous activity without stimulus presentation and later tried to evoke activity with visual stimulation. In ferrets younger than P21, we consistently failed

to evoke activity by visual stimulation despite using a wide range of stimulus parameters. We did, however, observe spontaneous activity in such young ferrets. The youngest age at which we were able to perform stable imaging of calcium signals was P19. In this ferret and in a P23 animal, we observed spontaneous activity, but no visually evoked responses (**Figure 3-5**). This allowed us to determine the onset of visually evoked activity at around ten days prior to eye-opening (P31). This is in agreement to earlier electrophysiological studies showing that visually evoked activity did not occur before P18 in the LGN and visual cortex of the ferret (Krug *et al.* 2001; Akerman *et al.* 2002).

We first quantified spontaneous events in both animals in which visual stimulation did not evoke any activity (**Figure 3-5**). By this, we noted that it was consistently more difficult to stain the tissue in these very young animals in order to obtain a high contrast between individual cell somata and the neuropil (**Figure 3-5a, d**). However, it was possible to extract cell bodies from the surrounding background at depths up to 145 μm. We then determined the levels of activity by automatically detecting all events being two standard deviations above baseline and peaks had to be at least three frames apart. In these two young animals (P19, P23), the mean rate of spontaneous events was 0.042 Hz ± 0.0048 Hz (mean ± s. e. m.). The calcium responses tended to occur in bursts with occasionally very large events ($\Delta F/F > 50\%$) lasting several seconds and exhibiting generally long quiescence between those (**Figure 3-5b, e**). Furthermore, the spontaneous activity of neurons was not spatially clustered or restricted to certain areas within the labelled region. The activity was rather global and synchronised between cells. But other than synchronous global activity, we did not detect any patterned activity such as propagating waves (Colonnese and Khazipov 2010) or spatial restricted bursts of spontaneous activity (Chiu and Weliky 2001), reported previously in mice and ferrets during the development prior to eye opening. We would have been able to detect cortical waves which travel in the order of seconds, even with our relative slow scan rates (1–2 Hz). However, the absence of these events is not surprising, since these slow activity transients were usually only present in non-anaesthetized animals (Chiu and Weliky 2001; Colonnese and Khazipov 2010).

We next quantified the levels of spontaneous activity in 12 animals (P22–P35) which showed visually evoked activity. Before presenting any visual stimuli by the monitor, we recorded spontaneous activity in those animals. Spontaneous events in individual neurons
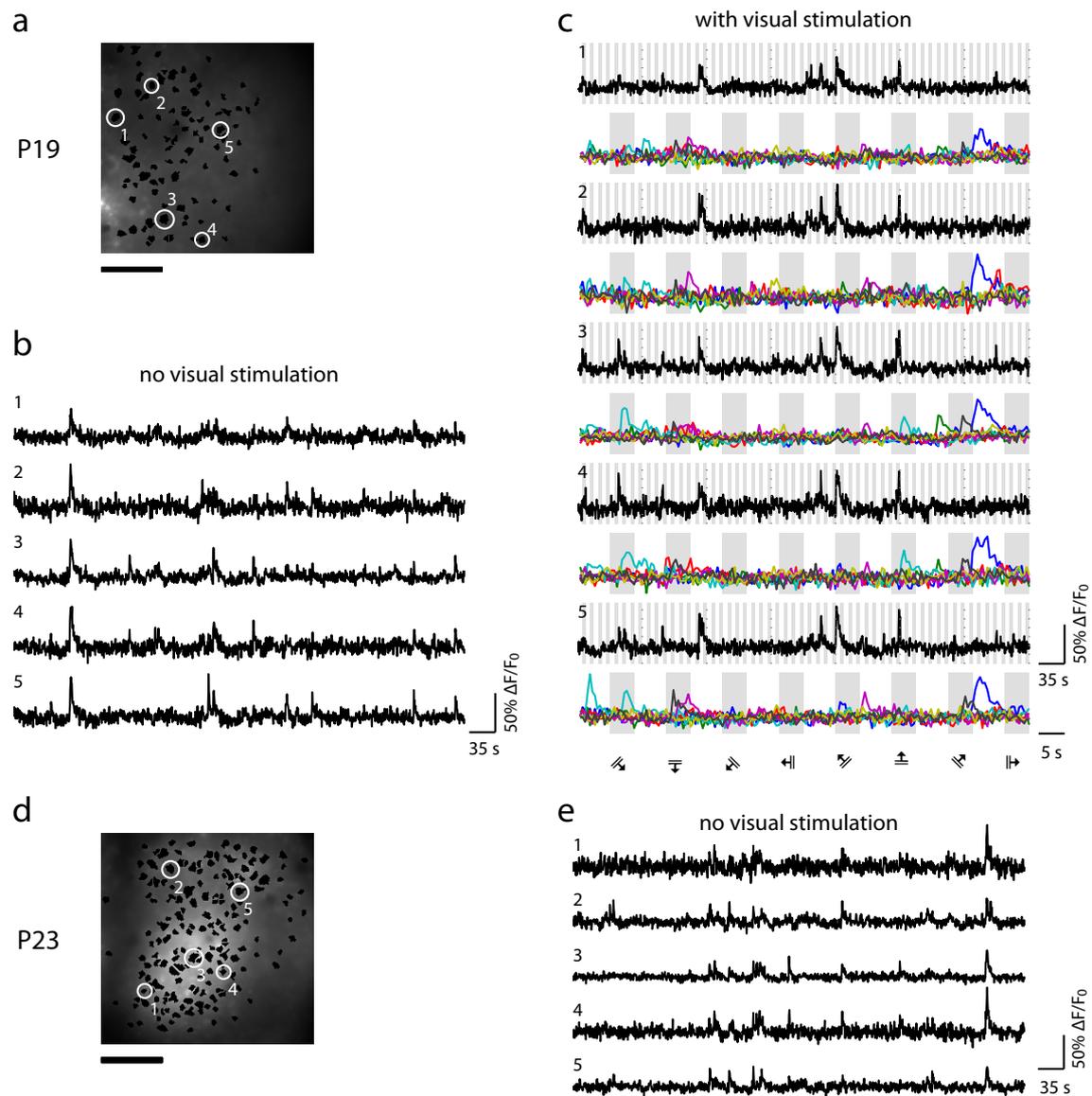
FIGURE 3-5: Spontaneous activity in early ferret visual cortex.

a and **d**, Cortical cells *in vivo* stained with OGB-1 AM. Regions of interest correspond to the cell somata which are shaded in black. Images were obtained in the absence of visual stimulation. Age is indicated to the left of each panel. Both examples were recorded at a depth of 124 μm. Scale bar, 100 μm.

b and **e**, Fluorescence time courses of spontaneous activity of individual cells. The positions of the cells are indicated in **a** and **d**, respectively. Note the strong correlation among cells.

c, Fluorescence time courses recorded during visual stimulation of the same cells as in **b**. Black traces are at the same time scale as used in **b**. Dotted lines demarcate stimulus cycles, which were presented in pseudo-randomized order. The coloured traces represent repetitions of each stimulus cycle after stimuli were shuffled into clockwise order. Note the different time scale as indicated by the legend. Grey bars indicate periods of visual stimulation.
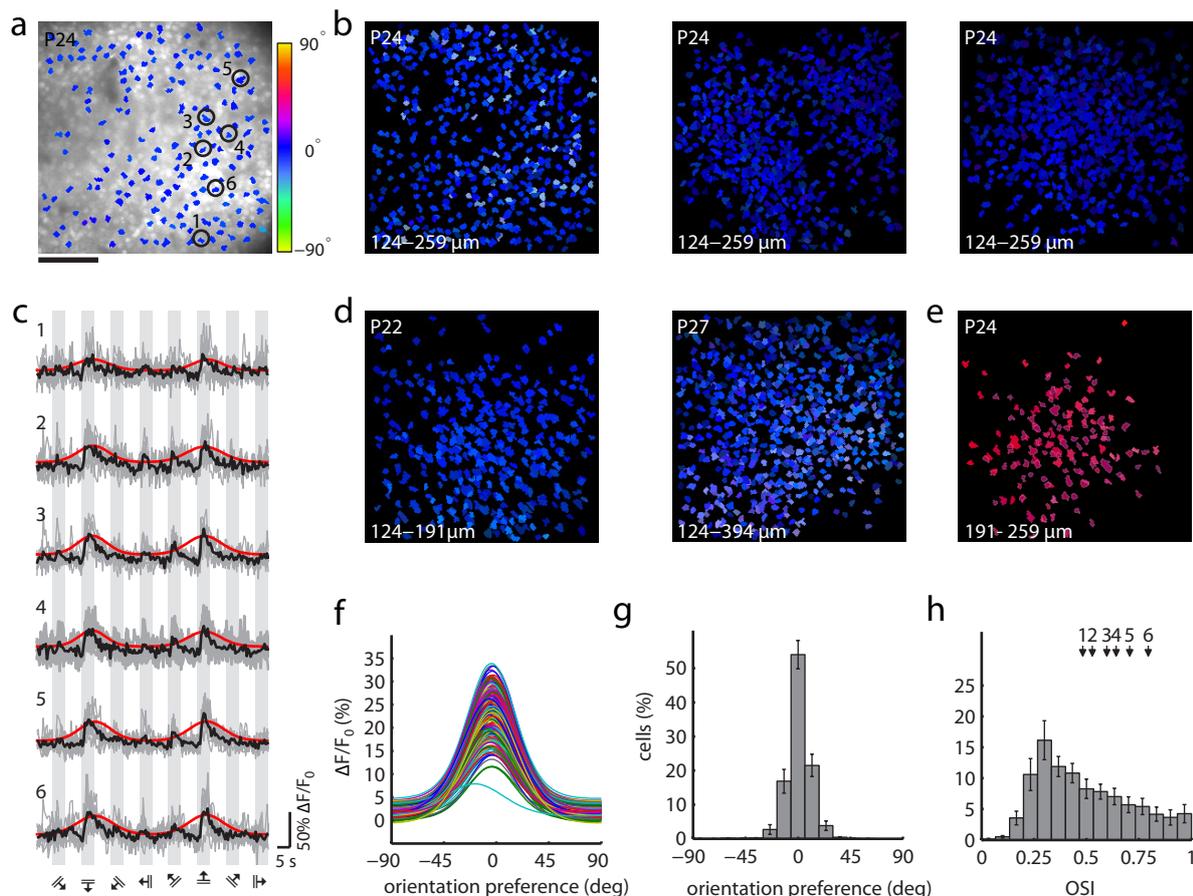
across all animals were generally very low, with a mean frequency of 0.039 Hz ± 0.0058 Hz (mean ± s. e. m.) which did not differ between ferrets in which visual activity could be evoked and ferrets that showed only spontaneous activity (t-test, *P = 0.82*). Furthermore, the response characteristics were very similar to those ones observed in animals lacking visual evoked signals.

One concern in our experiments was that the relatively low data acquisition rate (1 or 2 Hz) resulted in an underestimation of the frequency of spontaneous events due to missed fast events or failures to discriminate adjacent calcium transients. Therefore, we also imaged with higher frame rates of up to 7 Hz (but at lower resolution: 128 × 128 pixel) in a few ferrets. However, this did not significantly alter the mean frequency of spontaneous events (0.045 Hz; *n* = 3 animals; t-test, *P > 0.05*).

In summary, we did observe spontaneous activity in animals prior to the onset of visually evoked activity, but we could not, probably due to anaesthesia effects, study more complex patterns of spontaneous events as previously reported in awake mice and ferrets (Chiu and Weliky 2001; Colonnese *et al.* 2010; Colonnese and Khazipov 2010).

FIGURE 3-6: **Early orientation maps show a bias for horizontal orientation preference.**

a, Stained cortical tissue with overlays of somata of visually responsive cells. Colour encodes orientation preference as indicated by the legend. The data was recorded 191 μm below the cortical surface. Scale bar, 100 μm.

b, Depth-projected HLS maps calculated cell-wise for visually responsive cells at three different cortical regions in one P24 ferret. The leftmost map includes data shown in **a**. Colour conventions as in FIGURE 3-2C.

c, Fluorescence time courses of selective cells indicated in **a** with the seven reshuffled single trials (grey) and average time course (black). Red traces represent the orientation tuning curves fitted with the sum of two circular Gaussian functions to the peak responses.

d, Different depth-projected HLS maps from a P22 ferret and a P27 ferret, demonstrating the characteristic all-horizontal functional organization during this period. In **b**, **d** and **e**, age and depth below the cortical surface are indicated.

e, Depth-projected HLS maps from a P24 ferret. In some animals, the all-horizontal bias could not be observed and was shifted e. g. to a different orientation preference, but with a similarly sharp tuning and uniform organization across the cortical surface.

f, Orientation tuning curves (arbitrarily coloured) of all selective cells in **a**. Peak responses were fitted with a Gaussian function (von Mises distribution).

g, Mean distribution of preferred orientation in all-horizontal maps (n = 34 regions, including 9,720 orientation visually responsive and selective cells from 16 ferrets). The bin width is 12°. Error bars, s. e. m.

h, Mean distribution of OSI values in all-horizontal maps. Cells shown in **a** and **c** are indicated. The bin width is 0.067. Error bars, s. e. m.

3.4 Early development of orientation preference

One of the main goals of this thesis is to investigate the development of orientation preference maps in ferret visual cortex, in particular in the 10 day period before eye opening (around P31), where intrinsic signal imaging failed to resolve the development (Chapman *et al.* 1996; Chapman and Bonhoeffer 1998), and electrophysiological studies did not allow to determine the spatial organization of emerging orientation preference (Chapman and Stryker 1993; Krug *et al.* 2001).

We initially carried out experiments mainly in postnatal week (PW) 4 animals. As early as P21, after the eyes lids had been artificially opened, individual cells responded to visual stimulation. Unexpectedly, these earliest visually responsive cells were sharply tuned

for stimulus orientation. Strikingly, most cells responded nearly exclusively to horizontal stimuli (**Figure 3-6**). The majority of ferrets in PW4 (11 out of 16 ferrets) displayed this pattern of all-horizontal tuning. In a few animals, we found overall sharp tuning, but cells were responding to orientations other than horizontal (**Figure 3-6e**). Two out of 16 ferrets in PW4 showed no visually driven responses.

As we had not expected to find in young ferrets such large numbers of highly selective cells, which moreover all had a strong preference for horizontal stimuli, we sought
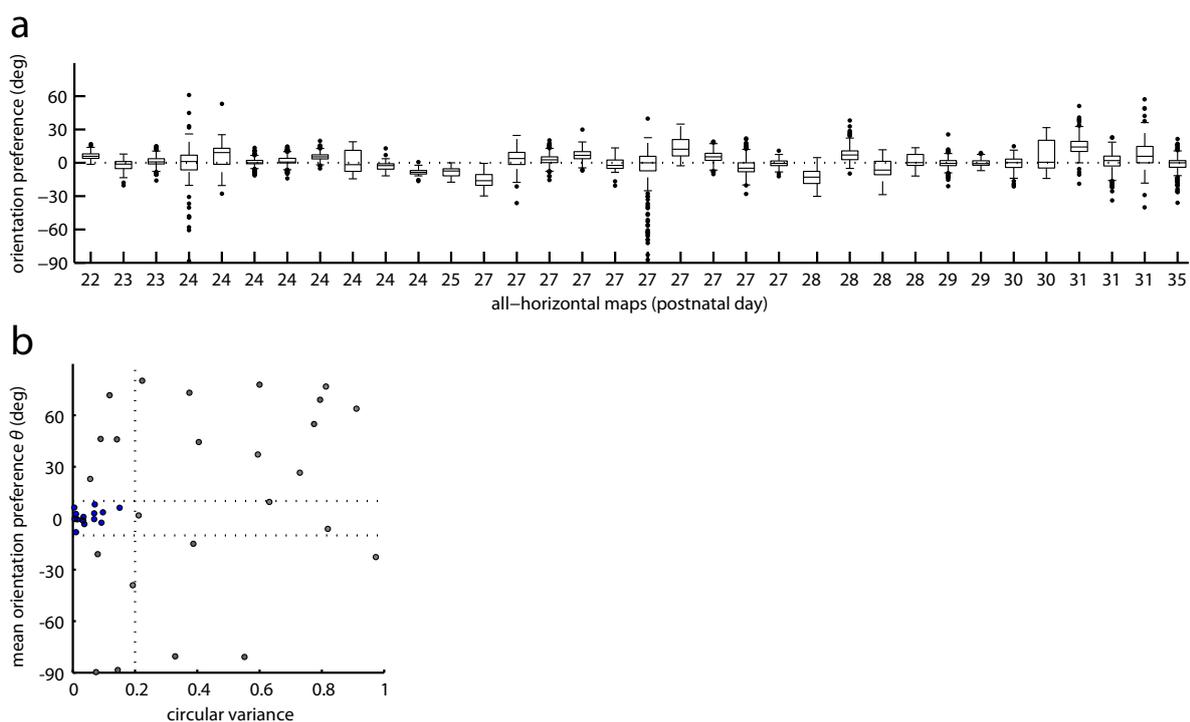
Figure 3-7: **Operational criterion defining the all-horizontal regime of functional organization.**

> **a**, Distributions of orientation selective cells for all 34 imaged maps in 16 animals with all-horizontal bias. A map refers to the set of cells z-projected from usually three cortical depths up to typically 400 μm below a single region on the cortical surface. Boxes indicate the median and inter-quartile range. Whiskers indicate 1.5 times the inter-quartile range. Outliers are plotted as individual points.
>
> **b**, All ferrets plotted in the clustering space defined by their mean orientation preference, with each orientation map weighted equally, and the circular variance of the distribution of orientation preferences, with each map weighted equally. The colours of the symbols indicate all-horizontal maps (blue) and non-horizontal maps (grey) from the entire dataset up to PW6. The central rectangular region delimited by the dotted bounds represents the operational criterion that we used to define all-horizontal ferrets (CV ≤ 0.2; -10° ≤ θ ≤ 10°).

to characterize these cells and their arrangement in the cortex in greater detail. Overall, 16 out of the 41 ferrets in this study were classified as "all-horizontal", that is, containing exclusively "all-horizontal" maps, based on the following operational definition: (1) the mean orientation preference of all cells in an "all-horizontal" ferret is within 10° of
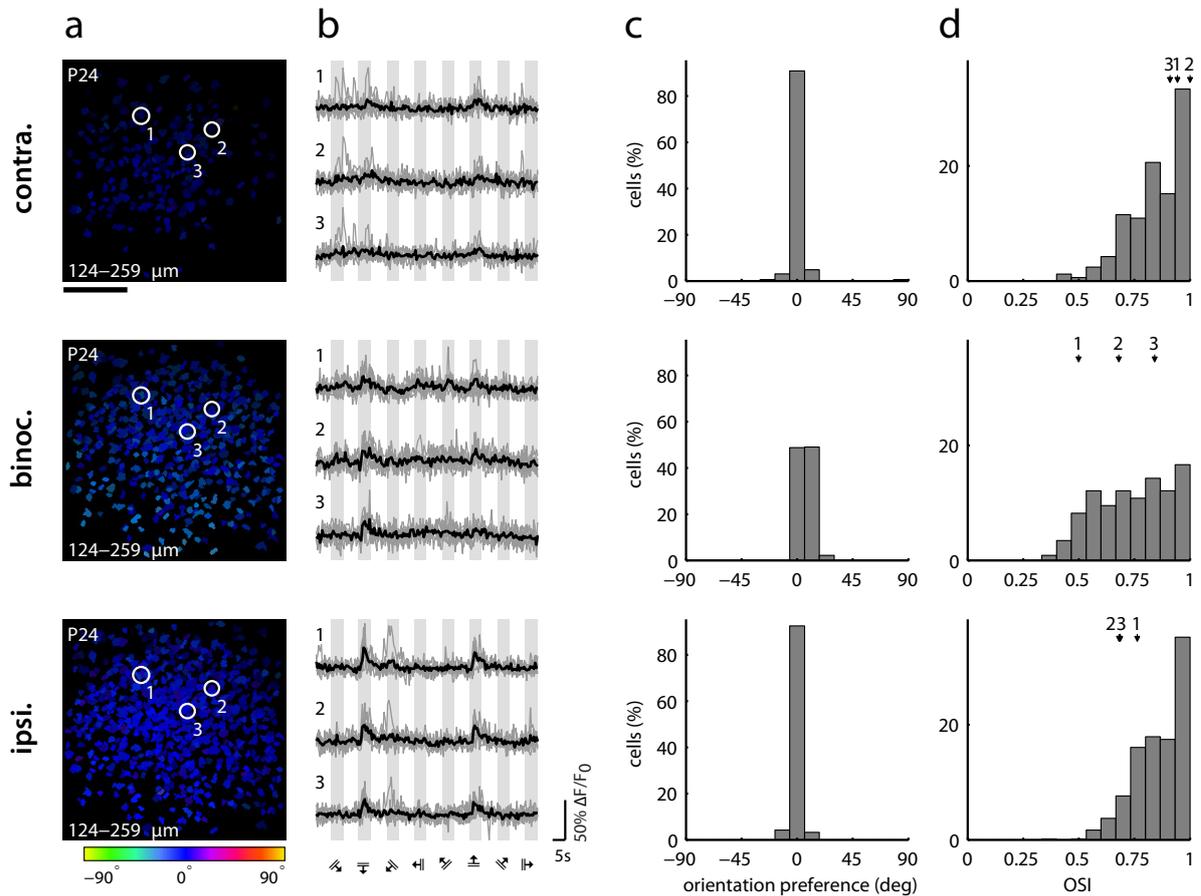
FIGURE 3-8: **Orientation preference maps with early all-horizontal tuning revealed with monocular and binocular visual stimulation.**

While recording from the same cells, visual stimulation was presented to the contralateral eye alone (top), the ipsilateral eye alone (bottom), or binocularly (middle).

a, Depth-projected HLS maps calculated cell-wise for visually responsive cells in one region of a P24 ferret. Scale bar 100 μm.

b, Fluorescence time courses of the cells indicated in **a**. Conventions as in FIGURE 3-2C.

c, Mean distribution of orientation preference (*n* = 165, 463, and 642 orientation selective cells, for contralateral, binocular, and ipsilateral stimulation, respectively).

d, Distribution of OSI values. Cells shown in **a** and **b** are indicated.

horizontal, and (2) the circular variance (CV) of orientation preference for these cells does not exceed 0.2 (**Figure 3-7**, see also **Methods 2.2.8.2, page 46**). Throughout, we use the term "map" to refer to the set of cells z-projected from usually three or more cortical depths up to typically 400 μm below a single region on the cortical surface.

We extracted on average 487 ± 48 labelled cells (16,574 cells in total) from 34 maps in 16 ferrets (**Figure 3-7**). Of these cells, 70.6% ± 3.8 % (mean ± s. e. m.; ANOVA, *P < 0.01*) were visually responsive and 79.4% were selective to the stimulus (ANOVA, *P < 0.01*) with a mean orientation preference of 0.8° (CV = 0.06), i. e. very close to horizontal. In the average all-horizontal map, the distribution of OSI values was skewed strongly rightwards, with a median OSI value of 0.49, corresponding to an orientation tuning width of ~29°. Cells in all-horizontal ferrets were thus as sharply tuned as cells in mature orientation maps from postnatal week 6 onwards (mixed-model ANOVA, *P = 0.45*).

In the youngest ferret exhibiting visually evoked responses, aged P21, only a few cells responded reliably, but those that did, were horizontally tuned. In the majority of visually responsive ferrets up to age P27, we observed a highly stereotyped pattern, with virtually all visually responsive cells preferring horizontal stimuli (**Figure 3-6g**). We also observed exclusive all-horizontal tuning in a few older ferrets, aged P28 (2 ferrets), P29, P30, P31 and P35. In all of these ferrets, cells exhibited a range of degrees of orientation selectivity, but the preference for horizontal stimuli was always very distinctive (**Figure 3-7a**).

In most experiments we stimulated both eyes. We therefore tested whether the horizontal tuning at early developmental ages was also seen with monocular stimulation. To this end, we recorded sequentially from the same cells in an optical section with contralateral, ipsilateral or binocular visual stimulation. Regardless of whether the contralateral or ipsilateral eye was stimulated, orientation preference and sharpness of tuning remained stable for cells in a given region (**Figure 3-8**). In some regions, ipsilateral visual stimulation was favoured (**Figure 3-8**) but in most cases contralateral stimuli elicited stronger signals and activated more cells.

Importantly, while not all animals in this age range showed a horizontal bias, we never observed a random mixing of sharply tuned cells with different orientation preference ("salt-and-pepper" organization).

3.4.1 Electrophysiological confirmation of early all-horizontal bias

The relationship between calcium signals and electrical activity in the developing cortex of very young ferrets has not been determined and might be different from the situation in adult animals. We therefore performed extracellular recordings with silicon microprobes, also aiming to confirm our observation of a strong horizontal bias obtained with calcium imaging in these young ferrets.
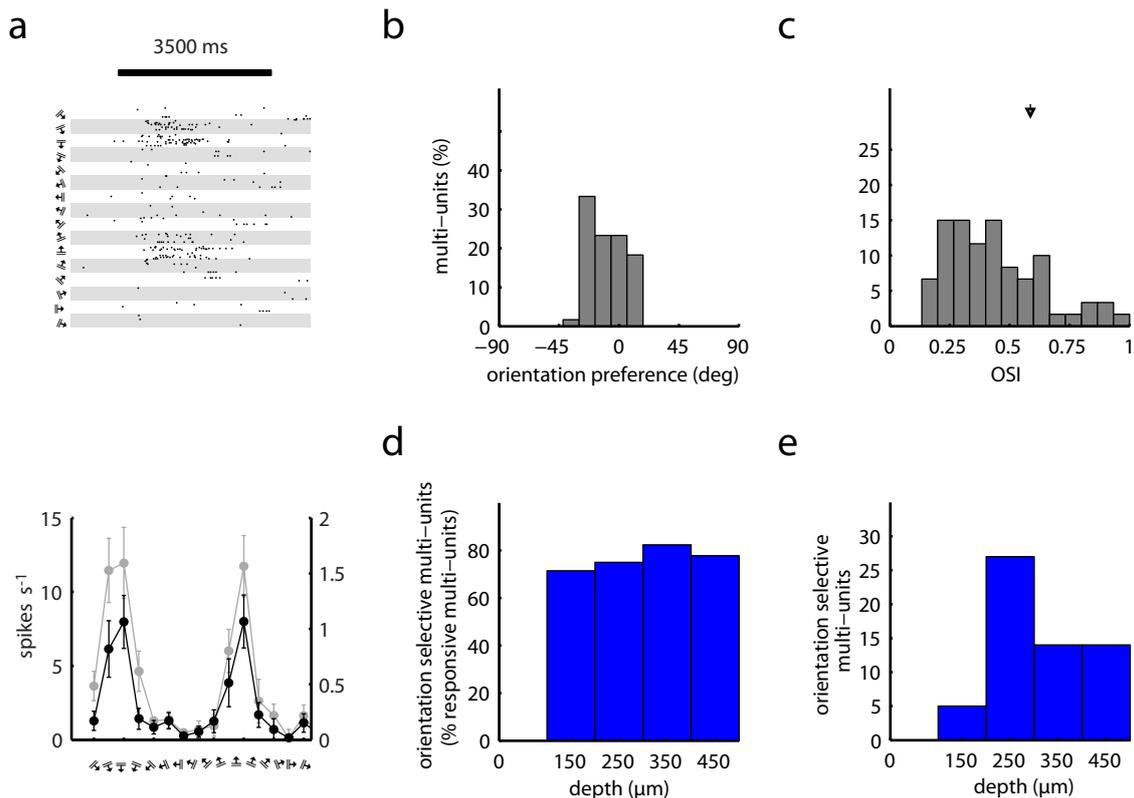
FIGURE 3-9: Electrical recordings confirm the all-horizontal bias.

a, Spike raster (top) and tuning curve (bottom, black) of a manually isolated single-unit from a P22 ferret. The bar in the spike raster plot indicates the period of visual stimulation. The tuning curve of the respective multi-unit (bottom) is shown in grey. Left- and right-hand ordinates indicate multi- and single-unit average firing rates above baseline, respectively. Error bars, s. e. m.

b, Orientation preference of electrically recorded multi-units (*n* = 60 multi-units from 10 penetrations in four all-horizontal ferrets aged P22, P25, P27, and P28).

c, Distribution of the orientation selectivity index for all recorded multi-units. The arrow indicates the multi-unit in **a**.

d, Distribution of orientation selective multi-units by depth (compare with **FIGURE 3-4F**).

e, Cumulative proportion of visually responsive multi-units that were orientation selective as a function of depth.

In four ferrets, aged P22, P25, P27, and P28, in which we had found entirely horizontal tuning using calcium imaging, we observed a consistently high proportion of orientation selective electrical multi-units, with over 70% of all visual responsive units (ANOVA, *P < 0.01*) at any 100 μm depth interval (**Figure 3-9d, e**), consistent with data from the imaging experiments. Electrical multi-unit activity also showed a strong preference for horizontally oriented stimuli (**Figure 3-9a**) with very similar tuning curves in comparison to those acquired with two-photon calcium imaging. These multi-units (n = 60) had an orientation preference of -9.3° (CV = 0.10; **Figure 3-9b**), and their distribution of OSI values was skewed strongly rightwards with a median OSI value of 0.41 (**Figure 3-9c**). Single-units, which we isolated manually (**Methods 2.2.8.5, page 50**), responded nearly exclusively to horizontal stimuli, consistent with the interpretation that multi-unit orientation selectivity reflects a universal preference for horizontal stimuli at the level of individual neurons (**Figure 3-9a**).

3.5 Development of orientation preference maps around eye opening

Having found that orientation preference during PW4 is mainly characterized by a strong horizontal bias, we continued to explore the development of orientation preference maps in PW5, the time around eye opening (ca. P31). During this period, the predominant functional organization for orientation preference changed markedly. Cortical neurons, while still clearly visually responsive, began to display very broad orientation tuning (**Figure 3-10**), despite occasional examples of horizontal tuning (**Figure 3-7**). While most cells were very broadly tuned, a few exhibited discernable orientation preferences, which spanned the complete range of orientations (**Figure 3-10e**). It follows that almost all cells had changed their preferred orientation in a concerted fashion within a very short time frame. However, we could not observe this remarkable switch between a horizontal bias with strong orientation tuning towards a very broad tuning exhibiting all orientation preferences within the course of an experiment. Importantly, despite the abundance of
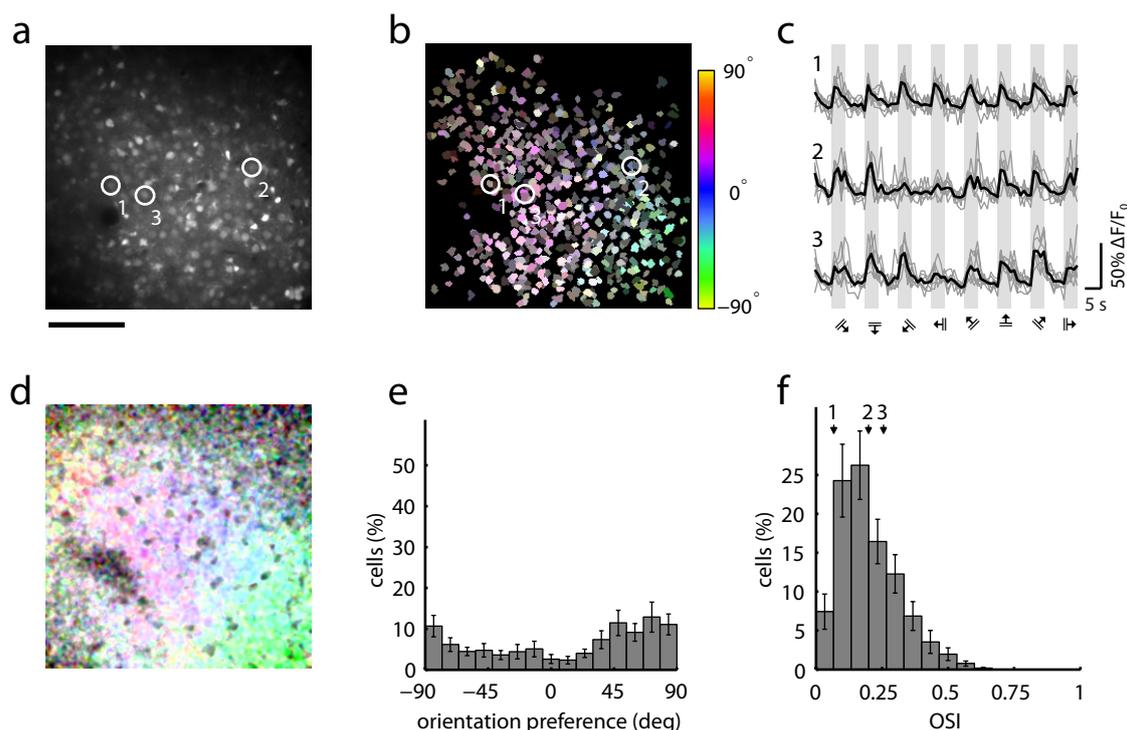
FIGURE 3-10: Orientation preference maps in postnatal week 5.

a, Stained cortical tissue from a P29 ferret. The image was recorded at a depth of 236 μm. Scale bar 100 μm.

b, Depth-projected HLS map calculated cell-wise for visually responsive cells at four different depths (135 - 304 μm) in the same ferret as shown in **a**. Note the low saturation of the cells indicating broad orientation tuning. Colouring conventions as in **FIGURE 3-2C**.

c, Time courses for three example cells indicated in **a** and **b**. Conventions as in **FIGURE 3-2H**.

d, Colour-coded orientation preference map calculated pixel-wise for the region shown in **a**.

e, Distribution of orientation preference for all 15 animals imaged in PW5 (*n* = 31 regions, 3,852 orientation selective cells). Bin width is 12°.

f, Mean distribution of the OSI for all animals. Bin width is 0.067.

Error bars indicate the standard error of the mean (s. e. m.).

weakly selective neurons, cells with similar orientation preferences were already spatially clustered during PW5, indicating the formation of an orientation map.

During PW5, we imaged 31 cortical regions in 15 animals. The observed orientation maps included the full range of orientation preferences (**FIGURE 3-10**). We found that 74.7% ± 3.7% (mean ± s. e. m.) of labelled cells were visually responsive. However, orientation selectivity of these cells was low, with only 34.1% ± 5.3% (mean ± s. e. m.) of visually

responsive cells showing selective tuning. In contrast to adult and juvenile ferrets (PW6+), orientation selectivity was significantly lower during PW5 (mixed-model ANOVA, $P < 10^{-3}$). The broad orientation tuning is reflected by a median OSI value of 0.20, pooled over all experiments in PW5 (**Figure 3-10f**).
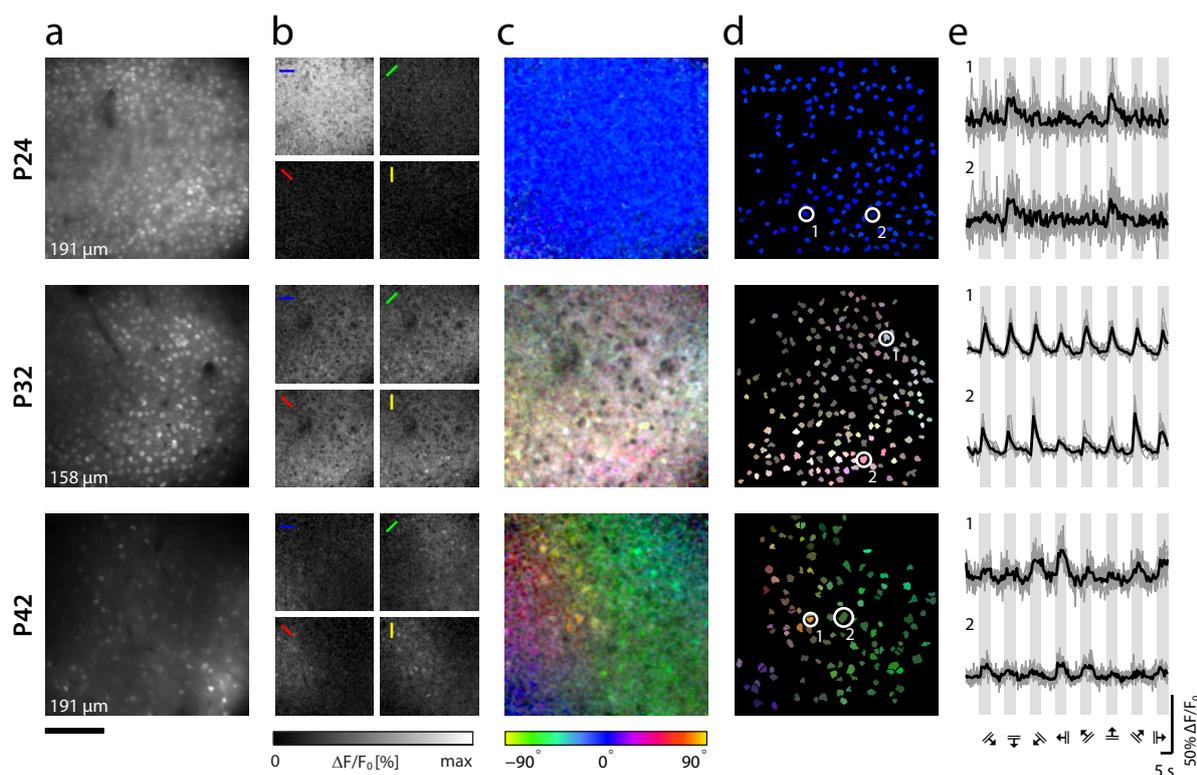
Figure 3-11: **Development of orientation maps in ferret visual cortex progresses through distinct phases.**

a, Cortical cells *in vivo* stained with OGB-1 AM. Each image is the average of all frames recorded during the visual stimulation protocol. Age is indicated to the left of each row. Indicated depths are with respect to the cortical surface. Scale bar, 100 μm.

b, Single-condition maps (quarter scale) calculated pixel-wise for the orientations indicated by the coloured bars in each map.

c, HLS maps calculated pixel-wise. Conventions as in **Figure 3-2c**.

d, HLS maps calculated cell-wise for visually responsive cells.

e, Fluorescence time courses of representative cells indicated in **d**. When necessary, responses were shuffled into clockwise order for presentation. In some cases, responses to additional intermediate stimuli are not shown. Light traces represent single trials. Heavy traces show average responses. Grey bars indicate periods of visual stimulation.

In earlier studies using intrinsic signal imaging (Chapman *et al.* 1996; Chapman and Bonhoeffer 1998; Li *et al.* 2006), structured orientation maps were found to emerge around the time of eye opening (**Figure 1-2d**). Using two-photon calcium imaging, we were able to detect an initial spatial clustering of orientation preference at single cell resolution a few days earlier.

The data described so far allows to answer one central question of my thesis. As one developmental scenario (**Figure 1-3**), I had proposed the early spatial clustering of orientation preference in emerging maps with initially broad tuning, which sharpens over time. This is indeed what we observed, starting in postnatal week 5. We can therefore reject a random distribution of strongly selective cells, referred as "salt-and-pepper" organization (**Figure 1-3**) which we never saw in any ferret.

Figure 3-11 summarizes the different stages of orientation map development with typical examples. Initially the majority of ferrets, with a few exceptions, exhibit a pattern of exclusive horizontal orientation tuning (**Figure 3-11 top**). This organization prevails throughout PW4. The sharp tuning for a single stimulus orientation vanishes in PW5, the time around eye opening, and is followed by broad tuning spanning the complete range of orientations (**Figure 3-11 middle**). During this period, we observed an initial spatial clustering of orientation preference. From PW6 onwards, most cells exhibited clear orientation tuning, and cells with similar orientation preferences were clearly clustered, forming mature orientation maps with occasional pinwheel discontinuities (**Figure 3-11 bottom**).

3.6 Fine scale analysis of the development of orientation preference maps

As a next step, we sought to examine our data in greater detail, analysing the development of orientation preference on a finer scale. When we analysed the data day by day, orientation selectivity was high in the initial all-horizontal phase of development, gradually fell to very low levels by the middle of PW5, and returned to mature, high levels by PW6 (**Figure 3-12a**). The proportion of visually responsive, but non-selective, cells exhibited
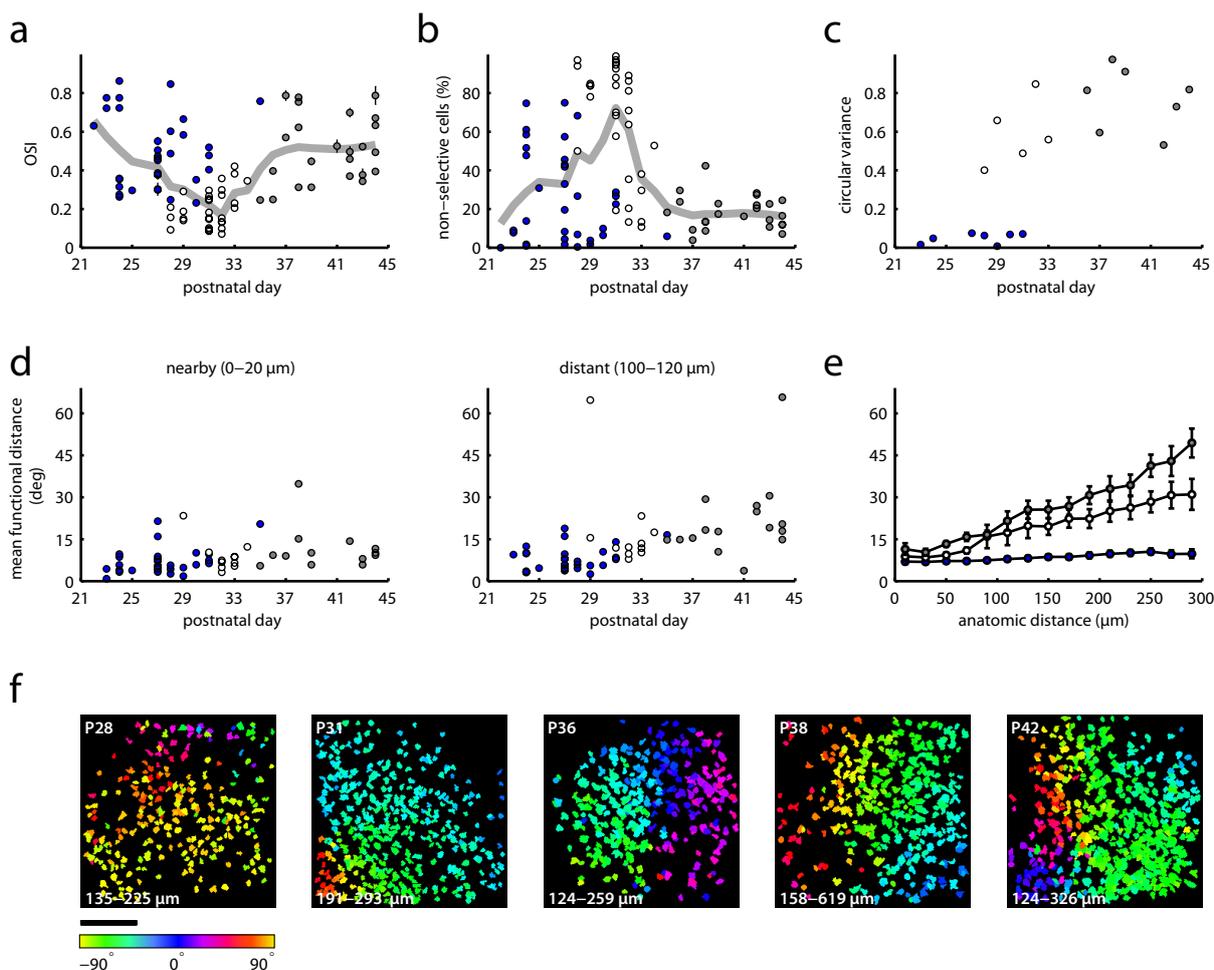
FIGURE 3-12: **Changes in fine scale functional organization of orientation preference maps over development.**

a, Mean OSI value versus postnatal age plotted for each map. Trend lines are local regressions using weighted linear least-squares and a 1st degree polynomial.

b, Proportion of non-selective but visually responsive cells plotted versus age for each map. Trend lines as in **a**.

c, Circular variance of orientation preference (CV) versus age. For this plot, maps were binned by day to ensure adequate sampling at all ages. Days on which less than three maps were obtained were excluded from this analysis.

d, Difference in orientation preference versus age for "nearby" cells separated by 0–20 μm, left, and "distant" pairs separated by 100–120 μm, right.

e, Mean difference in orientation preference versus anatomic distance between cells for the three phases of development. The analysis in **d** and **e** was carried out for all maps that did not contain a pinwheel centre. In **a-e**, blue indicates all-horizontal maps, white indicates full orientation maps from PW5, and grey indicates orientation maps from PW6+.

f, Pinwheel centres in depth-projected, cell-based orientation preference maps. In these maps, only preferred orientation is colour-coded.

Error bars, s. e. m. Scale bar, 100 μm.

a complementary developmental time course (**Figure 3-12b**). These gradual trends became even more robust when the orientation selectivity index and the responsive, but non-selective proportion of cells in a map were plotted against body weight, rather than age (**Figure 3-13**), suggesting that overall developmental state, rather than age *per se*, may determine the development of orientation maps. Nevertheless, this complementary developmental time course implies that all-horizontal maps develop into mature orientation preference maps by way of a brief, intermediate state during which the visual cortex remains visually responsive but loses its orientation selectivity almost entirely. Supporting this interpretation, the rise in OSI values over the course of PW5 and PW6+ was independent of orientation preference (**Figure 3-14**), indicating that horizontal tuning in more mature orientation preference maps is unlikely to be a holdover from the all-horizontal phase of development.

Given these gradual developmental changes, we wondered whether all-horizontal maps and mature orientation preference maps exist along a developmental continuum of functional organization. One possibility is that the distribution of preferred orientation is initially sharply peaked and broadens gradually over development. To test this hypothesis, we plotted the coefficient of variation (CV) of orientation preference as a function
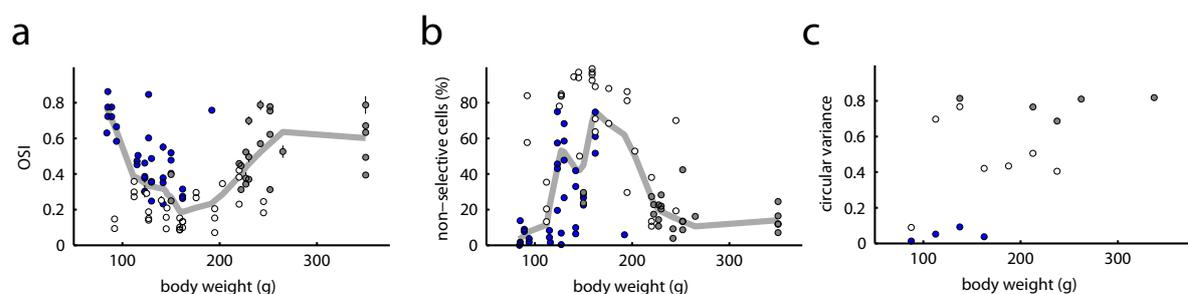
Figure 3-13: Changes in orientation selectivity and preferred orientation as a function of body weight.

a, A map's distribution of orientation selective cells by OSI as a function of body weight (mean ± s. e. m.).

b, The non-selective proportion of each map's visually responsive cells as a function of body weight. In **a** and **b**, trend lines are local regressions using weighted linear least-squares and a 1st degree polynomial.

c, Circular variance of the distribution of orientation preferences as a function of body weight. Maps were binned (bin width = 25 g) to ensure adequate sampling. Conventions as in **Figure 3-12a-c**.
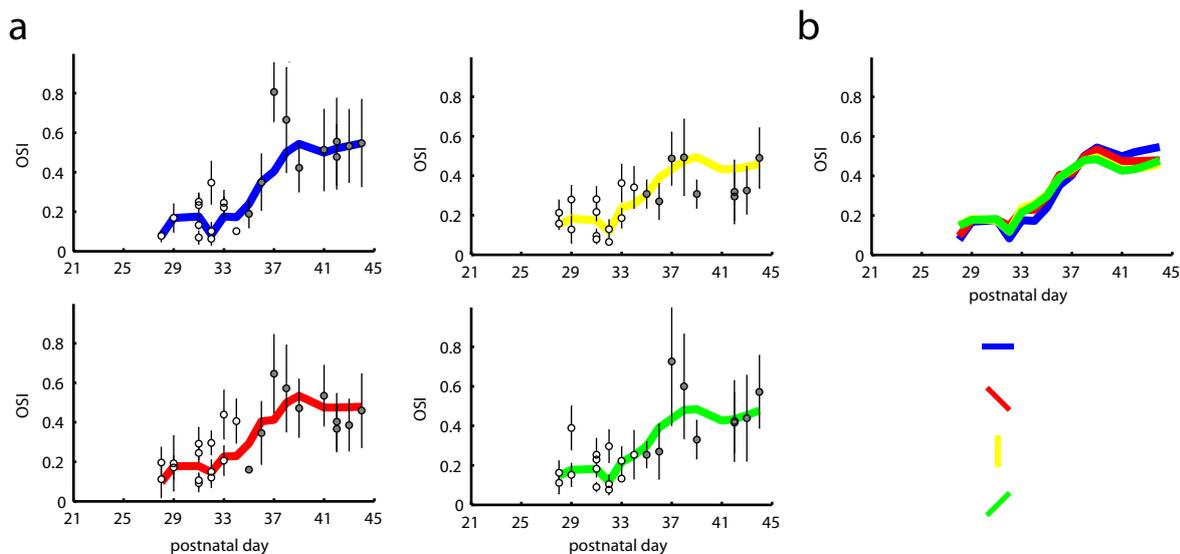
FIGURE 3-14: **Similar developmental changes in OSI for all orientation preferences.**

a, For each ferret, mean OSI for each of four orientation bins, centred around the cardinal and oblique orientations, versus age. Trend lines are local regressions using weighted linear least-squares and a 1st degree polynomial.

b, Trend lines from a plotted on the same axes. Conventions as in FIGURE 3-12A.

of age (FIGURE 3-12C). CV was uniformly low in the phase of development displaying the horizontal bias but then increased suddenly in PW5 and remained elevated in PW6+ (one-way ANOVA, $P < 10^{-7}$, with *post hoc* Tukey's tests using a $P = 0.01$ significance level; FIGURE 3-12C). This finding strongly suggests that, in contrast to the gradual developmental time course of orientation selectivity, the transition from all-horizontal maps to complete orientation preference maps occurs suddenly, within a few days around the time of eye opening.

Analysis of fine scale spatial organization emphasized the suddenness of this transition. "Nearby" cells, spaced ≤ 20 μm apart, were functionally similar regardless of age, and at this scale, all-horizontal maps were indistinguishable from complete orientation preference maps in either PW5 or PW6+ (one-way ANOVA, $P = 0.08$, with *post hoc* Tukey's tests using a $P = 0.01$ significance level; FIGURE 3-12D LEFT). Moreover, in all-horizontal maps, nearby cells were no more functionally dissimilar from one another than were "distant" cells, spaced 100-120 μm apart, emphasizing the uniformity of all-horizontal functional organization (Mann-Whitney U test, $P = 0.28$, FIGURE 3-12D RIGHT). By contrast, in full orientation preference maps in both PW5 and PW6+, distant cells were more functionally dissimilar than nearby cells (Mann-Whitney U test, $P = 0.02$ and $P < 10^{-3}$ for PW5 and

PW6+, respectively; **FIGURE 3-12D**), consistent with a mature functional organization in which functional similarity decreases with anatomic distance. When we plotted functional distance as a function of anatomic distance, indeed we observed that orientation preference varied smoothly across the cortex at comparable rates in PW5 and PW6+ orientation maps, while it remained nearly constant in all-horizontal maps (**FIGURE 3-12E**). Moreover, we found pinwheel discontinuities as early as P28, the earliest age at which we observed an orientation preference map that was not all-horizontal (**FIGURE 3-12F**). This analysis again stresses that during the transition from all-horizontal maps to full orientation preference maps, cells never assumed a "salt-and-pepper" organization with respect to their orientation preference.

In sum, the fine scale analysis further completes the comprehensive description the development of orientation preference maps at single cell resolution. The sudden, but exquisitely orchestrated change from all-horizontal to mature orientation preference maps suggests remarkable remodelling of the neuronal circuits underlying the generation of orientation preference.

3.7   Control experiments

In the following, I will describe the results of several sets of control experiments, which aim at elucidating possible explanations for the unexpected all-horizontal bias in orientation preference early in development. This bias might derive from incorrect positioning of the stimulus monitor or might be of biological cause at different levels of the visual system. Therefore, I examined closer the properties of the eyes and recorded visually evoked neuronal activity electrophysiologically from the LGN.

Furthermore, I had to control whether the analysis can discriminate calcium transients from neurons and other cell types.

3.7.1   Neuronal origin of calcium transients

The calcium indicator OGB-1 AM does not only stain neurons but also other classes of cells such as astrocytes, which also exhibit calcium transients. It has been proposed that these
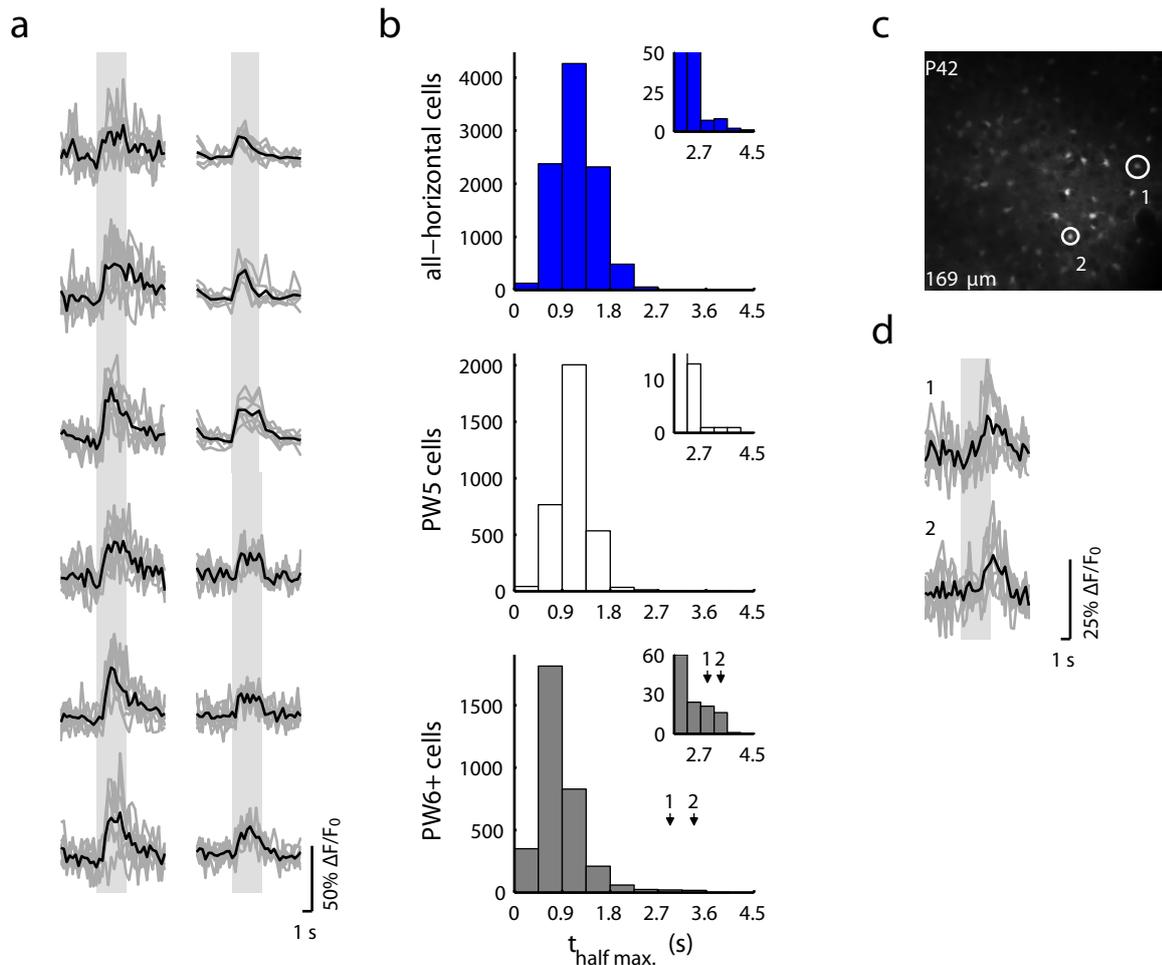
FIGURE 3-15: **Short and uniform latency of visually evoked calcium transients indicates neuronal origin.**

a, Calcium responses of the cells presented in FIGURES 3-3C and 3-10C evoked by the respective preferred orientations. Conventions as in FIGURE 3-2H. As in these examples, most visually responsive cells exhibited tonic, stimulus-locked fluorescence changes.

b, Distribution of calcium response latencies for visually responsive cells. We used $t_{half\ max}$, the time to reach half the maximum response magnitude as a measure for the response latency. Separate distributions are presented for all-horizontal (top), PW5 (middle), and PW6+ (bottom) ferrets. Only cells imaged at the higher (0.45 s frame⁻¹) of the two frame acquisition rates used were included. Inset histograms present the same data scaled to highlight the outliers of each distribution.

c, Anatomical image of cortical tissue. The two encircled cells are typical outliers of the bottom distribution in **b**, and given their intense labelling and characteristic short processes are putative astrocytes.

d, Calcium transients of the two cells indicated in **c**, evoked by their respective preferred orientations. Note the substantially longer delays than those in **a**. Conventions as in **a**.

transients indirectly reflect neuronal activity (Harder *et al.* 1998; Haydon and Carmignoto 2006). Moreover, a recent study in ferret visual cortex has shown that astrocytes respond to moving grating stimuli in a highly selective manner, even forming pinwheel-like patterns (Schummers *et al.* 2008). Astrocytes can be identified *in vivo* by the red dye sulforhodamine 101 (Nimmerjahn *et al.* 2004; Schummers *et al.* 2008), as well as by their slow onset responses in the range of several seconds (Schummers *et al.* 2008; Nimmerjahn 2009). In our experiments in very young ferrets it was not possible to consistently achieve successful labelling of astrocytes with sulforhodamine 101. We therefore used the following criteria to identify astrocytes: (1) brighter intensity of OGB-1 AM labelling in comparison to neurons (**Figure 3-15c**) (Stosiek *et al.* 2003; Ohki *et al.* 2005) and (2) response latency. As a measure of response latency, we determined the time to reach the half maximum response magnitude ($t_{half\ max}$).

Most visually responsive cells that we recorded, exhibited similarly tonic, stimulus-locked modulation of their fluorescence signals (**Figure 3-15a**). For all cells that were recorded with 0.45 s frame^{-1}, we determined the response latencies (**Figure 3-15b**). The distribution of response latencies revealed a few outliers with very long delays (**Figure 3-15b**), which were usually associated with cells showing stronger labelling and characteristic short processes (**Figure 3-15c-d**) identifying them as putative astrocytes. Moreover, astrocytes with their longer delays (**Figure 3-15d**) respond much less reliable to visual stimulation and therefore fail to fulfil our statistical criterion for responsiveness (ANOVA across blank and all direction periods, *P < 0.01*) and selectivity (ANOVA across all directions, *P < 0.01*) as also indicated by **Figure 3-2d, e**.

In summary, we conclude from this analysis that the vast majority of our data derives from neurons.

3.7.2   Mapping retinotopy in ferret visual cortex

In all experiments, we imaged from cortical regions corresponding to the centre of the visual field. Consequently, visual stimuli, subtending 80° in azimuth and 60° in elevation were presented in the centre of the animal's visual field. We ensured the correct positioning of the visual stimuli by mapping retinotopy, using two-photon calcium imaging and
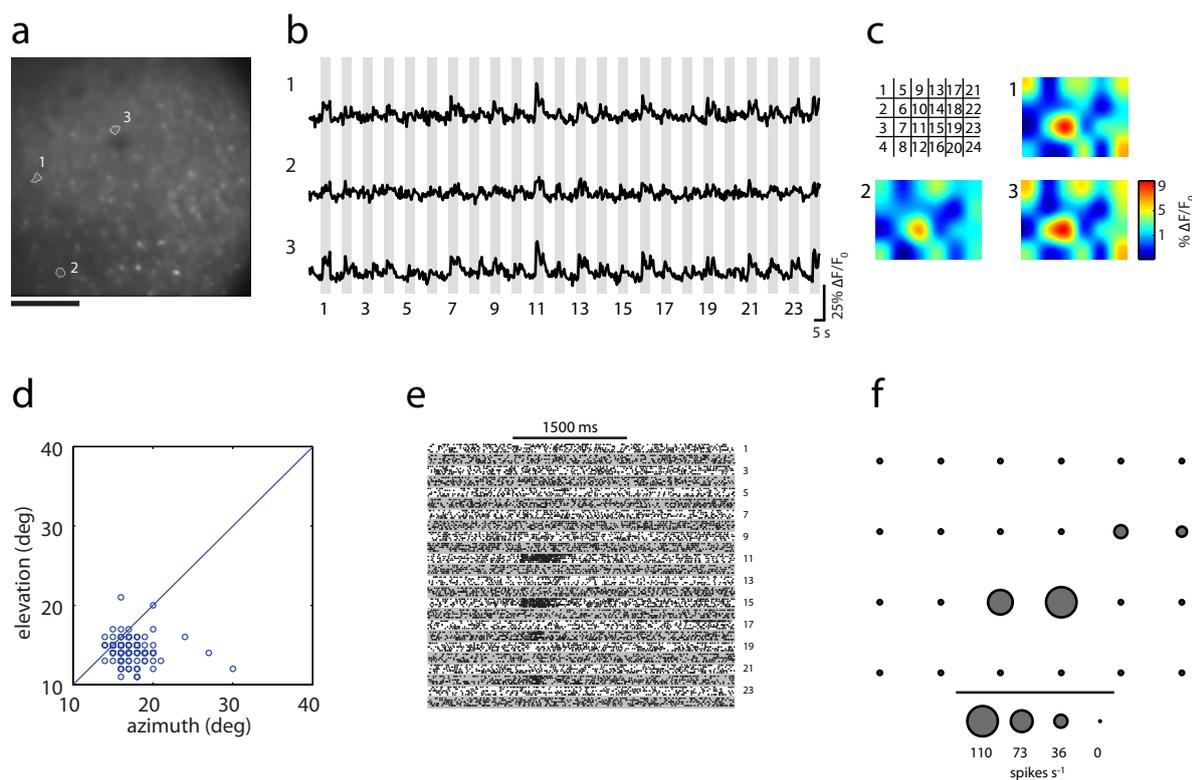
FIGURE 3-16: **Mapping receptive field extent with calcium imaging and electrophysiology.**

a, OGB-1 AM staining in a P24 ferret, 225 µm below cortical surface. Scale bar, 100 µm.

b, Averaged fluorescence time courses of selected cells (marked in **a**). The grey bars indicate periods of randomly interleaved visual stimulation at 24 positions in visual space (indicated in **c**). Time courses were re-shuffled afterwards. Individual patches were 13° in azimuth and 15° in elevation.

c, Receptive field maps of neurons shown in **a** and **b**. The averaged responses were interpolated with a Gaussian fit, and the response amplitude (ΔF/F) colour coded. The grid indicates stimulus position.

d, Many receptive fields are elongated in azimuth. The full width at half maximum (FWHM) in azimuth and elevation was calculated for all imaged cells in this ferret (n = 127). Some data points overlap.

e, Receptive field mapping with extracellular recordings. Spike raster of multi-unit activity from the same animal as shown in **a–d**. Visual stimuli were identical to the ones used in the imaging experiment shown in **b** and **c**. Ten sweeps were grouped by stimulus position as shown in **c**. The black bar indicates the period of stimulation.

f, The surface plot shows evoked electrical multi-unit activity at the different positions (**c**) of the visual field. The diameters of the data points correspond to the average firing indicated by the legend (bottom).

extracellular recording in a number of ferrets. The correct positioning of the monitor is important to avoid unexpected patterns of activity by clipping the receptive field of the recorded neurons due to partial visual stimulation and therefore resulting in an erroneous observed bias in orientation preference.

We employed the same stimulation paradigm as had been used for mapping the retinotopic structure of mouse visual cortex with intrinsic signal imaging (Schuett *et al*. 2002). In random order, small 13° × 15° stimulus patches out of a 6 × 4 array were presented with the monitor positioned in the central visual field. Individual patches consisted of moving gratings which rapidly changed to the next of eight directions in a random manner (**Figure 3-16c**). Evoked calcium signals or extracellular electrical activity was recorded.

Activity patterns evoked by centred patches on the monitor were consistent between electrical multi-unit recording and calcium imaging in the same cortical region (**Figure 3-16**). In some imaging experiments (3 out of 6), the mapped receptive fields were located on the bottom edge of the stimulus monitor, and we might therefore have stimulated only a part of the receptive fields in the recorded cells. Thus, the edge of the monitor might serve as strong horizontal edge causing a partial stimulation of the receptive field along elevation which could result in the observed horizontal bias. In order to test for this possibility, we deliberately stimulated neurons in ferrets exhibiting broad tuning with stimuli restricted to increasingly smaller fractions of their receptive fields. We were in fact able to induce apparent all-horizontal tuning under these conditions. However, this was only the case when the top part of a cell's receptive field, comprising less than 25% of its total area, was stimulated. In this case, we had to change drastically the monitor position by up 40° in elevation. This argues strongly that inadequate positioning of the stimulus monitor is unlikely to have caused the horizontal bias. Nonetheless, we will further investigate this unlikely possibility in future experiments.

We also determined the receptive field extent of single neurons which we imaged (**Figure 3-16c, d**). We noted a modest elongation in azimuth of receptive fields in PW4 ferrets (**Figure 3-16d**). These horizontally elongated receptive fields might cause horizontal gratings to drive cells stronger, potentially contributing to the horizontal bias in very young ferrets.

3.7.3 Early horizontal bias is not caused by optical properties of the ferret eye

In order to rule out potential confounders of our experimental design that could account for the horizontal bias we found in very young ferrets, we varied several parameters of the visual stimulation. In most experiments, we used gratings with a spatial frequency between 0.03 and 0.1 cycles degree^{-1}. It is conceivable that optical aberrations, such as astigmatism of the eyes' optics, could mask an underlying diversity of cortical orientation preferences. Ideally, this should be tested by measuring the optic properties of the ferrets' eye, including the lens. However, the extracorporeal examination of the eye is very error-prone, in particular due to potential distortions of the lens during enucleation.

Therefore, as an alternative approach, we employed eccentric photorefraction (Gekeler *et al.* 1997; Choi *et al.* 2000; see **METHODS 2.1.6, PAGE 36**) to determine a potential astigmatism of the ferret eye. In awake, 2 year old ferrets we could successful refract the eyes and did not find any indication for an astigmatism (**FIGURE 3-17B**). The refractive power along the horizontal and vertical meridian were between +12 and +15 dioptres (D). The apparent hyperopia is probably due to the conversant small eye artefact (Glickstein and Millodot

a   b   c
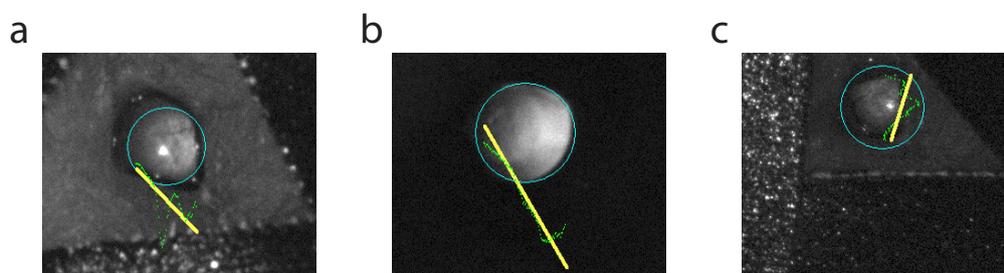
FIGURE 3-17: **Measurement of the refractive power in young and adult ferrets using eccentric photorefraction.**

a, Measurement of the refractive power (+9 D) along the horizontal meridian of the contralateral eye of a P28 anaesthetised ferret. The blue circle indicates the determined pupil diameter (2.8 mm). The yellow line indicates the linear regression of the intensity profile (green) . Note the faintly visible blood vessel pattern of the retina.

b, Eye of an adult ferret with refraction of +15 D along the horizontal meridian. The pupil diameter is 3.5 mm. The image appears blurred due to movements of the awake animal.

c, Eye of a P25 ferret (+3 D along the vertical meridian). The pupil diameter is 2.6 mm.

1970). Young ferrets, with their eye lids still closed, were anaesthetized before the eyes were artificially opened. Measurements of the refraction, however, failed in most cases, due to opacification of the crystalline lens. Anaesthesia might have caused opacification, as has been reported in mice (de la Cera *et al.* 2006). We were nonetheless able to determine the refractive power in two animals (P25 and P28), which had values between +3 and +9 D
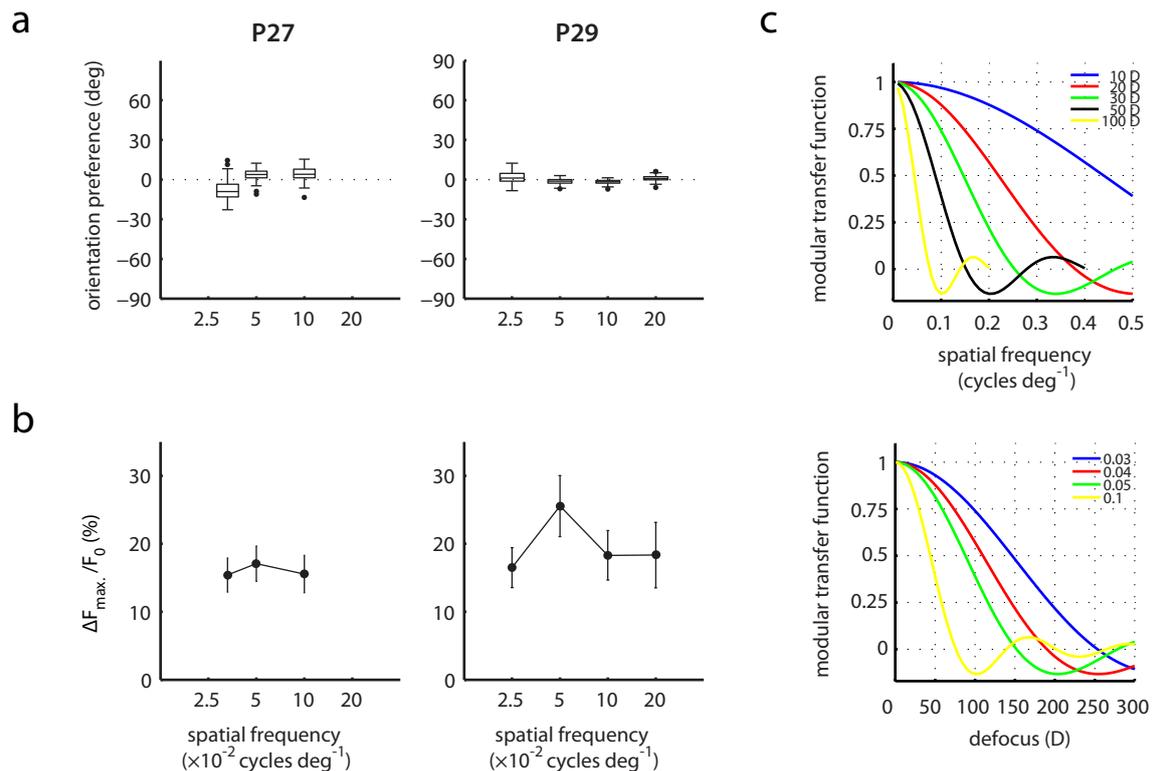
FIGURE 3-18: All-horizontal tuning is independent of stimulus spatial frequency.
Age of ferrets is indicated above each column.

a, For orientation selective cells imaged at a single depth, their distributions of orientation preference at different spatial frequencies are displayed in a box plot. Boxes indicate the median and inter-quartile range. Whiskers indicate 1.5 times the inter-quartile range. Outliers are plotted individually as dots.

b, Magnitude of the best response (mean ± s. e. m.) as a function of spatial frequency.

c, The theoretical effect of defocusing, e. g. through a possible astigmatism, on the geometrically calculated modulation transfer function (MTF). Top panel shows the modulation as a function of the spatial frequency for different magnitudes of defocusing (10, 20, 30, 50 and 100 D). The modulation turns 0 at 0.77, 0.39, 0.26, 0.16 and 0.08 cycles deg^{-1}, respectively. The bottom panel displays the different MTF as a function of defocusing for certain spatial frequencies used for stimulation. First roots of the functions are at 254, 191, 153 and 77 D, respectively.

(**Figure 3-17a, c**). Although we were not able to measure the refractive power of the eyes in a sufficient number of young ferrets, this result indicates that there is, if at all, only a small axial astigmatism present.

A very different approach to assess the potential role of astigmatic eyes for biases in orientation preference is based on the idea that an axial astigmatism would cause spatial contrast sensitivity to depend on stimulus orientation. We therefore also determined the orientation preference of neurons in two animals exhibiting an all-horizontal bias, using a variety of different spatial frequencies.

We observed that a strong horizontal preference and all-horizontal maps were maintained over a wide range of spatial frequencies, rendering a strong astigmatism to cause this bias unlikely. As shown in **Figure 3-18a**, the distributions of orientation preference vary only marginally with changing spatial frequency. Furthermore, the magnitude of the best response peaks in both animals at a spatial frequency of 0.05 cycles deg^{-1}, confirming that the spatial frequency used for mapping orientation preference during this age was optimally chosen. (**Figure 3-18b**).

Theoretical considerations, also suggest that an astigmatism is unlikely to cause an anisotropy of orientation preference in young ferrets: The eye would have to be defocused by over 100 dioptres before the contrast of gratings appears to vanish with the used spatial frequencies (Schaeffel and Queiroz 1990; **Figure 3-18c**). The residual contrast, or modulation, of the grating on the retina can be described by the modulation transfer function (**Methods 2.2.8.6, page 51**). The modulation drops to a minimum between 77 and 254 D for spatial frequencies ranging 0.03 to 0.1 cycles deg^{-1}. Although refraction of the eyes of young developing ferrets was probably not very exact, and we therefore cannot completely reject an astigmatism, a theoretical defocus of 100 D would still yield 50% modulation of the gratings at spatial frequencies smaller than 0.05 cycles deg^{-1} (**Figure 3-18c**).

3.7.4 Electrical recordings in the lateral geniculate nucleus

Having excluded optical aberrations as a cause for the horizontal bias, we next studied whether this bias originates in the lateral geniculate nucleus (LGN). We used tungsten electrodes instead of silicon probes to record from the LGN (**Figure 3-19**), thus avoiding
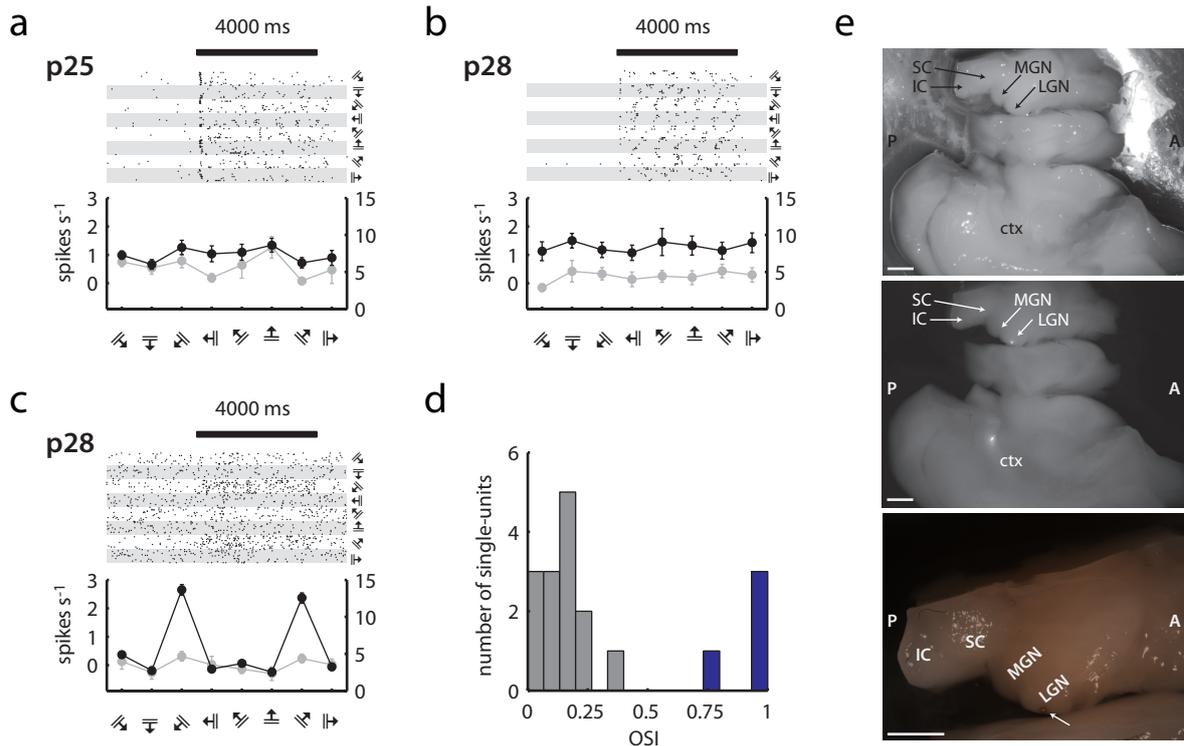
FIGURE 3-19: **Electrical recordings in LGN and visual cortex.**

a, Visually evoked responses in the LGN recorded in a P25 ferret. Spike raster (top) and tuning curve (bottom, black) of an isolated single-unit from the LGN. The bar in the spike raster plot indicates the period of visual stimulation. The tuning curve of the respective multi-unit (bottom) is shown in grey. Left- and right-hand ordinates indicate multi- and single-unit average firing rates above baseline, respectively. Error bars, s. e. m.

b, Visual responses in the LGN obtained in a P28 animal. Conventions as in **a**.

c, Visual responses of a cortical single-unit and its corresponding multi-unit recorded in the same animal as in **b**. Conventions as in **a**.

d, Distribution of the orientation selectivity index for all recorded single-units from the cortex (n = 4) and LGN (n = 19). Distribution of geniculate neurons (grey) is skewed leftwards whereas OSI scores of cortical neurons (blue) are skewed rightwards.

e, Anatomical confirmation for the correct positioning of the electrode into the LGN. The two hemispheres of fixated cortex were separated and flipped aside resting mainly on the dorsal side. Bright light image (top) shows the right cortical hemisphere together with the thalamus and brain-stem (dorsal surface up) which have the correct anterior-posterior position relative to the cortex. The electrode was painted with DiI to visualize the penetration in the LGN (middle) and viewed under epi-fluorescence illumination (excitation: BP 545/25; emission: BP 605/70). The bottom image is an overlay of bright light and epi-fluorescent images confirming the electrode track (arrow) to be in the LGN. Scale bars, 2 mm. ctx – cortex, IC – inferior colliculus, LGN – lateral geniculate nucleus, MGN – medial geniculate nucleus, SC – superior colliculus; A – anterior, P – posterior

excessive damage to the overlying visual cortex. For comparison, we recorded electrically activity in the visual cortex of the same animals (**Figure 3-19**), again using tungsten electrodes to facilitate comparison. After carrying out cortical recordings, we extended the craniotomy to allow positioning the electrode for recordings in the LGN using stereotactic coordinates reported for young ferrets in an earlier study (Krug *et al.* 2001). The electrodes were painted with DiI (DiCarlo *et al.* 1996; Niell and Stryker 2008) for *post hoc* identification of the LGN (**Figure 3-19e**).

We targeted the LGN in two animals (P25 and P28) and could isolate 19 single-units in total (5 penetrations) from our recordings (**Figure 3-19a, b**). LGN responses from some single-units had bursts of spikes starting with the onset of the visual stimulation and these patterns of activity were consistent through multiple repetitions (**Figure 3-19b**). These bursts of activity were absent in cortical recordings (**Figure 3-19c**, **Figure 3-4a**, **Figure 3-9a**). Other LGN cells responded in more tonic manner (**Figure 3-19a**). Both response characteristics were also previously described for geniculate cells in cat and ferret (Guido and Sherman 1998; Krug *et al.* 2001; Kara *et al.* 2002). However, all LGN single-units showed no orientation tuning. Their distribution of OSI values was skewed leftwards with a median OSI of 0.14 (**Figure 3-19d**). Conversely, the few single-units (*n* = 4) recorded from the visual cortex of the same animals exhibited high orientation tuning (**Figure 3-19c, d**). The distributions of the OSI values from cortical and geniculate neurons closely resemble the results from an earlier study assessing neuronal responses in the visual cortex and LGN by visual stimulation through closed eye-lids (Krug *et al.* 2001). Thus, we conclude that the all-horizontal bias of orientation preference observed mainly in postnatal week 4 is most likely of cortical origin.

Discussion

In this thesis, I have examined the formation of orientation preference maps in ferret visual cortex. I have focussed on early steps of development, since previous studies using intrinsic signal imaging or electrophysiology were not able to resolve the precise sequence of developmental changes leading to mature orientation preference maps. Combining *in vivo* two-photon calcium imaging with extracellular recordings allowed me to obtain cell-resolution orientation preference maps in the developing ferret visual cortex.

In the majority of animals imaged during the fourth postnatal week, before natural eye opening, all visually responsive neurons were sharply tuned and strongly preferred horizontally oriented stimuli. These neurons were distributed uniformly across the cortex.

In ferrets imaged one week later, around the time of eye opening, most visually responsive neurons responded to all orientations. Despite such broad orientation tuning, I observed a clear tendency for spatial clustering of preferred orientations. During these early stages of development, a random distribution of sharply tuned neurons ("salt-and-pepper" organization) was never observed. In still older animals, an increase in orientation selectivity was concomitant with the appearance of normal, mature orientation maps.

4.1   Two-photon calcium imaging

Two-photon calcium imaging (Stosiek *et al.* 2003; Ohki *et al.* 2005; Svoboda and Yasuda 2006) monitors changes in the intracellular calcium concentration of neurons associated with neuronal activity, thus allowing determining the functional properties of neurons in the visual cortex *in vivo*. Although neuronal spiking is only indirectly inferred by this method, several studies have shown that the observed somatic calcium transients are the result of suprathreshold rather than subthreshold activity and reliably reflect action potential firing (Smetters *et al.* 1999; Mao *et al.* 2001; Berger *et al.* 2007; Kerlin *et al.* 2010). Some calcium indicators such as OGB-1 AM (used in this study) can also detect subthreshold fluctuations (Bandyopadhyay *et al.* 2010) which lead to fluorescence changes of about 1%. These are unlikely to have a substantial effect on the signals obtained in the visual cortex (Bandyopadhyay *et al.* 2010), where visual stimulation evokes large calcium transients (up to 30% and more) caused by high spike rates (Ohki *et al.* 2005; Ohki *et al.* 2006; Li *et al.* 2008; Schummers *et al.* 2008). Further, the amplitude of the somatic calcium transients seems to be a good predictor of the firing rate of a given neuron (Mao *et al.* 2001; Kerr *et al.* 2005; Kerlin *et al.* 2010). Two-photon calcium imaging is therefore a powerful tool for monitoring spiking activity of large populations of neurons deep inside the intact cerebral cortex (Helmchen and Denk 2005).

This imaging method has, as laser scanning microscopy in general, a low temporal resolution, caused by the serial scanning of each pixel. The low scanning rate of 1–2 Hz, used in most of the experiments described here, poses a possible limitation to data acquisition and might lead to a smoothing if not an omission of the initial peak of a calcium transient. However, as discussed above, the calcium indicator OGB-1 AM can in principle

detect single action potentials, and the decay time constant of calcium transients ranges in the order of seconds (Yaksi and Friedrich 2006), permitting reliable detection of calcium responses. Moreover, we have chosen a relative long period for each visual stimulus (4 s) to evoke strong and sustained responses in ferret visual cortex. When we compared data acquired with low and high frame rates (up to 7 Hz), we did not detect any substantial differences in the shape of the visually evoked calcium signals. Thus, under these conditions even a relative low temporal resolution does allow faithful recordings of overall neuronal spiking activity. Moreover, our results are in very good agreement with our own electrophysiological recordings as well as with data from other laboratories (Chapman and Stryker 1993; Krug *et al.* 2001).

Recent technical improvements and different scanning strategies (Göbel *et al.* 2007; Grewe *et al.* 2010) diminish the problem of temporal resolution and will facilitate high-speed imaging in future studies.

Despite these potential shortcomings, two-photon calcium imaging offers several major advantages over conventional methods like intrinsic optical imaging and electrophysiological recordings to measure and map neuronal activity evoked by visual stimulation. First, the activity of hundreds of neurons can be assessed simultaneously on a fine spatial scale (at ca. 1 μm resolution) over different depths below the cortical surface. Second, not only somatic calcium transients can be measured, but also the activity of the neuropil surrounding cell bodies, which reflects the bulk average of pre- and postsynaptic events (Kerr *et al.* 2005; Jia *et al.* 2010). Third, two-photon calcium imaging allows distinguishing different cell types, for example neurons and astrocytes (Nimmerjahn *et al.* 2004). Fourth, visualization of all cells allows quantifying the proportions of responsive as well as unresponsive cells for a given visual stimulus, thus avoiding potential sampling biases encountered during electrical recordings. Taken together, two-photon calcium imaging is very well suited to study functional properties like orientation preference in the developing visual cortex.

4.2 All-horizontal bias in early orientation preference maps

The most unexpected finding of our study is the presence of all-horizontal orientation preference maps very early in development (**FIGURE 3-6**). How might this finding be explained?

4.2.1 Role of eyes' optics

Optical aberrations, such as astigmatism of the eyes' optics, could mask an underlying diversity of cortical orientation preferences, providing a trivial explanation of our finding. Acting on the assumption that immature ferrets have a strong axial astigmatism, a grating stimulus of a given spatial frequency could result in blurring effects of different extent: For example, a horizontal grating would be correctly focused on the retina, while vertical ones are heavily blurred. By this, a horizontal bias in orientation preference in the visual cortex could be explained. Nevertheless, it can be expected to observe a wider range of orientation preferences with stimuli of substantially lower spatial frequencies. However, the fact that a strong horizontal preference in all-horizontal orientation preference maps was maintained over a wide range of spatial frequencies of drifting gratings makes this explanation unlikely (**FIGURE 3-18**).

As a more direct test, we attempted to refract the eyes in immature ferrets (**FIGURE 3-17**). Because of the opacification of the crystalline lens in the eye under anaesthesia, we were not able to completely determine the refractive power in very young animals and could not rule out a small astigmatism. There is also little knowledge in the literature about the refraction of the eye and ocular biometry in adult and juvenile ferrets (Hernández-Guerra *et al.* 2007). However, calculating the effect of defocusing on the modulation transfer function suggests that defocusing of up to several hundred dioptres, depending on the spatial frequency, would be necessary to diminish any contrast (**FIGURE 3-18**). Such high amount of defocusing, leading to a potential astigmatism, is not supported by our ocular measurements of the refractive power in adult and juvenile ferrets, despite the limited accuracy of our measurements.

4.2.2   Impact of visual experience

Could all-horizontal orientation preference maps result from activity-dependent shaping of early neuronal connections? Visual experience plays a key role in the development of another functional map, the one for direction selectivity (Li *et al.* 2006; Li *et al.* 2008). In addition to their orientation preference, many neurons in the visual cortex also show a preference for a particular direction of stimulus motion, and such cells are spatially clustered, resulting in direction preference maps. Dark-reared animals lack these direction preference maps, suggesting that their development relies on visual experience (Li *et al.* 2006). However, the emergence of direction preference maps succeeds the formation of orientation preference maps and begins only during natural eye opening.

In turn, visual experience, while possible through the closed eyelids (Krug *et al.* 2001), is unlikely to influence the early development of orientation preference maps. Almost normal orientation preference maps are formed in ferrets that were dark-reared from P21 onwards, the onset of visual responses in cortical neurons (White *et al.* 2001). This suggests that the developmental time course described by our data does not depend on visual experience, which is rather important for the strengthening of already existing, premature maps (White *et al.* 2001).

Previous intrinsic signal imaging studies reported an early bias of orientation preference towards cardinal, i. e. horizontal and vertical, orientations in juvenile ferrets (Chapman and Bonhoeffer 1998; Coppola *et al.* 1998). Due to already discussed technical limitations of this method, the strongest overrepresentation has been observed around eye opening, right at the time when orientation preference maps are first detectable using this method. Nevertheless, during this time, the cortical surface is in particular devoted to horizontal orientations, underlying the general cardinal bias. This horizontal bias has also been seen in cats using electrophysiological recordings (Li *et al.* 2003). Single-units responded preferentially more to horizontal than to vertical (and other) orientations with much narrower tuning. The general cardinal bias declines however after visual experience starts with natural eye opening while in dark-reared animals (from P21 to start of the experiment after eye opening) an anisotropic representation of orientation preference could still be observed (Coppola and White 2004). In summary, visual experience diminishes rather than magnifies this overrepresentation of cardinal orientations. However, it

remains unknown whether the all-horizontal bias in orientation preference, observed in our experiments, has the same origin as the cardinal overrepresentation discussed above.

4.2.3 Influence of spontaneous activity

Spontaneous activity in the form of retinal waves (Maffei and Galli-Resta 1990; Meister *et al.* 1991; Wong *et al.* 1993; Feller *et al.* 1997), which are transmitted to downstream targets (Mooney *et al.* 1996; Chiu and Weliky 2001; Hanganu *et al.* 2006), could play an instructive role for map formation. Indeed, wave propagation in isolated early postnatal retinas of the mouse appears to have a directional bias (Stafford *et al.* 2009). However, this reported directional bias persists only along the nasal-temporal axis of the retina, i. e. 90° offset to the horizontal bias in orientation preference in ferret visual cortex determined by our data. But similar patterns of retinal waves in the ferret might exhibit a different directional bias during early development and could potentially drive the formation of all-horizontal maps.

Retinal waves might not be the only explanation for the all-horizontal bias of orientation preference, but correlated spontaneous activity was also reported for the immature sensory cortex in rodents (Garaschuk *et al.* 2000; Adelsberger *et al.* 2005; Yang *et al.* 2009; Colonnese and Khazipov 2010) which either originates from a cortical generator or could be caused by relayed retinal activity. We attempted to study patterned spontaneous activity in the developing visual cortex, but were not able to detect any spatial or temporal patterns of spontaneous activity such as travelling waves (Colonnese and Khazipov 2010). We assume that anaesthesia levels disrupted such spatiotemporal pattern as previously reported in mice and ferrets (Chiu and Weliky 2001; Colonnese and Khazipov 2010).

Nevertheless, there is evidence that spontaneous activity in the ferret contributes to the formation of topographic structures in the LGN and visual cortex. Spontaneous activity is more correlated among neurons in layers of the LGN which receive inputs from the same eye as between layers receiving inputs from the opposite eye (Weliky and Katz 1999). Moreover in ferret visual cortex, synchronous bursts of spontaneous activity occur in patchy patterns around one week before natural eye opening (Chiu and Weliky 2001). These correlated patches of activity resembles contra- and ipsilateral eye domains (ocular dominance columns) and become indeed associated with those during development (Chiu

and Weliky 2002). Moreover, this form of activity can be altered by transection of the optic nerve (Chiu and Weliky 2001) suggesting that it depends on external inputs provided by retinal waves (Kerschensteiner and Wong 2008; Blankenship *et al.* 2009) and transformations in the LGN (Weliky and Katz 1999; Chiu and Weliky 2001).

To this point, it can only hypothesized, that patterns of spontaneous activity in the retina, LGN or visual cortex share similar contributions to development of early orientation preference.

4.2.4   Biases in early axon ingrowth

At this time, the most parsimonious explanation for the presence of early all-horizontal maps seems to be that early axons form spatially asymmetric patterns during ingrowth into the lateral geniculate nucleus or the cortex.

In rodents, during the first two postnatal weeks, axons from retinal ganglion cells project to multiple targets in visual regions of the brain, among them the superior colliculus (SC) and the LGN. Retinocollicular projections form a continuous topographic map in the SC and LGN, and in addition inputs from both eyes remain separated in the LGN by specifically projecting to two non-overlapping geniculate domains. Anatomical tracing studies of the retinocollicular and retinogeniculate pathways have revealed that during the first postnatal week the initial axonal projections are less accurate by either overshooting to topographically incorrect positions in the SC or by forming overlapping domains in the LGN (Godement *et al.* 1984; So *et al.* 1990; Simon and O'Leary 1992; Plas *et al.* 2005). Retinocollicular projections terminating diffusely in their target region early in development were also found in the ferret (Chalupa and Snider 1998). In rodents, this coarse axon ingrowth undergoes refinement processes in the next postnatal week to generate precise adult-like connectivity patterns. The refinement of these projections probably relies on distinct activity pattern such as retinal waves (Stafford *et al.* 2009).

Although spatially asymmetric axonal ingrowth patterns and in particular an overshooting of retinogeniculate and even geniculocortical axons have not been yet described in the ferret,they might impose an early orientation bias on cortical neurons.

4.3 Absence of random mixing of orientation preference during development

In this study, we never observed any "salt-and-pepper" arrangement of orientation selective neurons during development. Early orientation preference maps in the fifth postnatal week exhibit already a weak spatial clustering of orientation preference, though with broad tuning. This early homogeneity of orientation preference implies that following the initial all-horizontal phase neurons must change their connectivity such that their orientation preference becomes similar to that of their neighbours. How can this specific connectivity be achieved during development?

4.3.1 Possible role of molecular factors

In principle, molecules can guide axons to their specific targets. Several examples for the involvement of molecular cues in the formation of maps in the visual system have been described. Molecular guidance cues in axons (Goodman and Shatz 1993) or cell adhesion molecules (Yamagata *et al.* 2002) can precisely instruct the formation of connections between neurons.

Cell surface proteins of the Eph-receptor/ephrin family play key roles in the formation of retinotopic maps in the LGN and SC by guiding axons of retinal ganglion cells to their correct partners in the midbrain and thalamus (McLaughlin and O'Leary 2005; Flanagan 2006). Moreover, gradients of ephrins and their Eph-receptors also control retinotopic mapping between LGN and the visual cortex (Cang *et al.* 2005; Cang *et al.* 2008).

In many carnivore and primate species, axonal projections from eye-specific layers of the LGN maintain their segregation in the primary visual cortex by forming ocular dominance columns (ODCs). Visual experience shapes the layout of these ODCs during a critical period by Hebbian-type plasticity (Hensch 2004). However, in the ferret the initial formation of ODCs occurs long before natural eye opening (Crowley and Katz 2000; Katz and Crowley 2002) and might be controlled by molecular mechanisms (Crowley and Katz 1999; Weliky and Katz 1999). While specific molecules mediating the initial formation of ODCs have not yet been identified (Huberman 2008), ODCs might be another example of a map which is instructed by molecular guidance cues.

The greater complexity of orientation preference maps in comparison to retinotopic maps and ODCs might *per se* not be a strong argument for discarding the idea of molecular guidance cues acting during the development of orientation preference maps. The probably most striking example for the establishment of a topographic map with high complexity is found in the mammalian olfactory system (Wilson and Mainen 2006). Here, sensory neurons in the olfactory epithelium make precise and specific connections to the olfactory bulb by relying on perhaps hundreds of molecular cues that lead spatially widely distributed receptor cells to terminate within a single glomerulus (Wang *et al*. 1998; Chen and Flanagan 2006). If similarly such molecular cues were present during the development of orientation preference maps, they would presumably be transient and present at very early times during development, while geniculocortical afferents are still arriving in layer 4.

On the other hand, orientation selectivity is not based on the termination of selective geniculate inputs preferring horizontal, vertical or oblique orientations but on the specific spatial arrangement of ON-centre and OFF-centre receptive fields in the cortex (**Introduction 1.2, page 15**). It is hard to imagine how such a complex alignment could rely on molecular cues, and so far there is no experimental evidence for the notion that the generation of orientation selectivity in the cortex is guided through molecular factors. Rather, this property seems to be triggered initially by spontaneous activity and later by visual experience.

4.3.2   Neuronal activity shapes orientation selectivity

During development, neuronal activity plays an important role for the maturation of orientation selectivity. The crucial function of spontaneous activity is evidenced by experiments showing that the blockade of spontaneous neuronal activity in the visual cortex following direct infusion of the sodium channel blocker tetradotoxin (TTX) into the visual cortex completely abolished the maturation of orientation selectivity (Chapman and Stryker 1993). In a related study, pharmacological silencing of retinal mGlu6 glutamate receptors by intravitreal injections of DL-2-amino-4-phosphonobutyric acid (APB) to selectively disrupt the activity of the retinal ON pathway (Chapman and Gödecke 2000) prevented the

maturation of orientation selectivity. This indicates that the balance of ON and OFF centre cell activity is important for the development of orientation selective receptive fields.

An alternative approach to alter patterned retinal activity was used by Weliky and Katz (1997). The correlation of retinal ganglion cells during development was artificially enhanced by electric stimulation of the optic nerves, a procedure resulting in a weakening of orientation selectivity. These results fit nicely to a correlation-based model, which proposed that activity-dependent interactions between retinal ganglion cells of the ON and OFF centre pathways result in the subfield segregation of oriented simple cells in the cortex (Miller 1992, 1994). Furthermore, this model might also explain the effects of different rearing conditions during the development of orientation preference maps (White *et al.* 2001). While dark-rearing leads to nearly normally developed but less selective orientation preference maps, binocular eyelid suture disrupts orientation selectivity very strongly, resulting in a rudimentary orientation preference map. Strongly reduced visual experience by eyelid suture may still activate ON and OFF geniculate inputs to cortical target cells, but over a broader spatial extent than in normally reared animals. The increasing correlation of these inputs would therefore prevent the segregation of the ON and OFF subfields of the cortical target neurons (Miller *et al.* 1999).

The relative broad orientation tuning of neurons in layer 4 compared to layer 2/3 undergoes little maturation from the time of eye opening (Chapman and Stryker 1993). It suggests that ON and OFF geniculate inputs projecting to cortical target cells in layer 4 are already arranged with receptive fields aligned in space (Chapman *et al.* 1991; Reid and Alonso 1995; Ferster *et al.* 1996), in turn generating orientation selectivity in this layer with the onset of visual responsiveness in the cortex. The local correlation of the geniculate inputs may serve as a base for the emergence of a map structure. Subsequent maturation of orientation selectivity occurring later in layer 2/3 is mediated by the establishment and refinement of feedforward and recurrent connections. In particular, the refinement of local circuits relies on visual experience (Durack and Katz 1996; White *et al.* 2001). Furthermore, the instructive role of visual experience to neighbouring neurons has been demonstrated for direction selectivity maps in ferret visual cortex (Li *et al.* 2006; Li *et al.* 2008). The emergence of direction selectivity and its spatial clustering requires visual experience and can be suppressed by dark-rearing (Li *et al.* 2006) or biased by training with a visual stimulus

moving in two opposite directions (Li *et al.* 2008). An effect could already be observed after eight hours of biased visual training, resulting in an increasing overrepresentation for the trained directions of motion over time. Spatial analysis of cells in layer 2/3 revealed that visual experience induced by motion training has a local constructive effect by changing the direction selectivity of individual neurons to be like their neighbours. Interestingly, the authors also noted small but significant changes in orientation preference induced by training. But it remains to be elucidated whether such mechanisms also act during the development of orientation preference and if so, how connections, probably feedforward and recurrent, are established and remodelled to correlate orientation (or direction) preference of adjacent neurons among each other within a map.

4.4 Functional organization of orientation preference maps

Orientation preference maps, obtained with intrinsic signal imaging or two-photon calcium imaging, exhibit areas in which orientation preference changes smoothly across the cortical surface, interrupted by pinwheels and fractures, discontinuities of rapidly changing orientation preference (Bonhoeffer and Grinvald 1991; Ohki *et al.* 2006). Why these structures and orientation preference maps in general emerge remains still unclear (Horton and Adams 2005). It is also an open question why some species such as cats, ferrets and primates (Hubel and Wiesel 1963; Bonhoeffer and Grinvald 1991; Blasdel 1992; Rao *et al.* 1997; Ohki *et al.* 2006) show this elaborate functional organization, whereas others like rodents (Metin *et al.* 1988; Girman *et al.* 1999; Ohki *et al.* 2005) lack spatial clustering but do have orientation selective cells ("salt-and-pepper" organization). One way to disentangle this question is to investigate the emergence and maturation of orientation preference maps. Our data, as discussed above, support the idea that orientation preference maps do not follow a phase of "salt-and-pepper" organization during early development in the ferret (**FIGURE 3-12**). Adjacent neurons in emerging maps always prefer similar orientations.

The different spatial layouts of orientation selective neurons across the cortical surface in various species might derive from different rules of connectivity, already present during development. A given set of neurons in the network might be physically arranged in a different way but still show similar functional connectivity. Relevant intracortical

connections are for example horizontal short-range and long-range connections in the upper and lower layers that span up to millimetres across the cortex. Short-range connections (< 500 μm) in species with orientation preference maps may tend to link cells with similar functional properties. However, close to singularities like pinwheel centres, the situation is more akin to species without maps. Here, neurons might either connect unselectively to just any adjacent neighbouring cell, or they might form specific connections to neurons with similar functional properties, avoiding close neighbours.

Two studies in macaque (Malach *et al.* 1993) and tree shrew (Bosking *et al.* 1997) combined intrinsic signal imaging and anatomical tracing to study a potential relationship between short-range connections and orientation preference maps. Anatomically determined connections were overlaid with the orientation preference map and showed that short-range connections are however rather unselective with respect to orientation preference of a given neuron. Furthermore, intracellular recording studies in cats found a broader tuning for neurons near pinwheel centres than within iso-orientation domains (Schummers *et al.* 2002; Mariño *et al.* 2005). Strong subthreshold responses of cells near pinwheel centres to all stimulus orientations, even including the one orthogonal to a cell's preferred orientation, indicate that these cells receive inputs in a rather unselective manner (Schummers *et al.* 2002). But studies, like Maldonado *et al.* (1997), also report similar orientation tuning width of spiking activity for cells close to pinwheel centres and those further away. However, a recent study (Nauhaus *et al.* 2008) carried out in macaque and cat combining intrinsic signal imaging with electrode array recordings found that the degree of orientation tuning of individual neurons was correlated with the homogeneity of the local orientation preference map. Neurons in centre of an iso-orientation domain exhibited the sharpest tuning, while cells near pinwheel centres tended to have broad tuning (Ohki *et al.* 2006; Nauhaus *et al.* 2008). Moreover, narrower orientation tuning in iso-orientation domains was also found to depend on pinwheel density. In comparison to macaques, cats have low densities of pinwheel centres, equivalent to higher levels of homogeneity, which is in turn reflected by sharper orientation tuning of neurons (Nauhaus *et al.* 2008).

Most studies of local connectivity rely on anatomical bulk labelling or indirect inference of synaptic connectivity (whole-cell recordings, spike train correlations). It would be critical to learn more about local connectivity rules by combing functional imaging with

genetic tools to identify distinct cell types or trace individual cells and their connections (Wickersham *et al.* 2007).

A recent study in mouse using genetic labels and calcium imaging showed that inhibitory neurons resemble closely orientation tuning of the local network whereas excitatory neurons exhibit strong orientation tuning independent of the surrounding population response (Kerlin *et al.* 2010). It suggests that different connectivity rules may apply for different cell types which led to ambivalent results in studies examining the degree of orientation tuning of individual neurons within an orientation preference map (Maldonado *et al.* 1997; Schummers *et al.* 2002; Nauhaus *et al.* 2008).

Together, these data seem to suggest that local intracortical connections are relatively unspecific, and that a given neuron simply pools the preferred orientations of its local neighbours. In line with this, species lacking orientation maps at all (Metin *et al.* 1988) show slightly weaker overall orientation tuning (Ohki *et al.* 2005).

One example for highly specific connections are long-range axons which form clusters and link domains that share the same preferred orientation (Gilbert and Wiesel 1989; Malach *et al.* 1993; Bosking *et al.* 1997). This patchy layout of horizontal connectivity was not observed in species lacking orientation preference maps (Burkhalter 1989; Rumberger *et al.* 2001) raising the question whether neurons with similar orientation preferences are connected in rodents.

Although our current knowledge about connectivity does not explain the potential biological function of orientation preference maps, there is theoretical evidence that intracortical connectivity and wiring length optimisation could give rise to different functional architectures in different species. Overlapping maps of orientation preference, ocular dominance and spatial frequency are arranged in an optimal fashion to maximise coverage (Swindale *et al.* 2000), i.e. maps are a solution for the optimal mapping of a multi-dimensional feature space onto a two-dimensional cortical surface, as also predicted by theoretical models (Swindale 1992). However, randomly intermingled cells result in much better coverage, however with the cost of disrupting map continuity, which is thought to be important for minimizing the length of axons (Durbin and Mitchison 1990; Swindale *et al.* 2000).

Further models suggested that differences in the connectivity rules of intracortical circuits account for different functional layouts. The existence of pinwheels and fractures are necessary to optimise wiring length in some cases, whereas a "salt-and-pepper" layout of orientation selectivity, as seen in rodents, is more efficient for other forms of intracortical connectivity (Koulakov and Chklovskii 2001; Chklovskii and Koulakov 2004).

4.5 Perspectives for future research

Earlier studies using optical imaging followed the development of orientation preference maps chronically in the same animal (Chapman *et al.* 1996; Gödecke *et al.* 1997). While synthetic calcium indicators are not suitable for chronic imaging, the advent of novel genetically encoded calcium indicators (Mank *et al.* 2008; Tian *et al.* 2009) raises the opportunity to selectively follow the transition between different developmental stages of map formation in individual neurons in the same animal. Cell-type specific labelling and identification (Kerlin *et al.* 2010; Runyan *et al.* 2010) will allow further insights into the complexity of cortical circuits during development. In conjunction with chronic imaging, the use of optogenetic tools (Boyden *et al.* 2005; Zhang *et al.* 2007) to reduce or perturb activity patterns in the immature cortex will foster the investigation of the role of intrinsic activity and its potential influence on the emergence and stabilization of orientation preference maps (Weliky and Katz 1997; Schuett *et al.* 2001; Sohal *et al.* 2009). Ideally, such experiments should be carried out in awake animals, since patterned network activity is partially occluded by anaesthesia (Chiu and Weliky 2001; Colonnese and Khazipov 2010).

In conclusion, the results of this thesis demonstrate that the development of orientation preference maps is a process not only of refinement but also of functional reorganization, which is exquisitely coordinated between cells. Understanding the mechanisms of functional reorganization during development will certainly gain knowledge to model cortical dynamics, and may also lead towards complementary insights into the integration of neurons into mature networks.

Bibliography

Adelsberger, H., Garaschuk, O., Konnerth, A. 2005. Cortical calcium waves in resting new-born mice. *Nature Neuroscience,* 8:988-90.

Adorjan, P., Levitt, J. B., Lund, J. S., Obermayer, K. 1999. A model for the intracortical origin of orientation preference and tuning in macaque striate cortex. *Visual Neuroscience,* 16:303-18.

Akerman, C. J., Grubb, M. S., Thompson, I. D. 2004. Spatial and temporal properties of visual responses in the thalamus of the developing ferret. *Journal of Neuroscience,* 24:170-82.

Akerman, C. J., Smyth, D., Thompson, I. D. 2002. Visual experience before eye-opening and the development of the retinogeniculate pathway. *Neuron,* 36:869-79.

Alonso, J. M., Usrey, W. M., Reid, R. C. 1996. Precisely correlated firing in cells of the lateral geniculate nucleus. *Nature,* 383:815-9.

Bandyopadhyay, S., Shamma, S. A., Kanold, P. O. 2010. Dichotomy of functional organization in the mouse auditory cortex. *Nature Neuroscience,* 13:361-8.

Barlow, H. B., Pettigrew, J. D. 1971. Lack of specificity of neurones in the visual cortex of young kittens. *Journal of Physiology,* 218:98-100.

Bartfeld, E., Grinvald, A. 1992. Relationships between orientation-preference pinwheels, cytochrome oxidase blobs, and ocular-dominance columns in primate striate cortex. *Proceedings of the National Academy of Sciences of the United States of America,* 89:11905-9.

Bass, M., DeCusatis, C., Enoch, J. M., Lakshminarayanan, V., Li, G., MacDonald, C., Stryland, E. V. 2010. *The Handbook of Optics* (3rd ed. Vol. 3): McGraham-Hill.

Batschelet, E. 1981. *Circular Statistics in Biology*. London: Academic Press.

Bauer, R., Dow, B. M., Vautin, R. G. 1980. Laminar distribution of preferred orientations in foveal striate cortex of the monkey. *Experimental Brain Research,* 41:54-60.

Ben-Yishai, R., Bar-Or, R. L., Sompolinsky, H. 1995. Theory of orientation tuning in visual cortex. *Proceedings of the National Academy of Sciences, USA,* 92:3844-8.

Berger, T., Borgdorff, A., Crochet, S., Neubauer, F. B., Lefort, S., Fauvet, B., Ferezou, I., Carleton, A., Lüscher, H.-R., Petersen, C. C. H. 2007. Combined voltage and calcium epifluorescence imaging in vitro and in vivo reveals subthreshold and suprathreshold dynamics of mouse barrel cortex. *Journal of Neurophysiology,* 97:3751-62.

Bishop, P. O., Burke, W., Davis, R. 1958. Synapse discharge by single fibre in mammalian visual system. *Nature,* 182:728-30.

Bishop, P. O., Burke, W., Davis, R. 1962. The interpretation of the extracellular response of single lateral geniculate cells. *Journal of Physiology,* 162:451-72.

Bishop, P. O., Coombs, J. S., Henry, G. H. 1973. Receptive fields of simple cells in the cat striate cortex. *Journal of Physiology,* 231:31-60.

Bishop, P. O., Henry, G. H. 1972. Striate neurons: receptive field concepts. *Investigative Ophthalmology,* 11:346-54.

Blakemore, C., Sluyters, R. C. V. 1975. Innate and environmental factors in the development of the kitten's visual cortex. *Journal of Physiology,* 248:663-716.

Blankenship, A. G., Ford, K. J., Johnson, J., Seal, R. P., Edwards, R. H., Copenhagen, D. R., Feller, M. B. 2009. Synaptic and extrasynaptic factors governing glutamatergic retinal waves. *Neuron,* 62:230-41.

Blasdel, G. G. 1992. Orientation selectivity, preference, and continuity in monkey striate cortex. *Journal of Neuroscience,* 12:3139-61.

Blasdel, G. G., Fitzpatrick, D. 1984. Physiological organization of layer 4 in macaque striate cortex. *Journal of Neuroscience,* 4:880-95.

Blasdel, G. G., Salama, G. 1986. Voltage-sensitive dyes reveal a modular organization in monkey striate cortex. *Nature,* 321:579-85.

Bonhoeffer, T., Grinvald, A. 1991. Iso-orientation domains in cat visual cortex are arranged in pinwheel-like patterns. *Nature,* 353:429-31.

Bonhoeffer, T., Grinvald, A. 1993. The layout of iso-orientation domains in area 18 of cat visual cortex: optical imaging reveals a pinwheel-like organization. *Journal of Neuroscience,* 13:4157-80.

Bonhoeffer, T., Grinvald, A. 1996. Optical imaging based on intrinsic signals: The Methodology. In Toga, A. W. & Mazziotta, J. C. (Eds.), *Brain Mapping: The Methods* (1 ed., pp. 75-97): Academic Press.

Bonhoeffer, T., Kim, D. S., Malonek, D., Shoham, D., Grinvald, A. 1995. Optical imaging of the layout of functional domains in area 17 and across the area 17/18 border in cat visual cortex. *European Journal of Neuroscience,* 7:1973-88.

Borg-Graham, L. J., Monier, C., Fregnac, Y. 1998. Visual input evokes transient and strong shunting inhibition in visual cortical neurons. *Nature,* 393:369-73.

Bosking, W. H., Zhang, Y., Schofield, B., Fitzpatrick, D. 1997. Orientation selectivity and the arrangement of horizontal connections in tree shrew striate cortex. *Journal of Neuroscience,* 17:2112-27.

Bourgeois, J. P., Rakic, P. 1993. Changes of synaptic density in the primary visual cortex of the macaque monkey from fetal to adult stage. *Journal of Neuroscience,* 13:2801-20.

Bourne, H. R., Nicoll, R. 1993. Molecular machines integrate coincident synaptic signals. *Cell,* 72:65-75.

Bowling, D. B., Caverhill, J. I. 1989. ON/OFF organization in the cat lateral geniculate nucleus: sublaminae vs. columns. *Journal of Computational Biology,* 283:161-8.

Boyden, E. S., Zhang, F., Bamberg, E., Nagel, G., Deisseroth, K. 2005. Millisecond-timescale, genetically targeted optical control of neural activity. *Nature Neuroscience,* 8:1263-8.

Brainard, D. H. 1997. The Psychophysics Toolbox. *Spatial Vision,* 10:433-6.

Bullier, J., Henry, G. H. 1980. Ordinal position and afferent input of neurons in monkey striate cortex. *Journal of Comparative Neurology,* 193:913-35.

Burkhalter, A. 1989. Intrinsic connections of rat primary visual cortex: laminar organization of axonal projections. *Journal of Comparative Neurology,* 279:171-86.

Cang, J., Kaneko, M., Yamada, J., Woods, G., Stryker, M. P., Feldheim, D. A. 2005. Ephrin-as guide the formation of functional maps in the visual cortex. *Neuron,* 48:577-89.

Cang, J., Niell, C. M., Liu, X., Pfeiffenberger, C., Feldheim, D. A., Stryker, M. P. 2008. Selective disruption of one Cartesian axis of cortical maps and receptive fields by deficiency in ephrin-As and structured activity. *Neuron,* 57:511-23.

Chalupa, L. M., Snider, C. J. 1998. Topographic specificity in the retinocollicular projection of the developing ferret: an anterograde tracing study. *Journal of Comparative Neurology,* 392:35-47.

Chan, C., Smith, G., Jacobs, R. J. 1985. Simulating refractive errors: source and observer methods. *American Journal of Optometry and Physiological Optics,* 62:207-16.

Chapman, B., Bonhoeffer, T. 1998. Overrepresentation of horizontal and vertical orientation preferences in developing ferret area 17. *Proceedings of the National Academy of Sciences of the United States of America,* 95:2609-14.

Chapman, B., Gödecke, I. 2000. Cortical cell orientation selectivity fails to develop in the absence of ON-center retinal ganglion cell activity. *Journal of Neuroscience,* 20:1922-30.

Chapman, B., Stryker, M. P. 1993. Development of orientation selectivity in ferret visual cortex and effects of deprivation. *Journal of Neuroscience,* 13:5251-62.

Chapman, B., Stryker, M. P., Bonhoeffer, T. 1996. Development of orientation preference maps in ferret primary visual cortex. *Journal of Neuroscience,* 16:6443-53.

Chapman, B., Zahs, K. R., Stryker, M. P. 1991. Relation of cortical cell orientation selectivity to alignment of receptive fields of the geniculocortical afferents that arborize within a single orientation column in ferret visual cortex. *Journal of Neuroscience,* 11:1347-58.

Chen, Y., Flanagan, J. G. 2006. Follow your nose: axon pathfinding in olfactory map formation. *Cell,* 127:881-4.

Chiu, C., Weliky, M. 2001. Spontaneous activity in developing ferret visual cortex in vivo. *Journal of Neuroscience,* 21:8906-14.

Chiu, C., Weliky, M. 2002. Relationship of correlated spontaneous activity to functional ocular dominance columns in the developing visual cortex. *Neuron,* 35:1123-34.

Chklovskii, D. B., Koulakov, A. A. 2004. Maps in the brain: What can we learn from them? *Annual Review of Neuroscience,* 27:369-92.

Choi, M., Weiss, S., Schaeffel, F., Seidemann, A., Howland, H. C., Wilhelm, B., Wilhelm, H. 2000. Laboratory, clinical, and kindergarten test of a new eccentric infrared photorefractor (PowerRefractor). *Optometry and Vision Science,* 77:537-48.

Chung, S., Ferster, D. 1998. Strength and orientation tuning of the thalamic input to simple cells revealed by electrically evoked cortical suppression. *Neuron,* 20:1177-89.

Clarke, P. G., Donaldson, I. M., Whitteridge, D. 1976. Binocular visual mechanisms in cortical areas I and II of the sheep. *Journal of Physiology,* 256:509-26.

Cleland, B. G., Dubin, M. W., Levick, W. R. 1971a. Simultaneous recording of input and output of lateral geniculate neurones. *Nature New Biology,* 231:191-2.

Cleland, B. G., Dubin, M. W., Levick, W. R. 1971b. Sustained and transient neurones in the cat's retina and lateral geniculate nucleus. *Journal of Physiology,* 217:473-96.

Colonnese, M. T., Kaminska, A., Minlebaev, M., Milh, M., Bloem, B., Lescure, S., Moriette, G., Chiron, C., Ben-Ari, Y., Khazipov, R. 2010. A conserved switch in sensory processing prepares developing neocortex for vision. *Neuron,* 67:480-98.

Colonnese, M. T., Khazipov, R. 2010. "Slow activity transients" in infant rat visual cortex:a spreading synchronous oscillation patterned by retinal waves. *Journal of Neuroscience,* 30:4325-37.

Cooper, H. M., Herbin, M., Nevo, E. 1993. Visual system of a naturally microphthalmic mammal: the blind mole rat, Spalax ehrenbergi. *Journal of Comparative Neurology,* 328:313-50.

Coppola, D. M., White, L. E. 2004. Visual experience promotes the isotropic representation of orientation preference. *Visual Neuroscience,* 21:39-51.

Coppola, D. M., White, L. E., Fitzpatrick, D., Purves, D. 1998. Unequal representation of cardinal and oblique contours in ferret visual cortex. *Proceedings of the National Academy of Sciences, USA,* 95:2621-3.

Cragg, B. G. 1975. The development of synapses in the visual system of the cat. *Journal of Comparative Neurology,* 160:147-66.

Crair, M. C., Gillespie, D. C., Stryker, M. P. 1998. The role of visual experience in the development of columns in cat visual cortex. *Science,* 279:566-70.

Crowley, J. C., Katz, L. C. 1999. Development of ocular dominance columns in the absence of retinal input. *Nature Neuroscience,* 2:1125-30.

Crowley, J. C., Katz, L. C. 2000. Early development of ocular dominance columns. *Science,* 290:1321-4.

de la Cera, E. G., Rodriguez, G., Llorente, L., Schaeffel, F., Marcos, S. 2006. Optical aberrations in the mouse eye. *Vision Research,* 46:2546-53.

DiCarlo, J. J., Lane, J. W., Hsiao, S. S., Johnson, K. O. 1996. Marking microelectrode penetrations with fluorescent dyes. *Journal of Neuroscience Methods,* 64:75-81.

Douglas, R. J., Martin, K. A. C. 2004. Neuronal circuits of the neocortex. *Annual Review of Neuroscience,* 27:419-51.

Durack, J. C., Katz, L. C. 1996. Development of horizontal projections in layer 2/3 of ferret visual cortex. *Cerebral Cortex,* 6:178-83.

Durbin, R., Mitchison, G. 1990. A dimension reduction framework for understanding cortical maps. *Nature,* 343:644-7.

Enroth-Cugell, C., Robson, J. G. 1966. The contrast sensitivity of retinal ganglion cells of the cat. *Journal of Physiology,* 187:517-52.

Erisir, A., Harris, J. L. 2003. Decline of the critical period of visual plasticity is concurrent with the reduction of NR2B subunit of the synaptic NMDA receptor in layer 4. *Journal of Neuroscience,* 23:5208-18.

Felleman, D. J., Van Essen, D. C. 1991. Distributed hierarchical processing in the primate cerebral cortex. *Cerebral Cortex,* 1:1-47.

Feller, M. B., Butts, D. A., Aaron, H. L., Rokhsar, D. S., Shatz, C. J. 1997. Dynamic processes shape spatiotemporal properties of retinal waves. *Neuron,* 19:293-306.

Ferster, D., Chung, S., Wheat, H. 1996. Orientation selectivity of thalamic input to simple cells of cat visual cortex. *Nature,* 380:249-52.

Ferster, D., Lindstrom, S. 1983. An intracellular analysis of geniculo-cortical connectivity in area 17 of the cat. *Journal of Physiology,* 342:181-215.

Flanagan, J. G. 2006. Neural map specification by gradients. *Current Opinion in Neurobiology,* 16:59-66.

Freeman, R. D., Sclar, G., Ohzawa, I. 1983. An electrophysiological comparison of convergent and divergent strabismus in the cat: visual evoked potentials. *Journal of Neurophysiology,* 49:227-37.

Freygang, W. H., Jr. 1958. An analysis of extracellular potentials from single neurons in the lateral geniculate nucleus of the cat. *Journal of General Physiology,* 41:543-64.

Gao, W. J., Newman, D. E., Wormington, A. B., Pallas, S. L. 1999. Development of inhibitory circuitry in visual and auditory cortex of postnatal ferrets: immunocytochemical localization of GABAergic neurons. *Journal of Comparative Neurology,* 409:261-73.

Gao, W. J., Wormington, A. B., Newman, D. E., Pallas, S. L. 2000. Development of inhibitory circuitry in visual and auditory cortex of postnatal ferrets: immunocytochemical localization of calbindin- and parvalbumin-containing neurons. *Journal of Comparative Neurology,* 422:140-57.

Garaschuk, O., Linn, J., Eilers, J., Konnerth, A. 2000. Large-scale oscillatory calcium waves in the immature cortex. *Nature Neuroscience,* 3:452-9.

Gekeler, F., Schaeffel, F., Howland, H. C., Wattam-Bell, J. 1997. Measurement of astigmatism by automated infrared photoretinoscopy. *Optometry and Vision Science,* 74:472-82.

Gilbert, C. D. 1977. Laminar differences in receptive field properties of cells in cat primary visual cortex. *Journal of Physiology,* 268:391-421.

Gilbert, C. D., Wiesel, T. N. 1989. Columnar specificity of intrinsic horizontal and cortico-cortical connections in cat visual cortex. *Journal of Neuroscience,* 9:2432-42.

Girman, S. V., Sauve, Y., Lund, R. D. 1999. Receptive field properties of single neurons in rat primary visual cortex. *Journal of Neurophysiology,* 82:301-11.

Glickstein, M., Millodot, M. 1970. Retinoscopy and eye size. *Science,* 168:605-6.

Göbel, W., Kampa, B. M., Helmchen, F. 2007. Imaging cellular network dynamics in three dimensions using fast 3D laser scanning. *Nature Methods,* 4:73-9.

Gödecke, I., Kim, D. S., Bonhoeffer, T., Singer, W. 1997. Development of orientation preference maps in area 18 of kitten visual cortex. *European Journal of Neuroscience,* 9:1754-62.

Godement, P., Salaun, J., Imbert, M. 1984. Prenatal and postnatal development of retinogeniculate and retinocollicular projections in the mouse. *Journal of Comparative Neurology,* 230:552-75.

Goodman, C. S., Shatz, C. J. 1993. Developmental mechanisms that generate precise patterns of neuronal connectivity. *Cell,* 72:77-98.

Grewe, B. F., Langer, D., Kasper, H., Kampa, B. M., Helmchen, F. 2010. High-speed in vivo calcium imaging reveals neuronal network activity with near-millisecond precision. *Nat Methods,* 7:399-405.

Grinvald, A., Lieke, E., Frostig, R. D., Gilbert, C. D., Wiesel, T. N. 1986. Functional architecture of cortex revealed by optical imaging of intrinsic signals. *Nature,* 324:361-4.

Guido, W., Sherman, S. M. 1998. Response latencies of cells in the cat's lateral geniculate nucleus are less variable during burst than tonic firing. *Visual Neuroscience,* 15:231-7.

Hammond, P. 1994. Binocular attributes of length summation and end stopping in cat striate cortex. *Proceedings: Biological Sciences,* 258:169-74.

Hanganu, I. L., Ben-Ari, Y., Khazipov, R. 2006. Retinal waves trigger spindle bursts in the neonatal rat visual cortex. *Journal of Neuroscience,* 26:6728-36.

Harder, D. R., Alkayed, N. J., Lange, A. R., Gebremedhin, D., Roman, R. J. 1998. Functional hyperemia in the brain: hypothesis for astrocyte-derived vasodilator metabolites. *Stroke,* 29:229-34.

Hawken, M. J., Parker, A. J. 1984. Contrast sensitivity and orientation selectivity in lamina IV of the striate cortex of Old World monkeys. *Experimental Brain Research,* 54:367-72.

Haydon, P. G., Carmignoto, G. 2006. Astrocyte control of synaptic transmission and neurovascular coupling. *Physiological Reviews,* 86:1009-31.

Heimel, J. A., Hooser, S. D. V., Nelson, S. B. 2005. Laminar organization of response properties in primary visual cortex of the gray squirrel (Sciurus carolinensis). *Journal of Neurophysiology,* 94:3538-54.

Helmchen, F., Denk, W. 2005. Deep tissue two-photon microscopy. *Nature Methods,* 2:932-40.

Henry, G. H., Bishop, P. O., Dreher, B. 1974. Orientation, axis and direction as stimulus parameters for striate cells. *Vision Research,* 14:767-77.

Hensch, T. K. 2004. Critical period regulation. *Annual Review of Neuroscience,* 27:549-79.

Hernández-Guerra, A. M., Rodilla, V., López-Murcia, M. M. 2007. Ocular biometry in the adult anesthetized ferret (Mustela putorius furo). *Veterinary Ophthalmology,* 10:50-2.

Hirsch, J. A., Alonso, J. M., Reid, R. C. 1995. Visually evoked calcium action potentials in cat striate cortex. *Nature,* 378:612-6.

Horton, J. C., Adams, D. L. 2005. The cortical column: a structure without a function. *Philosophical Transactions of the Royal Society of London. Series B, Biological Sciences,* 360:837-62.

Hubel, D. H., Wiesel, T. N. 1959. Receptive fields of single neurones in the cat's striate cortex. *Journal of Physiology,* 148:574-91.

Hubel, D. H., Wiesel, T. N. 1961. Integrative action in the cat's lateral geniculate body. *Journal of Physiology,* 155:385-98.

Hubel, D. H., Wiesel, T. N. 1962. Receptive fields, binocular interaction and functional architecture in the cat's visual cortex. *Journal of Physiology,* 160:106-54.

Hubel, D. H., Wiesel, T. N. 1963. Shape and arrangement of columns in cat's striate cortex. *Journal of Physiology,* 165:559-68.

Hubel, D. H., Wiesel, T. N. 1977. Ferrier lecture. Functional architecture of macaque monkey visual cortex. *Proceedings of the Royal Society of London, Series B: Biological Sciences,* 198:1-59.

Hubel, D. H., Wiesel, T. N., Stryker, M. P. 1978. Anatomical demonstration of orientation columns in macaque monkey. *Journal of Comparative Neurology,* 177:361-80.

Hübener, M., Bonhoeffer, T. 2002. Optical Imaging of Functional Architecture in Cat Primary Visual Cortex. In Payne, B. R. & Peters, A. (Eds.), *The Cat Primary Visual Cortex* (pp. 131-66). San Diego: Academic Press.

Hübener, M., Shoham, D., Grinvald, A., Bonhoeffer, T. 1997. Spatial relationships among three columnar systems in cat area 17. *Journal of Neuroscience,* 17:9270-84.

Huberman, A. D., Feller, M. B., Chapman, B. 2008. Mechanisms underlying development of visual maps and receptive fields. *Annual Review of Neuroscience,* 31:479-509.

Humphrey, A. L., Norton, T. T. 1980. Topographic organization of the orientation column system in the striate cortex of the tree shrew (Tupaia glis). I. Microelectrode recording. *Journal of Comparative Neurology,* 192:531-47.

Jackson, C. A., Hickey, T. L. 1985. Use of ferrets in studies of the visual system. *Laboratory Animal Science,* 35:211-5.

Jia, H., Rochefort, N. L., Chen, X., Konnerth, A. 2010. Dendritic organization of sensory input to cortical neurons in vivo. *Nature,* 464:1307-12.

Kaplan, E., Purpura, K., Shapley, R. M. 1987. Contrast affects the transmission of visual information through the mammalian lateral geniculate nucleus. *Journal of Physiology,* 391:267-88.

Kara, P., Pezaris, J. S., Yurgenson, S., Reid, R. C. 2002. The spatial receptive field of thalamic inputs to single cortical simple cells revealed by the interaction of visual and electrical stimulation. *Proceedings of the National Academy of Sciences of the United States of America,* 99:16261-6.

Katz, L. C., Crowley, J. C. 2002. Development of cortical circuits: lessons from ocular dominance columns. *Nature Reviews: Neuroscience,* 3:34-42.

Kerlin, A. M., Andermann, M. L., Berezovskii, V. K., Reid, R. C. 2010. Broadly tuned response properties of diverse inhibitory neuron subtypes in mouse visual cortex. *Neuron,* 67:858-71.

Kerr, J. N. D., Denk, W. 2008. Imaging in vivo: watching the brain in action. *Nature Reviews Neuroscience,* 9:195-205.

Kerr, J. N. D., Greenberg, D., Helmchen, F. 2005. Imaging input and output of neocortical networks in vivo. *Proceedings of the National Academy of Sciences of the United States of America,* 102:14063-8.

Kerschensteiner, D., Wong, R. O. 2008. A precisely timed asynchronous pattern of ON and OFF retinal ganglion cell activity during propagation of retinal waves. *Neuron,* 58:851-8.

Koulakov, A. A., Chklovskii, D. B. 2001. Orientation preference patterns in mammalian visual cortex: a wire length minimization approach. *Neuron,* 29:519-27.

Krubitzer, L., Kaas, J. 2005. The evolution of the neocortex in mammals: how is phenotypic diversity generated? *Current Opinion in Neurobiology,* 15:444-53.

Krug, K., Akerman, C. J., Thompson, I. D. 2001. Responses of neurons in neonatal cortex and thalamus to patterned visual stimulation through the naturally closed lids. *Journal of Neurophysiology,* 85:1436-43.

Kuffler, S. W. 1953. Discharge patterns and functional organization of mammalian retina. *Journal of Neurophysiology,* 16:37-68.

Law, M. I., Zahs, K. R., Stryker, M. P. 1988. Organization of primary visual cortex (area 17) in the ferret. *Journal of Comparative Neurology,* 278:157-80.

Lemke, G., Reber, M. 2005. Retinotectal mapping: new insights from molecular genetics. *Annual Review of Cell and Developmental Biology,* 21:551-80.

Leventhal, A. G., Thompson, K. G., Liu, D., Zhou, Y., Ault, S. J. 1995. Concomitant sensitivity to orientation, direction, and color of cells in layers 2, 3, and 4 of monkey striate cortex. *Journal of Neuroscience,* 15:1808-18.

Levick, W. R., Cleland, B. G., Dubin, M. W. 1972. Lateral geniculate neurons of cat: retinal inputs and physiology. *Investigative Ophthalmology,* 11:302-11.

Li, B., Peterson, M. R., Freeman, R. D. 2003. Oblique effect: a neural basis in the visual cortex. *Journal of Neurophysiology,* 90:204-17.

Li, Y., Fitzpatrick, D., White, L. E. 2006. The development of direction selectivity in ferret visual cortex requires early visual experience. *Nature Neuroscience,* 9:676-81.

Li, Y., Hooser, S. D. V., Mazurek, M., White, L. E., Fitzpatrick, D. 2008. Experience with moving visual stimuli drives the early development of cortical direction selectivity. *Nature,* 456:952-6.

Linden, D. C., Guillery, R. W., Cucchiaro, J. 1981. The dorsal lateral geniculate nucleus of the normal ferret and its postnatal development. *Journal of Comparative Neurology,* 203:189-211.

Maffei, L., Galli-Resta, L. 1990. Correlation in the discharges of neighboring rat retinal ganglion cells during prenatal life. *Proceedings of the National Academy of Sciences, USA,* 87:2861-4.

Majewska, A., Yiu, G., Yuste, R. 2000. A custom-made two-photon microscope and deconvolution system. *Pflugers Archiv,* 441:398-408.

Malach, R., Amir, Y., Harel, M., Grinvald, A. 1993. Relationship between intrinsic connections and functional architecture revealed by optical imaging and in vivo targeted biocytin injections in primate striate cortex. *Proceedings of the National Academy of Sciences, USA,* 90:10469-73.

Maldonado, P. E., Gödecke, I., Gray, C. M., Bonhoeffer, T. 1997. Orientation selectivity in pinwheel centers in cat striate cortex. *Science,* 276:1551-5.

Mank, M., Santos, A. F., Direnberger, S., Mrsic-Flogel, T. D., Hofer, S. B., Stein, V., Hendel, T., Reiff, D. F., Levelt, C., Borst, A., Bonhoeffer, T., Hübener, M., Griesbeck, O. 2008. A genetically encoded calcium indicator for chronic in vivo two-photon imaging. *Nature Methods,* 5:805-11.

Mao, B. Q., Hamzei-Sichani, F., Aronov, D., Froemke, R. C., Yuste, R. 2001. Dynamics of spontaneous activity in neocortical slices. *Neuron,* 32:883-98.

Mardia, K. V. 1972. *Statistics of directional data*. London: Academic Press.

Mariño, J., Schummers, J., Lyon, D. C., Schwabe, L., Beck, O., Wiesing, P., Obermayer, K., Sur, M. 2005. Invariant computations in local cortical networks with balanced excitation and inhibition. *Nature Neuroscience,* 8:194-201.

Martinez, L. M., Wang, Q., Reid, R. C., Pillai, C., Alonso, J. M., Sommer, F. T., Hirsch, J. A. 2005. Receptive field structure varies with layer in the primary visual cortex. *Nature Neuroscience,* 8:372-9.

McConnell, S. K., LeVay, S. 1986. Anatomical organization of the visual system of the mink, Mustela vison. *Journal of Comparative Neurology,* 250:109-32.

McLaughlin, D., Shapley, R., Shelley, M., Wielaard, D. J. 2000. A neuronal network model of macaque primary visual cortex (V1): orientation selectivity and dynamics in the input layer 4Calpha. *Proceedings of the National Academy of Sciences, USA,* 97:8087-92.

McLaughlin, T., O'Leary, D. D. 2005. Molecular gradients and development of retinotopic maps. *Annual Review of Neuroscience,* 28:327-55.

Meister, M., Wong, R. O., Baylor, D. A., Shatz, C. J. 1991. Synchronous bursts of action potentials in ganglion cells of the developing mammalian retina. *Science,* 252:939-43.

Metin, C., Godement, P., Imbert, M. 1988. The primary visual cortex in the mouse: receptive field properties and functional organization. *Experimental Brain Research,* 69:594-612.

Miller, K. D. 1992. Development of orientation columns via competition between ON- and OFF-center inputs. *Neuroreport,* 3:73-6.

Miller, K. D. 1994. A model for the development of simple cell receptive fields and the ordered arrangement of orientation columns through activity-dependent competition between ON- and OFF-center inputs. *Journal of Neuroscience,* 14:409-41.

Miller, K. D., Erwin, E., Kayser, A. 1999. Is the development of orientation selectivity instructed by activity? *Journal of Neurobiology,* 41:44-57.

Monier, C., Chavane, F., Baudot, P., Graham, L. J., Frégnac, Y. 2003. Orientation and direction selectivity of synaptic inputs in visual cortical neurons: a diversity of combinations produces spike tuning. *Neuron,* 37:663-80.

Mooney, R., Penn, A. A., Gallego, R., Shatz, C. J. 1996. Thalamic relay of spontaneous retinal activity prior to vision. *Neuron,* 17:863-74.

Murphy, E. H., Berman, N. 1979. The rabbit and the cat: a comparison of some features of response properties of single cells in the primary visual cortex. *The Journal of Comparative Neurology,* 188:401-27.

Murphy, P. C., Sillito, A. M. 1987. Corticofugal feedback influences the generation of length tuning in the visual pathway. *Nature,* 329:727-9.

Nauhaus, I., Benucci, A., Carandini, M., Ringach, D. L. 2008. Neuronal selectivity and local map structure in visual cortex. *Neuron,* 57:673-9.

Niell, C. M., Stryker, M. P. 2008. Highly selective receptive fields in mouse visual cortex. *Journal of Neuroscience,* 28:7520-36.

Nimmerjahn, A. 2009. Astrocytes going live: advances and challenges. *Journal of Physiology,* 587:1639-47.

Nimmerjahn, A., Kirchhoff, F., Kerr, J. N. D., Helmchen, F. 2004. Sulforhodamine 101 as a specific marker of astroglia in the neocortex in vivo. *Nature Methods,* 1:31-7.

Ohki, K., Chung, S., Ch'ng, Y. H., Kara, P., Reid, R. C. 2005. Functional imaging with cellular resolution reveals precise micro-architecture in visual cortex. *Nature,* 433:597-603.

Ohki, K., Chung, S., Kara, P., Hübener, M., Bonhoeffer, T., Reid, R. C. 2006. Highly ordered arrangement of single neurons in orientation pinwheels. *Nature,* 442:925-8.

Ohki, K., Reid, R. C. 2007. Specificity and randomness in the visual cortex. *Current Opinion in Neurobiology,* 17:401-7.

Pelli, D. G. 1997. The VideoToolbox software for visual psychophysics: transforming numbers into movies. *Spatial Vision,* 10:437-42.

Pettigrew, J. D. 1974. The effect of visual experience on the development of stimulus specificity by kitten cortical neurones. *Journal of Physiology,* 237:49-74.

Pfleger, B., Bonds, A. B. 1995. Dynamic differentiation of GABAA-sensitive influences on orientation selectivity of complex cells in the cat striate cortex. *Experimental Brain Research,* 104:81-8.

Plas, D. T., Lopez, J. E., Crair, M. C. 2005. Pretarget sorting of retinocollicular axons in the mouse. *Journal of Comparative Neurology,* 491:305-19.

Poskanzer, K., Needleman, L. A., Bozdagi, O., Huntley, G. W. 2003. N-cadherin regulates ingrowth and laminar targeting of thalamocortical axons. *Journal of Neuroscience,* 23:2294-305.

Priebe, N. J., Ferster, D. 2005. Direction selectivity of excitation and inhibition in simple cells of the cat primary visual cortex. *Neuron,* 45:133-45.

Ramoa, A. S., Mower, A. F., Liao, D., Jafri, S. I. 2001. Suppression of cortical NMDA receptor function prevents development of orientation selectivity in the primary visual cortex. *Journal of Neuroscience,* 21:4299-309.

Rao, S. C., Toth, L. J., Sur, M. 1997. Optically imaged maps of orientation preference in primary visual cortex of cats and ferrets. *Journal of Comparative Neurology,* 387:358-70.

Reid, R. C., Alonso, J. M. 1995. Specificity of monosynaptic connections from thalamus to visual cortex. *Nature,* 378:281-4.

Reid, R. C., Alonso, J. M. 1996. The processing and encoding of information in the visual cortex. *Current Opinion in Neurobiology,* 6:475-80.

Roberts, E. B., Ramoa, A. S. 1999. Enhanced NR2A subunit expression and decreased NMDA receptor decay time at the onset of ocular dominance plasticity in the ferret. *Journal of Neurophysiology,* 81:2587-91.

Rumberger, A., Tyler, C. J., Lund, J. S. 2001. Intra- and inter-areal connections between the primary visual cortex V1 and the area immediately surrounding V1 in the rat. *Neuroscience,* 102:35-52.

Runyan, C. A., Schummers, J., Van Wart, A., Kuhlman, S. J., Wilson, N. R., Huang, Z. J., Sur, M. 2010. Response features of parvalbumin-expressing interneurons suggest precise roles for subtypes of inhibition in visual cortex. *Neuron,* 67:847-57.

Ruthazer, E. S., Stryker, M. P. 1996. The role of activity in the development of long-range horizontal connections in area 17 of the ferret. *Journal of Neuroscience,* 16:7253-69.

Sato, H., Katsuyama, N., Tamura, H., Hata, Y., Tsumoto, T. 1996. Mechanisms underlying orientation selectivity of neurons in the primary visual cortex of the macaque. *Journal of Physiology,* 494:757-71.

Schaeffel, F., Farkas, L., Howland, H. C. 1987. Infrared photoretinoscope. *Applied Optics,* 26:1505-9.

Schaeffel, F., Queiroz, A. d. 1990. Alternative Mechanisms of Enhanced Underwater Vision in the Garter Snakes Thamnophis melanogaster and T. couchii. *Copeia,* 1:50-8.

Schuett, S., Bonhoeffer, T., Hubener, M. 2002. Mapping retinotopic structure in mouse visual cortex with optical imaging. *Journal of Neuroscience,* 22:6549-59.

Schuett, S., Bonhoeffer, T., Hübener, M. 2001. Pairing-induced changes of orientation maps in cat visual cortex. *Neuron,* 32:325-37.

Schummers, J., Mariño, J., Sur, M. 2002. Synaptic integration by V1 neurons depends on location within the orientation map. *Neuron,* 36:969-78.

Schummers, J., Yu, H., Sur, M. 2008. Tuned responses of astrocytes and their influence on hemodynamic signals in the visual cortex. *Science,* 320:1638-43.

Sengpiel, F., Stawinski, P., Bonhoeffer, T. 1999. Influence of experience on orientation maps in cat visual cortex. *Nature Neuroscience,* 2:727-32.

Shapley, R., Hawken, M., Ringach, D. L. 2003. Dynamics of orientation selectivity in the primary visual cortex and the importance of cortical inhibition. *Neuron,* 38:689-99.

Sherman, S. M. 1985. Functional organization of the W-, X-, and Y-cell pathways in the cat: A review and hypothesis. In Spraque, J. M. & Epstein, A. N. (Eds.), *Progress in Psychobiology and Physiological Psychology* (pp. 233-314). Orlando, Florida: Academic Press.

Shichida, Y., Matsuyama, T. 2009. Evolution of opsins and phototransduction. *Philosophical Transactions of the Royal Society of London, Series B: Biological Sciences,* 364:2881-95.

Sillito, A. M. 1975. The contribution of inhibitory mechanisms to the receptive field properties of neurones in the striate cortex of the cat. *Journal of Physiology,* 250:305-29.

Simon, D. K., O'Leary, D. D. 1992. Development of topographic order in the mammalian retinocollicular projection. *Journal of Neuroscience,* 12:1212-32.

Sirotin, Y. B., Das, A. 2009. Anticipatory haemodynamic signals in sensory cortex not predicted by local neuronal activity. *Nature,* 457:475-9.

Smetters, D., Majewska, A., Yuste, R. 1999. Detecting action potentials in neuronal populations with calcium imaging. *Methods,* 18:215-21.

Smith, A. L., Thompson, I. D. 1999. Spatiotemporal patterning of glutamate receptors in developing ferret striate cortex. *European Journal of Neuroscience,* 11:923-34.

Smith, W. J. 2008. Modern Optical Engineering (4th ed., pp. 365-408): McGraham-Hill.

So, K. F., Campbell, G., Lieberman, A. R. 1990. Development of the mammalian retino-geniculate pathway: target finding, transient synapses and binocular segregation. *Journal of Experimental Biology,* 153:85-104.

Sohal, V. S., Zhang, F., Yizhar, O., Deisseroth, K. 2009. Parvalbumin neurons and gamma rhythms enhance cortical circuit performance. *Nature,* 459:698-702.

Stafford, B. K., Sher, A., Litke, A. M., Feldheim, D. A. 2009. Spatial-temporal patterns of retinal waves underlying activity-dependent refinement of retinofugal projections. *Neuron,* 64:200-12.

Stosiek, C., Garaschuk, O., Holthoff, K., Konnerth, A. 2003. In vivo two-photon calcium imaging of neuronal networks. *Proceedings of the National Academy of Sciences, USA,* 100:7319-24.

Stryker, M. P., Zahs, K. R. 1983. On and off sublaminae in the lateral geniculate nucleus of the ferret. *Journal of Neuroscience,* 3:1943-51.

Svoboda, K., Yasuda, R. 2006. Principles of two-photon excitation microscopy and its applications to neuroscience. *Neuron,* 50:823-39.

Swindale, N. V. 1992. Elastic nets, travelling salesmen and cortical maps. *Current Biology,* 2:429-31.

Swindale, N. V. 2000. How many maps are there in visual cortex? *Cerebral Cortex,* 10:633-43.

Swindale, N. V., Grinvald, A., Shmuel, A. 2003. The spatial pattern of response magnitude and selectivity for orientation and direction in cat visual cortex. *Cerebral Cortex*, 13:225-38.

Swindale, N. V., Shoham, D., Grinvald, A., Bonhoeffer, T., Hübener, M. 2000. Visual cortex maps are optimized for uniform coverage. *Nature Neuroscience,* 3:822-6.

Thibos, L. N., Levick, W. R. 1985. Orientation bias of brisk-transient y-cells of the cat retina for drifting and alternating gratings. *Experimental Brain Research,* 58:1-10.

Thurlow, G. A., Bowling, D. B., Cooper, R. M. 1993. ON and OFF activity gradients in the lateral geniculate nucleus of the cat: a combined 14C 2-deoxyglucose and D,L-2-amino-4-phosphonobutyric acid study. *Visual Neuroscience,* 10:1027-33.

Tian, L., Hires, S. A., Mao, T., Huber, D., Chiappe, M. E., Chalasani, S. H., Petreanu, L., Akerboom, J., McKinney, S. A., Schreiter, E. R., Bargmann, C. I., Jayaraman, V., Svoboda, K., Looger, L. L. 2009. Imaging neural activity in worms, flies and mice with improved GCaMP calcium indicators. *Nature Methods,* 6:875-81.

Tiao, Y. C., Blakemore, C. 1976. Functional organization in the visual cortex of the golden hamster. *Journal of Comparative Neurology,* 168:459-81.

Troyer, T. W., Krukowski, A. E., Priebe, N. J., Miller, K. D. 1998. Contrast-invariant orientation tuning in cat visual cortex: thalamocortical input tuning and correlation-based intracortical connectivity. *Journal of Neuroscience,* 18:5908-27.

Ts'o, D. Y., Frostig, R. D., Lieke, E. E., Grinvald, A. 1990. Functional organization of primate visual cortex revealed by high resolution optical imaging. *Science,* 249:417-20.

Tsai, P. S., Nishimura, N., Yoder, E. J., Dolnick, E. M., White, G. A., Kleinfeld, D. 2002. Principles, design and construction of a two-photon laser-scanning microscope for in vitro and in vivo brain imaging. In Frostig, R. D. (Ed.), *In vivo optical imaging of brain function* (pp. 113-71). Boca Raton: CRC Press.

Tsodyks, M., Kenet, T., Grinvald, A., Arieli, A. 1999. Linking spontaneous activity of single cortical neurons and the underlying functional architecture. *Science,* 286:1943-6.

Usrey, W. M., Reppas, J. B., Reid, R. C. 1999. Specificity and strength of retinogeniculate connections. *Journal of Neurophysiology,* 82:3527-40.

van Hooser, S. D. 2007. Similarity and diversity in visual cortex: is there a unifying theory of cortical computation? *The Neuroscientist,* 13:639-56.

van Hooser, S. D., Heimel, J. A., Chung, S., Nelson, S. B. 2006. Lack of patchy horizontal connectivity in primary visual cortex of a mammal without orientation maps. *Journal of Neuroscience,* 26:7680-92.

van Hooser, S. D., Heimel, J. A. F., Chung, S., Nelson, S. B., Toth, L. J. 2005. Orientation selectivity without orientation maps in visual cortex of a highly visual mammal. *Journal of Neuroscience,* 25:19-28.

Wang, F., Nemes, A., Mendelsohn, M., Axel, R. 1998. Odorant receptors govern the formation of a precise topographic map. *Cell,* 93:47-60.

Wässle, H. 2004. Parallel processing in the mammalian retina. *Nature Reviews: Neuroscience,* 5:747-57.

Wässle, H., Boycott, B. B. 1991. Functional architecture of the mammalian retina. *Physiological Reviews,* 71:447-80.

Weliky, M. 2000. Correlated neuronal activity and visual cortical development. *Neuron,* 27:427-30.

Weliky, M., Katz, L. C. 1994. Functional mapping of horizontal connections in developing ferret visual cortex: experiments and modeling. *Journal of Neuroscience,* 14:7291-305.

Weliky, M., Katz, L. C. 1997. Disruption of orientation tuning in visual cortex by artificially correlated neuronal activity. *Nature,* 386:680-5.

Weliky, M., Katz, L. C. 1999. Correlational structure of spontaneous neuronal activity in the developing lateral geniculate nucleus in vivo. *Science,* 285:599-604.

White, L. E., Coppola, D. M., Fitzpatrick, D. 2001. The contribution of sensory experience to the maturation of orientation selectivity in ferret visual cortex. *Nature,* 411:1049-52.

White, L. E., Fitzpatrick, D. 2007. Vision and cortical map development. *Neuron,* 56:327-38.

Wickersham, I. R., Lyon, D. C., Barnard, R. J. O., Mori, T., Finke, S., Conzelmann, K.-K., Young, J. A. T., Callaway, E. M. 2007. Monosynaptic restriction of transsynaptic tracing from single, genetically targeted neurons. *Neuron,* 53:639-47.

Wielaard, D. J., Shelley, M., McLaughlin, D., Shapley, R. 2001. How simple cells are made in a nonlinear network model of the visual cortex. *Journal of Neuroscience,* 21:5203-11.

Wiesel, T. N., Hubel, D. H. 1974. Ordered arrangement of orientation columns in monkeys lacking visual experience. *Journal of Comparative Neurology,* 158:307-18.

Williams, B. H. 2000. Therapeutics in Ferrets. *Veterinary Clinics Of North America: Exotic Animal Practice,* 3:131-53.

Williams, R. W., Herrup, K. 1988. The control of neuron number. *Annual Review of Neuroscience,* 11:423-53.

Wilson, R. I., Mainen, Z. F. 2006. Early events in olfactory processing. *Annual Review of Neuroscience,* 29:163-201.

Wixson, S. K. 1999. Anesthesia and Analgesia in Laboratory Animals. In Kohn, D. F., Wixson, S. K., White, W. J. & Benson, G. J. (Eds.), (pp. 274-9): Academic Press.

Wong, R. O. 1999. Retinal waves and visual system development. *Annual Review of Neuroscience,* 22:29-47.

Wong, R. O., Meister, M., Shatz, C. J. 1993. Transient period of correlated bursting activity during development of the mammalian retina. *Neuron,* 11:923-38.

Wörgötter, F., Eysel, U. T. 1987. Quantitative determination of orientational and directional components in the response of visual cortical cells to moving stimuli. *Biological Cybernetics,* 57:349-55.

Yaksi, E., Friedrich, R. W. 2006. Reconstruction of firing rate changes across neuronal populations by temporally deconvolved Ca2+ imaging. *Nature Methods,* 3:377-83.

Yamagata, M., Weiner, J. A., Sanes, J. R. 2002. Sidekicks: synaptic adhesion molecules that promote lamina-specific connectivity in the retina. *Cell,* 110:649-60.

Yang, J. W., Hanganu-Opatz, I. L., Sun, J. J., Luhmann, H. J. 2009. Three patterns of oscillatory activity differentially synchronize developing neocortical networks in vivo. *Journal of Neuroscience,* 29:9011-25.

Zandvliet, M. 2005. Electrocardiography in Psittacine Birds and Ferrets. *Seminars in Avian and Exotic Pet Medicine,* 14:34-51.

Zhang, F., Wang, L.-P., Brauner, M., Liewald, J. F., Kay, K., Watzke, N., Wood, P. G., Bamberg, E., Nagel, G., Gottschalk, A., Deisseroth, K. 2007. Multimodal fast optical interrogation of neural circuitry. *Nature,* 446:633-9.

Acknowledgements

It is a pleasure to thank those who made this thesis possible. First, it is hard to overstate my gratitude to Prof. Dr. Mark Hübener for being a great, friendly and helpful supervisor. With his overwhelming scientific enthusiasm paired with coruscating wit, he generated a wonderful working atmosphere and gave me the inspiration and vigour to finish my thesis. He was always disposed to discuss ideas or problems (even during nightly experimental sessions) and gave thoroughly advice on scientific and personal issues.

I am also very grateful to Prof. Dr. Tobias Bonhoeffer for giving me the opportunity to accomplish my Ph.D. thesis in his excellent research department. I experienced him as an enthusiastic scientist who shares his expertise and passion with his students.

I owe my deepest gratitude to my close collaborator in this project, Jonathan Leong, with whom I spent days and nights in the laboratory during the experimental periods. He became a good friend who inspired me in many scientific and cultural respects with his vivid spirit.

I am very thankful to Prof. Dr. Frank Schaeffel for helping with the photorefraction and for enduringly answering questions to ophthalmic optics.

I would like to thank my thesis committee, Prof. Dr. Axel Borst and Dr. Felix Felmy, for enriching discussions and invaluable suggestions and I thank Prof. Dr. Benedikt Grothe for reviewing this thesis.

I really enjoyed working in the Max Planck Institute. I am indebted to the whole *in vivo* group and my colleagues for providing a stimulating and fun environment in which to learn and grow.

Frank Voss und Volker Staiger have made available their support in a number of ways to start and complete successfully numerous experiments. Special thanks also to Max Sperling for his support with programming and computer concerns.

I also would like to thank Dr. Brandstetter, Dr. Hesse, Mrs. Kuenzel and the entire team of the animal facility who zealously helped to provide the best and adequate care for the ferrets and their kits.

I appreciate the graduate programmes "Orientation and Motion in Space" (GRK 1091) and the International Max Planck Research School for Molecular and Cellular Life Sciences for generous funding. I really enjoyed the stimulating courses and extracurricular activities.

I wish to thank my entire family for providing me a loving environment. Lastly, and most importantly, I wish to thank my parents. They bore me, raised me, supported me, believed in me, and loved me. To them I dedicate this thesis.

Curriculum vitae
Marcus Leinweber

PERSONAL AND CONTACT DETAILS

Date of birth	12. January 1980, Berlin, Germany
Address	Max Planck Institute of Neurobiology
	Am Klopferspitz 18
	82152 Martinsried, Germany
Email	leinweber@neuro.mpg.de

EDUCATION

since 03/2006	*Max Planck Institute of Neurobiology, Martinsried* Ph.D. thesis with Prof. Dr. Mark Hübener and Prof. Dr. Tobias Bonhoeffer
04/2006 – 04/2009	*DFG Graduate School "Orientation and Motion in Space", Munich*
since 10/2005	*International Max Planck Research School for Molecular and Cellular Life Sciences, Martinsried*
10/2000 – 09/2005	*Studies at the University of Leipzig* Subject: Biochemistry Degree: Diplom (1.5)
10/2002 – 06/2003	*Studies at the University of Glasgow, Great Britain* Subject: Biochemistry Degree: Bachelor of Science (GPA 14 of 16)
09/1990 – 07/1999	*High School in Freudenstadt (Baden-Württemberg)* Degree: Abitur (1.7)

RESEARCH EXPERIENCE

04 – 09/2005	*Max Planck Institute for Evolutionary Anthropology, Leipzig* Project: Investigation of gene expression variation in the transcriptoms of humans and primates. Position: diploma student PI: Prof. Dr. Pääbo
01/2004 – 03/2005	*Max Planck Institute for Evolutionary Anthropology, Leipzig* Project: Transcriptomics in humans and different primates using DNA-microarrays (Affymetrix). Position: student assistent PI: Prof. Dr. Svante Pääbo
10 – 12/2003	*Biotechnological-Biomedical Centre, Leipzig* Project: High-throughput screening for crystallization conditions of proteins. Position: student assistent PI: Prof. Dr. Nobert Sträter

07 – 09/2003	*Max Planck Institute for Biophysics, Frankfurt/M.*
	Project: Overexpression and crystallization of membrane proteins and X-Ray crystallography.
	Position: practical student
	PI: Prof. Dr. Hartmut Michel

PUBLICATIONS

Khaitovich P., Hellmann I., Enard W., Nowick K., Leinweber M., Franz H., Weiss G., Lachmann M., Pääbo S. 2005: Parallel Patterns of Evolution in the Genomes and Transcriptomes of Humans and Chimpanzees. *Science*, 309: 1850-4.

CONFERENCE CONTRIBUTIONS

Leinweber, M., Leong, J. C. S., Mrsic-Flogel, T. D., Bonhoeffer, T., Hübener, M. 2009. Changing functional organization during initial development of orientation maps in the visual cortex. *Abstracts of the 9th Annual Meeting of the German Society of Neuroscience, Göttingen, Germany.*

Leinweber, M., Leong, J. C. S., Mrsic-Flogel, T. D., Bonhoeffer, T., Hübener, M. 2008. Two-photon calcium imaging reveals early development of orientation maps in ferret visual cortex. *Abstracts of the 5th Annual Meeting of the Lemanic Neuroscience Programs, Les Diablerets, Switzerland.*

Leong, J. C. S., Leinweber, M., Mrsic-Flogel, T. D., Bonhoeffer, T., Hübener, M. 2007. Functional organization of orientation preference in the developing cortex. *Abstracts of the 36th Annual Meeting of the Society of Neuroscience, San Diego, USA.*